Embedded sensing for advanced robotic applications

Markellos Ntagios

School of Engineering,

College of Science and Engineering

University of Glasgow

A thesis submitted in fulfilment for the degree of Doctor of Philosophy

January 2022

Supervisor:

Prof. Ravinder Dahiya

ABSTRACT

The human skin has several sensors with different properties and responses to different stimuli, such as pressure, temperature, and pain. Tactile sensors are generally modelled after the biological sense of cutaneous touch; these are able to detect stimuli resulting from mechanical stimulation. Pressure sensors are the most common types of receptors that enable the manipulation of foreign objects. Their application in robotics is rapidly developing, mainly driven by the prospect of autonomous and intelligent robots that can interact with the environment. Robotic end-effectors, prosthesis and wearable devices benefit from the development of tactile technology. This tries to mimic the properties of human skin not only as a protective shell, but also to provide sensory information from the outside environment. Many attempts have been made to create tactile sensors with various techniques and materials, leading to a variety of devices. Most of these are based on the human skin's functionality and appearance and resemble small patches of the skin with various degrees of flexibility and occasionally stretchability, such as electronic skin (Eskin).

New manufacturing techniques such as Additive Manufacturing (AM) are currently used to develop complex structures via layer-by-layer deposition methods. Complex shapes are possible using 3D printing as deposition is controlled from the electronics. Antennas, interconnects and 3D printed circuit boards are now possible to be manufactured using this technology. Moreover, tactile sensing devices embedded in the core structure of robotic parts intrinsically can be made. This has the potential to produce a new generation of tactile sensors without the issues noted in Eskins. This thesis presents an investigation in the development of complex, smart and intelligent devices, particularly for robotic end-effectors.

This new approach presented in this thesis developed complex three-dimensional (3D) intelligent structures using innovative designs and multi-material AM technology. It covers current 3D printing systems with the ability of past-like extruder mechanism and traditional filament deposition modelling (FDM), resulting in 3D printed structures with various materials for complex applications. The enhanced 3D printer can print a variety of materials from food-based materials (chocolate, condiment etc) to conductive materials and dielectrics.

This methodology was used to produce distal phalanges for a 3D printed hand with inherent capacitive pressure sensors and embedded electronics. Materials such as thermoplastic polyurethane (TPU), silver paint, conductive polylactic acid composite, graphite ink, etc. are explored to develop different variants of the sensors using 3D printing. The best-performing 3D printed soft capacitive touch sensors, formed with silver paint and soft rubber (Ecoflex 00-30), are integrated on the distal phalanges of the 3D printed robotic hand. These sensors exhibit a stable response with sensitivity of 0.00348 kPa^{-1} for pressure <10 kPa and 0.00134 kPa^{-1} for higher pressure. A 3D printed hand was designed, fabricated and integrated with the sensors. The robotic hand was also provided with harvesting generating devices for autonomous operation.

As 3D printing provides design freedom for complex shapes, a soft, flexible and low-cost capacitive pressure-sensitive insole was developed using a single-step 3D printing method. Developed using elastomeric materials, the soft and robust sensory sole can bend and twist, without altering its performance. The sensors exhibit a sensitivity of 2.4MPa^{-1} for the range of 0-60kPa and 0.526MPa^{-1} for 60kPa and above while tested for forces up to 1000N.

As capacitive sensors are slow to respond/read a piezoresistive sensor was embedded using 3D printing for faster response on dynamic conditions. The devices fabricated use graphite paste encapsulated in a two-part rubber material and embedded using a 3D printer in TPU. The devices are tested for their response in the time and frequency domain.

While the above focuses on devices, fabrication difficulties arose. A novel closed-loop feedback 3D printer extruder was developed to expand 3D printers' capabilities and eliminate current problems and short-comings of current state 3D printers. The system expands the range of materials that can be printed with the

advantage of printing multi-part materials such as two-part polymers without preparation. Experimentation was done using various materials showing good flow control at high printing speeds.

LIST OF PUBLICATIONS

Journal Articles

1. **M. Ntagios,** H. Nassar, A. Pullanchiyodan, W.T. Navaraj and R. Dahiya, "Robotic Hands with Intrinsic Tactile Sensing via 3D Printed Soft Pressure Sensors", *Advanced Intelligent Systems*, vol.2, 6, 2020.

2. M. Soni, M. Bhattacharjee, **M. Ntagios** and R. Dahiya, "Printed Temperature Sensor Based on PEDOT: PSS-Graphene Oxide Composite," *IEEE Sensors Journal*, vol. 20, 14, 2020.

3. P. Escobedo, **M. Ntagios**, D. Shakthivel, W. T. Navaraj and R. Dahiya, "Energy Generating Electronic Skin With Intrinsic Tactile Sensing Without Touch Sensors," *IEEE Transactions on Robotics*, vol. 37, 2, 2021.

4. A. Christou, **M. Ntagios***, A. Hart and R. Dahiya "GlasVent—The Rapidly Deployable Emergency Ventilator". *Global Challenges* vol.4, 12, 2020.

5. O. Ozioko, P. Karipoth, P. Escobedo, **M. Ntagios**, A. Pullanchiyoda and R. Dahiya. "SensAct: The Soft and Squishy Tactile Sensor with Integrated Flexible Actuator" *Advanced Intelligent Systems*, vol.3, 3, 2021.

6. F. Nikbakhtnasrabadi, H. El Matbouly, **M. Ntagios**, and R. Dahiya, "Textile-Based Stretchable Microstrip Antenna with Intrinsic Strain Sensing". *ACS Applied Electronic Materials*, vol.3, 5, 2021.

7. A. Pullanchiyodan, L. Manjakkal, **M. Ntagios**, and R. Dahiya, "MnOx-Electrodeposited Fabric-Based Stretchable Supercapacitors with Intrinsic Strain Sensing" *ACS Applied Materials & Interfaces*, vol. 13, 40, 2021.

8. **M. Ntagios,** H. Nassar and R. Dahiya, "Closed-Loop Direct Ink Extruder For Multi-Part Materials", (in progress).

9. **M. Ntagios** and R. Dahiya, "3D Printed Soft and Flexible Insole with Intrinsic Pressure Sensing Capability," *IEEE Sensors Journal*, 2022.

* *Equal contribution*

Conference Articles

1. H. Nassar, **M. Ntagios**, W. T. Navaraj and R. Dahiya, "Multi-Material 3D Printed Bendable Smart Sensing Structures," *2018 IEEE SENSORS*, 2018.

2. **M. Ntagios**, W. T. Navaraj and R. Dahiya, "3D Printed Phalanx Packaged with Embedded Pressure Sensor," *2018 IEEE SENSORS*, 2018.

3. **M. Ntagios**, P. Escobedo and R. Dahiya, "3D Printed Robotic Hand with Embedded Touch Sensors," *2020 IEEE International Conference on Flexible and Printable Sensors and Systems (FLEPS)*, 2020.

4. P. Escobedo, L. Manjakkal, **M. Ntagios** and R. Dahiya, "Flexible Potentiostat Readout Circuit Patch for Electrochemical and Biosensor Applications," *2020 IEEE International Conference on Flexible and Printable Sensors and Systems (FLEPS)*, 2020.

5. P. Escobedo, **M. Ntagios** and R. Dahiya, "Electronic Skin with Energy Autonomous Proximity Sensing for Human-Robot Interaction," *2020 IEEE SENSORS*, 2020.

6. **M. Ntagios**, P. Escobedo and R. Dahiya, "3D printed packaging of photovoltaic cells for energy autonomous embedded sensors," *2020 IEEE SENSORS*, 2020.

7. R. Chirila, **M. Ntagios** and R. Dahiya, "3D Printed Wearable Exoskeleton Human-Machine Interfacing Device," *2020 IEEE SENSORS*, 2020.

8. **M. Ntagios**, S. Dervin and R. Dahiya, "3D Printed Capacitive Pressure Sensing Sole for Anthropomorphic Robots," *2021 IEEE International Conference on Flexible and Printable Sensors and Systems (FLEPS)*, 2021.

9. X. Karagiorgis, **M. Ntagios**, P. Skabara, "3D printed Elastomer foam based soft capacitive pressure sensors", 2022 *IEEE International Conference on Flexible and Printable Sensors and Systems (FLEPS)*, 2022.

Book Chapters

1. A. S. Dahiya, Y. Kumaresan, O. Ozioko, **M. Ntagios** and R. Dahiya, "Soft Sensors for Electronic Skin" *Elsevier*, (In press).

2. **M. Ntagios**, O. Ozioko and R. Dahiya, "Biomimetic Skin with integrated Tactile Sensing, Actuation and Computing", *MIT Press*, (In press)

Awards

1. 3rd Place Best Student Paper Award to **M. Ntagios**, P. Escobedo and R. Dahiya for "3D Printed Robotic Hand with Embedded Touch Sensors" *IEEE FLEPS 2020*,

ACKNOWLEDGMENT

I would like to express my most worm-heartly gratitude to my supervisor Professor Ravinder Dahiya for his invaluable support and guidance. His knowledge and leadership throughout the period of my research led me to this point. Without his encouragement and discussion, this work would not be possible. I would like to thank Dr. Bernd Porr my second supervisor for his inputs. I also would like to thank Rich Walker director of Shadow Robot Company for his advice and support to this project. His invaluable inside on robotics and sensing shaped the work and encouraged me to push my boundaries to new high. Also, I would like to express my gratitude to the entire Shadow Robot Company for their support, especially Dr. Annagiulia Morachioli. I am eternally grateful to UKRI for funding this PhD and Shadow Robot Company, as well as EPSRC and the IEEE community. I would like to thank Dr. William Taube Navaraj for his support and time he spent helping me with my initial steps in my research. To Dr. Oliver Ozioko, Dr. Abhilash Pullanchiyodan I would like to thank him for supporting my research. To my dearest friend and colleague Habib Nassar I would like to heartily thank for his collaboration, support and discussion and ideas he provided through the four years we worked together. Lastly, I would like to thank all members of the Bendable Electronics and Sensing Technologies (B.E.S.T.) group for their help, support and collaboration, as well as the University of Glasgow and especially the technicians for the fabrication of PCBs. Special thanks go to my friends from the group Dr. Nivasan Yogeswaran, Dr. Tasos Viliouras, Adamos Christou, Fatemeh Nikbakht, Xenofon Karagiorgis, Radu Chirila, Ayoub Zumeit, Joan Neto, Sihang Ma. To Dr. Abhishek Dahiya I would like to thank him for his amazing support and encouragement in completion of this work.

There are no words to describe my eternal gratitude to my partner and best friend Eleni Charla. The support, strength, tolerance and love I received in the last four years of my endeavours, cannot be written in words, or repaid. To her, I give her all my love and support to her endeavours.

I would like to thank my entire family. Especially, my great father Dr. Stavros Ntagios for believing in me and supporting me without hesitation. His infinite wisdom was, is and will guide me to move forwards. To my beloved mother I

cannot express my love, for her, with words. Her love is priceless to me, even when I do not deserve it. To both, they have my eternal thankfulness for supporting me all my life.

I dedicate this thesis to my family

members that are currently

not with us and hopefully in a better place

DECLARATION

I, Markellos Ntagios, hereby declare that, except where explicitly reference is made to the contribution of others, this thesis is the result of the work of my own work and has not been submitted for any other degree at the University of Glasgow or any other institution.

TABLE OF CONTENT

LIST OF TABLES

LIST OF FIGURES

List of Acronyms

Acronym	Full Name
ABS	acrylonitrile butadiene styrene
AI	Artificial Intelligence
AM	Additive Manufacturing
ASA	acryloni-trile styrene acrylate
BIS	Beam Interference Solidification
CAD	Computer-aided design
CDC	Capacitive to Digital Converter
CNT	Carbon nanotubes
DIW	Direct Ink Writing
DMD	Direct metal deposition
DMLS	Direct metal laser sintering
DoA	Degrees-of-Actuation
DoF	Degrees-of-Freedom
DUT	device under test
EDA	Electronic Design Automation
EMIM-ES	1-ethyl-3-methylimidazolium ethyl sulfate
Eskin	Electronic Skin
FDM	Filament Deposition Modelling
FET	Field-Effect-Transistors
FFF	Fused Filament Fabrication
FSR	Force Sensitive Resistors
GUI	Graphical-User-Interface
HIS	Holographic Interference solidification
HRI	Human Robot Interaction
I2C	Inter-Integrated Circuit
IC	Integrated Circuit
IoT	Internet of things
ITO	Indium tin oxide
LPD	Laser powder deposition
LTP	Liquid thermal polymerization
MCU	microcontroller unit
MEM	microelectromechanical
MUX	multiplexer
PCB	Printed Circuit Board
PCB	Personal Computer
PDMS	Polydimethylsiloxane
PEDOT:PSS	polymer—poly(3,4-ethyl-enedioxythiophene–poly(styrenesulfonate)
PEI	polyetherimide
PEMA	Printed Electrode membrane assembly
PLA	polyactic acid
PMMA	poly(methyl methacrylate)
PPS	Pre-Pressure-Subsystem
PWM	Pulse Width Modulation
SDS	Screw-Driven-Subsystem

SGC	Solid ground Curing
SLA	Stereolithography
SLC	Selective laser cladding
SLM	Selective laser melting
SLS	Selective laser Sintering
SMU	Source/Measure Unit
TPU	thermoplastic polyurethane
UART	Universal Asynchronous Receiver/Transmitter
USB	Universal Serial Bus
UV	Ultraviolet

Chapter 1: Introduction

1.1 Motivation

Smart and intelligent structures involve the distribution of actuators, sensors and processing units that are able to analyse sensor response and use integrated control methods to trigger a response to a changing environment. Numerous applications, from the automotive industry to implants, benefit from smart structures. The field has attracted interest from many sectors as implementing such devices show a significant advantage. Smart structures can help in the robotic industry, from navigation systems to internal system conditions. However, robotic systems suffer from space limitations to implement such systems as bulk components, so a different approach is needed for robotic applications.

In addition, replicating biological organs to develop artificial equivalents and placing them on robotic systems is a growing scientific field with several challenges yet not fully resolved. Topics, such as soft robotics, Eskins, bionic limbs and more are attracting significant interest for the development of next-generation robots, moving from state-of-the-art robotics towards smart factories, assistive living and safe human-robot interaction. Moving from industrial use to urban areas (houses, hospitals) and unstructured environments (forests, mines etc.) it is crucial to equip such robots with human-skin capabilities, for safer interaction with humans. Soft and flexible electronics have driven progress in the field by conforming to the rigid and curved surfaces of robotic bodies with various level of success.

Robotic manipulators must be equipped with sensing modalities to provide information for achieving a specific task. Other fields such as the Internet-of-Things (IoT) are benefitting from the development of robots, able to provide tactile information on objects that are grasped, to the end-user/operator. Medical doctors are now able to perform surgery using such systems [1], which can provide valuable tactile information about the tissue of interest. Tactile sensing is also

used to extract information about material properties, such as softness and surface roughness and to classify materials using advancements in machine learning [2]–[6]. In addition, Eskins are used in humanoids, prostheses and wearable applications. However, the current state of technology still falls short on providing human-skin capabilities. Just by touch, a human is able to recognise properties of the grasped object such as size, shape, edges, roughness/softness, temperature, texture, curvature and many more. The human hand extracts this vast amount of information from different mechanoreceptors embedded at different depts in the skin. Electronic skin is unable to replicate this level of complexity. Furthermore, some of the most common issues involve mechanical flexibility, sensitivity, robustness, high fabrication cost, wear and tear and integration difficulties.

Additive Manufacturing, with the use of multi-material printing of smart and intelligent structure utilising layer-by-layer deposition shows promise for addressing most of the above challenges. This could enable the embedment of electronic components, the fabrication of active structures such as sensors and energy storage structures in compact and complex shapes.

This thesis aims to address problems with the current state of tactile sensors utilizing AM technologies and smart design by printing tactile sensors using multi-material printing. It enables the creation of sensors using 3D printing while the sensing elements can be embedded in the core structure of robotic bodies and take advantage of the available space, while simultaneously it could embed the accompanying electronic components necessary for reading the sensor’s state. This can provide a compact solution to the spatial problems of current technology and packaging. With the development of new materials and deposition methods, this could spark a new generation of smart compact structures for a plethora of applications, from robotics to food partials.

1.2 Objectives

Currently, there are three main pathways for developing smart and sensorised devices. The first is to develop tactile sensors using Eskin approach, this involves often costly processes and dedicated equipment of their fabrication. The second

is to purchase off-the-shelf sensors and use them as they are or encapsulate them, either using 3D printing or moulding. Lastly, the third method is to 3D print the devices on existing substrates and encapsulate them using methods such as drop-casting. Figure 1.1 presents the current approaches.

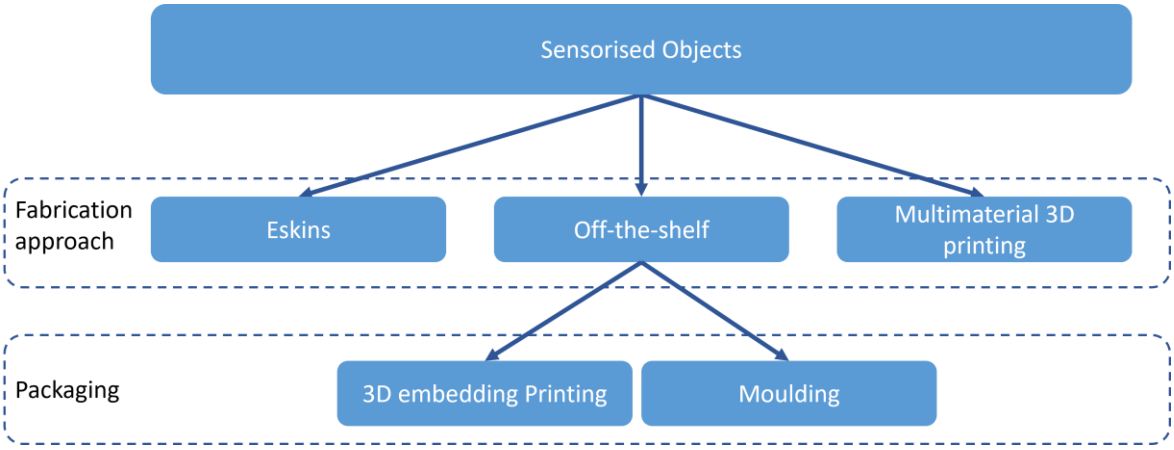

Figure 1.1 Sensorised object fabrication pathway

The objective of this thesis is the development of smart and intelligent systems for robotic applications. This thesis attempts to bridge the gap between packaging and fabrication of smart and sensorised devices. The current method of developing sensorised systems is to develop the sensing structure firstly while packaging the system is often overlooked and pushed to a later state after the development of the sensors. After their development, packaging issues are extremely difficult to overcome due to lack of oversight at the initial designing phase of the sensing structure. This problem is magnified when these systems need to perform for robotic body parts such as humanoid hands and feet. . For example, Eskins suffer from wear and tear, wiring and routing, and difficulties with wire bonding. This thesis presents an attempt to overcome these issues utilising AM technology. The versatility of the technology and rapid improvements can provide an alternative approach to the problem. Smart design and multi-material printing can provide a new solution to the problem. Multiple transducers have been developed using AM techniques for fabrication or encapsulation. This presents a new approach to fabrication of transducers for robotic application that minimises complexity, cuts the cost of fabrication and reduces the wear and tear of the sensing elements, thus introducing a cost-effective alternative.

The objectives are:

1. Development of smart devices with embedded sensors and electronics for advanced functionality. This includes tactile sensors for robotic/prosthetic hands, as feedback mechanisms for object manipulation using a cost-effective approach.

2. Improving the durability of Eskins. This includes the exploration of materials and dielectrics, packaging strategies and fabrication steps that could enhance the durability of tactile sensors.

3. Improving automation in smart devices. This includes the development and modification of 3D printers, if need be, for more specialised use. To achieve the above goals, new hardware/software might be required, and more complex fabrication techniques might need to be developed.

4. To investigate, develop and integrate energy harvesting systems for autonomous operation of robotic systems. To that end, a robotic hand and wrist have been developed with energy harvesting solar panels for harvesting and energy storing for autonomous operation. As current solar panel technology involves fragile materials, protecting them is a necessity.

1.3 Thesis Organisation

The thesis is organised as follows:

- Review of Literature (**Chapter 2**)

  Chapter 2 presents the state-of-the-art in physical sensors. Initially, it provides the fundamentals of transducing mechanisms that can be found in the human skin. Afterwards, it presents a plethora of transducing mechanisms and compares different realisation methods for various sensors. The chapter also introduces 3D printing used in smart structures and sensors.

- Design of sensors, end-effectors and peripherals (**Chapter 3**)

  Chapter 3 describes the design processes for making sensors and robotic parts. This involves the design of the robotic hand and wrist, followed by the design of capacitive and piezoresistive sensors, and covers of

photovoltaic cells. The chapter presents the designing freedom of using 3D printing processes.

- Electronics and embedded electronics using 3D printing (**Chapter 4**)

  Chapter 4 concerns the electronics used for the sensors and robotic parts. It presents designs of custom-made Printed Circuit Boards (PCBs), electronic circuits and their embedment using 3D printing for complex smart devices.

- Packaging and performance (**Chapter 5**)

  Chapter 5 explores how 3D printing was used as a fabrication tool to make different sensors and robotic parts, as well as the characterization of the different sensors and systems. The section discusses each of the fabrication processes required to make of each transducer and presents their performance and the reasoning for the materials used.

- Development of tools for autonomous fabrication of sensors (**Chapter 6**)

  Chapter 6 provide details on modifying of the 3D printers used in this thesis to increase their capabilities and to provide advanced functionalities. This section provides the design of a custom-made extruder mechanism, the related electronics used, and the accompanying software and controls. It presents the performance of the system while demonstrating the advantage of its use in an autonomous manner to fabricate smart structures.

- Conclusion and future prospective (**Chapter 7**)

  Chapter 8 summarises the key outcomes of this work on designing and creating smart structures, as well as advancements in 3D printers and provides some suggestions for future research.

Chapter 2: State-of-the-art of soft sensors and smart structures

This chapter presents a review of the state-of-the-art involving various processes for obtaining tactile sensors and smart intelligent structures. Initially, it provides a brief introduction to human skin modalities for a comprehensive understanding of the sense of touch in the human-skin. It continues with an extensive study of the existing artificial mechanoreceptors and different transducing methods, presenting advantages and disadvantages for each type. A variety of existing tactile devices that can be implemented on robotic systems are presented, together with the drawbacks in the current methodology. An introduction to 3D printing is presented with different technologies and its use in smart devices, embedded electronics and sensing modalities. This chapter provides the reasoning for the work carried out in this thesis.

2.1 Introduction

The human skin is the largest organ of the human body. Besides its protective role as a barrier between the external environment and the rest of the human body, it plays a significant role in humans' perspective of the outside world [7]–[9]. Interaction between humans and the environment is possible via the human skin and its sensing capabilities. The physical changes are captured via mechanoreceptors and thermoreceptors that can convey information about tactile and temperature information, while pain is detected by nociceptors existing in all layers of the skin. The sensors are embedded in all skin layers and can be found to overlap in some areas, providing a robust mechanism [10]. Mechanoreceptors are a type of somatosensory receptors transferring information of external stimuli, usually in the form of touch, pressure, stretching, vibration and motion [11]. There are four tactile mechanoreceptor types: Merkel cells, Meissner's corpuscles, Ruffini endings and Pacinian corpuscles, classified as Low-Threshold

Mechanoreceptors (LTM). A subclassification can be established based on the adaptation rate of each type. Fast or rapid adapting (FAI and FAII or RAI and RAII) fire only on the onset and offset of the stimuli. The second type is slow adapting (SAI and SAII) that fire throughout the duration of the stimulus [12].

- Meissner's corpuscles (FAI) have been found in the glabrous skin of all mammals and are mostly responsible for detecting a gentle touch. They have the highest sensitivity when sensing vibration. Lack of Meissner's corpuscles results in the loss of gentle touch and difficulties with sensorimotor control [13].

- Pacinian corpuscles (FAII) can be found in both glabrous and hirsute (hair) skin with a primarily responsibility for detecting vibrations. They respond, mostly, to disturbances and are highly sensitive to vibration frequencies of 250 Hz.

- Merkel cells (SAI) are oval-shaped and can be found in the epidermis. They are highly sensitive and respond to low vibration frequencies of 5-15 Hz and pressure over long periods. They are mostly found in the fingertips and toes [14], [15].

- Ruffini endings (SAII) can be found between the dermal and hypodermis tissue. They respond to skin stretching and contribute to the somatosensory controls. They respond to static pressure and have very slow adaptation.

Figure 2.1 presents the human skin and the mechanoreceptors embedded in the different layers.

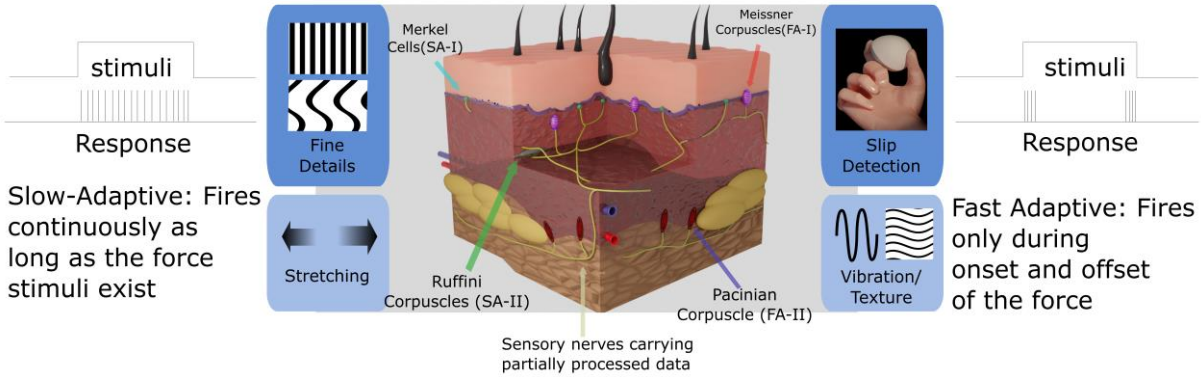

Figure 2.1: Human skin.
Presenting the spike trains, human skin receptors and signal response.

2.2 Transducing methods

All physical transducers' working principal is to convert mechanical stimuli to an electrical signal. There are multiple transduction mechanisms that the human skin can detect, such as pressure, vibration, shear and strain force. Tactile sensors implement different transduction methods to capture that information and the most commonly used sensors are capacitive, piezoresistive, piezoelectric, and optical sensors. Other less-used transduction mechanisms are ultrasonic and triboelectric, and have been used to detect pressure, vibration and other types of stimuli. All these transducer types can be found in many applications both for robots as well as in wearable applications for either feedback to robotics or for health monitoring, respectively[16]–[19].

2.2.1 Capacitive sensors

One of the most common transducing methods is capacitive. They are used in a parallel plate structure where device capacitance is defined as $C = \varepsilon_0 \varepsilon_r A/d$, where C is capacitance, ε_0 is the permittivity of free space, ε_r is relative permittivity, *A* is the surface area of the plate and *d* is the distance of the parallel plates. If an applied force, perpendicular from one of the plates, is exerted, then the dielectric material is compressed and the distance of the two plates decreases, resulting in an increase of capacitance. This change of capacitance can be measured and a relation between the capacitance and the applied force can be established.

A second type of morphology used in capacitive sensors is interdigitating electrodes. The structure resembles two combs facing each other on the same plane with each comb being an individual electrode. The capacitance occurs across a narrow pathway between the electrodes, which is typically filled with a dielectric material. The capacitance is given by: $C = \varepsilon * l[(N-3) * A_1 + A_2]$ where ε is the dielectric constant, l is the length of the interdigitated capacitive structure, N the number of periodicity of the structure, and A_1 and A_2 are derived

from the morphology of the substrate material and conductor [20]. While pressure is applied, the morphology of the structure changes, resulting in a change of capacitance. Figure 2.2 shows the two different morphologies.

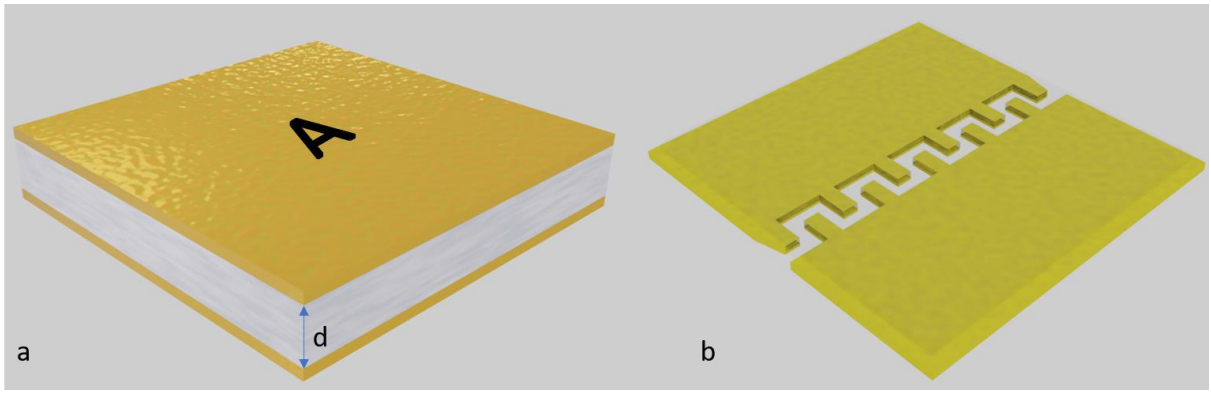

Figure 2.2: Capacitive sensor morphologies.
a) Parallel plate morphology b) Interdigitated morphology

2.2.2 Resistive/Piezoresistive sensors

Piezoresistive sensors utilise the effect of two surfaces changing their resistivity across them, while a force is applied perpendicular to them. Resistive/piezoresistive tactile sensors are now commonly made from conductive polymers. A force applied on the conductive polymer results in the decrease of the structure's resistance as the conductive materials come closer. The relationship between the applied force and resistance is more often a hyperbolic curve. This results in a rapid decrease of resistance for low amounts of pressure and is thought to be ideal for low-pressure applications. In general, there are two basic morphologies for the use of such sensors [21]. The first is a single-sided electrode contact and the second is a double-sided electrode contact. The second resembles the parallel-plate capacitive structure mentioned above (Figure 2.2a) and the first resembles the interdigitated structure, without the need of a comb morphology (Figure 2.2b).

Piezoresistive tactile sensors are commonly made using parallel electrode stripes on the top and bottom of the sensing material. The electrodes of one side are rotated at 90^{o} degrees against the other, thus allowing a crossing configuration. This arrangement enables a matrices structure sensor array. When a load is applied to the matrix, the sensing material in the local area changes its resistance, which can be measured at the crossing joints of the electrode stipes. This

approach can be used for large area sensor matrices and can offer high sensitivity with high pixel density [22]–[24].

2.2.3 Piezoelectric sensors

The term piezoelectricity refers to the ability of a material to generate electric charge or voltage potential across its surface when a mechanical stress is applied. At the same time, they have the property to exert force when a voltage is applied. These materials are asymmetric crystals, which still exist in an electrically natural state. When mechanical deformation, from an external force occurs, the atoms are pushed and conduct electricity. This piezoelectric effect can be used to develop devices able to utilise this effect to measure changes in pressure, acceleration and strain based on the electric charge generated [25]. Piezoelectric tactile sensors morphologically resemble capacitive structures with the difference being the use of a piezoelectric instead of a dielectric material. On such devices, when force is applied, it causes polarisation of the crystal and generates opposite charges on both electrodes. The efficiency of the material to convert mechanical stress to electricity is given by the piezoelectric constant (d_{33}).

These sensors are highly sensitive, with a high output even with relatively small amounts of force. A drawback to this transduction method is that when a load is maintained, the output decays quickly to zero. Piezoelectric devices are commonly used for sensing dynamic forces/vibration. As an upside, these devices do not require power supply for operation, exhibit high sensitivity, good linearity and high signal-to-noise ratio.

2.2.4 Optical Sensors

Optical transducers are an alternative method for tactile sensing used in robotics. Light is emitted in a transparent/translucent medium and when an applied force is acting upon the structure, it results in the change of the emitted light. A detector is used to capture this change and a relationship between the light intensity and the force can be obtained. There are three basic categories for such sensors [10].

i. Extrinsic optical transducers, which work when an applied force interacts with the light path.

ii. Intrinsic optical sensors, which change the phase, intensity or polarization of the light beam while an applied force is exerted and do not interrupt the optical path.

iii. Optical fibres can be used as well as transducers. They often transmit a light source from a broadband into the fibres, and when an applied force is exerted, the light is reflected or transmission is missing from the observed spectrum.

Optical sensors have been developed to cover large body parts in robotic systems. Commonly, cameras and markers are often used for tactile sensing as they provide a lot of information about the contact area, pressure, shear force and even temperature [26]–[28]. There are many works in the literature that use such techniques such as robotic limbs, fingertips, and E-skins. The main advantages of optical sensors are their immunity to external electromagnetic interference and high resolution. Drawbacks of optical sensor implementation are loss or alteration of the light due to signal distortion, bulky construction and the fact that are computationally intensive.

2.2.5 Comparison of tactile transducing methods

As described above, tactile transducers implemented different methodologies to extract information about the nature of an applied force. Each transduction methodology has inherent advantages and disadvantages. Table 2.1 presents a summary thereof for each method.

Table 2.1 Transducing modalities' benefits and drawbacks. Adopted from:[10]

Sensor Types	*Benefits*	*Drawbacks*
Capacitive	High Sensitivity Low Cost Scalability Simple Design	Complex electronics Cross-talk Hysteresis
Piezoresistive/ Resistive	High Sensitivity Low Cost Low noise Simple electronics	Non-linear response Hysteresis Signal drift Temperature sensitive

Piezoelectric	High sensitivity Dynamic Response High Bandwidth	Temperature Sensitive Unsuitable for static events Complex electronics
Optical	Immune to electromagnetic interference Fast response No interconnections	Complex electronics Relatively large size Power consumption

2.3 Tactile sensing devices

In the field of tactile sensing technologies, many transduction methods and materials are used to produce artificial skins for tactile feedback, using a variety of fabrication techniques. In the pursuit to develop such systems many attempts have been made to create sensors able to capture information from transducers, with various degrees of success. This section focuses on the development of sensors using a variety of techniques in traditional fabrication (clean-room) approaches.

2.3.1 Early tactile sensors

At first, tactile sensing technology was implemented for touch screens and prosthetics and initially rigid materials were used. Researchers began working on flexible electronics/sensors by exploring the use of organic/inorganic semiconductors [29], [30]. This started an explosion of scientific curiosity in flexible and smart devices able to conform to curved surfaces. This technology can be applied not only for tactile sensing but also in wearables, flexible displays, healthcare monitoring, soft robotics, human-machine interfaces and many others [31].

Even though interest in robotics started in the early 1950s, the tactile sensing field did not see any research interest as most problems involving robotics concerned mechanical aspects, such as motion [32]. One of the first implementations of tactile sensors was a manipulation system developed by the Massachusetts Institute of Technology (MIT). The computer-operated mechanical hand by Ernst was able to learn about its environment using tactile information [33]. As technology progressed, an optical touch sensor was developed by MIT researchers [34]. This sensor was able to produce optical information on a monitor for the

operator and it was used to study the operator's ability to recognise objects from a simple tactile pattern. The hand resembles a simple gripper system, with the camera attached outside the gripper. A coherent fibre bundle cable connected the camera's lens with one of the fingers [35].

With further advancements in the mechanical capabilities of hands, there was increased interest for tactile sensing to provide those manipulators feedback for grasping objects. The 1980s saw a variety of new devices, designs and transduction methods. This period, marked the rise of devices with surface pads with linear arrays [35], [36] and the use of elastomers made out of doped carbon or silicon, combined with rigid or discreet substrates to make resistive based sensors [37], [38]. Some of the most common materials, used even today, such as carbon fibers, were firstly introduced in this period. In 1981, Larcombe from the University of Warwick introduced the use of carbon fibres as a sensing material for a resistive pressure sensor [39]. Even today, we can see the use of such materials in many applications such as wearables [40]–[45]. At the end of the decade, Riberton and Walkden were able to produce a 256-element array made from carbon fibres using a row and column approach [46]. Many other transducing methods, such as piezoelectric, were used in this period. Quartz and ceramics were used to develop piezoelectric devices, but the use of those materials show inherent problems due to mechanical properties of the materials, especially due to fragility issues. Some of the polymers used are polyvinylidene fluoride (PVDF) but they do not exhibit piezoelectric properties in raw form. The use of high electric fields was used to make them piezoelectric/pyroelectric. In particular, a 128 PVDF sensor array was developed with conductive rubber as electrodes [47]. Capacitive structures were also explored but in general these types of devices were dismissed due to electromagnetic interference issues. However, attempts were made to develop transducers using this kind of system with a better practical implementation in a narrow range of applications. Most often they were made from orthogonal conductive strips in a row-column configuration and a dielectric layer in between. For example, Bell Labs, produced an 8x8 array and utilized a shield to reduce the interference. The bottom electrodes were etched on a flexible PCB with two analogue multiplexers (one attached to the bottom and the second to the top

electrodes) fixed to it [48]. This enables the user to have an image representation of the forces involved with the point of contact.

Over the next decade (1990s), the growth of tactile sensors continued with the exploration of many new materials. In this period, many topics were explored and expanded upon, not only in the design and fabrication but also in analysis and experimentation, data processing, application, multifingered hands, healthcare and others. Some of the concerns in field regarded device packaging and better performance, as previous works showed qualitative performance rather than quantitative results. Researchers started to explore mechanisms to increase the sensitivity of devices in order to extract fine texture details, stress and strain, slippage detection and other temporal contact events [32], [49]–[54]. All these features are important as more and more highly dexterous hands started to be developed and better and more accurate sensing was needed to operate those hands optimally. As the field showed significant progress at that time, there was an opportunity to develop sensors and manipulators that could inspire a new medical field in assistive medical robotics surgery, with robots guided by surgeons to perform difficult surgeries as they could have finer movements than the human counter-parts and tactile sensors on the manipulators could also transmit tactile information back to medical staff [55]–[57]. Most of the devices used transduction methodologies similar to those of previous decade, such as piezoresistive force sensors with silicon-based materials, piezoelectric PVDF film, silicon-based capacitive arrays and Complementary metal–oxide–semiconductor (CMOS) devices [53], [58]–[62]. Parallel to tactile sensing, for robotic hands, there was an interest in tactile sensing insoles as they provide an additional challenge due to the extreme pressure they exhibit. F-Scan was an attempt to introduce tactile sensing able to sense at pressures up to 1.7 MPa. However, the sensors are sensitive to temperature variations, loading speeds, surface condition and ununiform response [63]. Even though there was a significant advancement in the field of sensing in this period, many have pointed out the limitations of the mechanical properties of the materials used [50]. Force Sensing Resistor (FSR) was also commercialised in this period by interlink and is widely used in many experimental sensing devices [64]. These devices are used even today in many applications such as a joysticks,

tactile sensing insoles, tactile sensors for manipulators, wearables, health monitoring and many others [65]–[73].

The field of tactile sensing in these distinct periods showed exponential growth. The need for better control systems and algorithms for robotic systems drives the field towards better-performing devices. Automation, in particular, is heavily reliant on feedback mechanisms and tactile sensing is the first component in the development of such systems. In general, we see the scientific effort for such devices tripling every decade. Table 2.2 shows an approximate number of unique scientific publications in the 1970s, 1980s and 1990s both in conference works and journals. This clearly showcases the growth, importance and need for more and more advanced tactile sensors with better capabilities.

Table 2.2 Approximate Publications in the 1970s, 1980s and 1990s for tactile sensors. Adopted from [32]**.**

	1970s	*1980s*	*1990s*
Total number of publications	30	115	246

2.3.2 Recent advancements

In recent years, tactile sensing has become synonymous with the success of robotics in implementing complex tasks. Grasping and manipulation is heavily dependent on the ability to recognise an object's geometrical and physical characteristics [74]. This enables a safer environment for Human-Robot Interaction (HRI) as robotic vision is most often not enough to prevent accidents. As the pressure for more autonomous robots is increasing, due to unforeseen circumstances, such as pandemics, avoiding hazardous environments for humans, and a general need for higher skilled occupation, to fulfil low-skilled jobs, there is an increasing pressure on the development of such systems. In order to move robots from structured to unstructured environments, such as mines, urban areas and healthcare facilities, those machines need to be equipped with multiple

perception mechanisms such as visual, tactile and many others that humans possess [75].

Tactile sensing systems have now been integrated in robots for demonstration purposes and are able to be integrated into microcircuits. There is currently a plethora of solutions and technologies for the development of tactile systems. Unfortunately, not only design is affecting the performance of transducers, especially on large-scale devices, but also problems arise with wiring (wire routing, signal driving, ambient conditions and robotic platforms integration difficulties). Figure 2.3 presents tactile sensors with the aforementioned inherent problems of current approaches used in making of these devices.

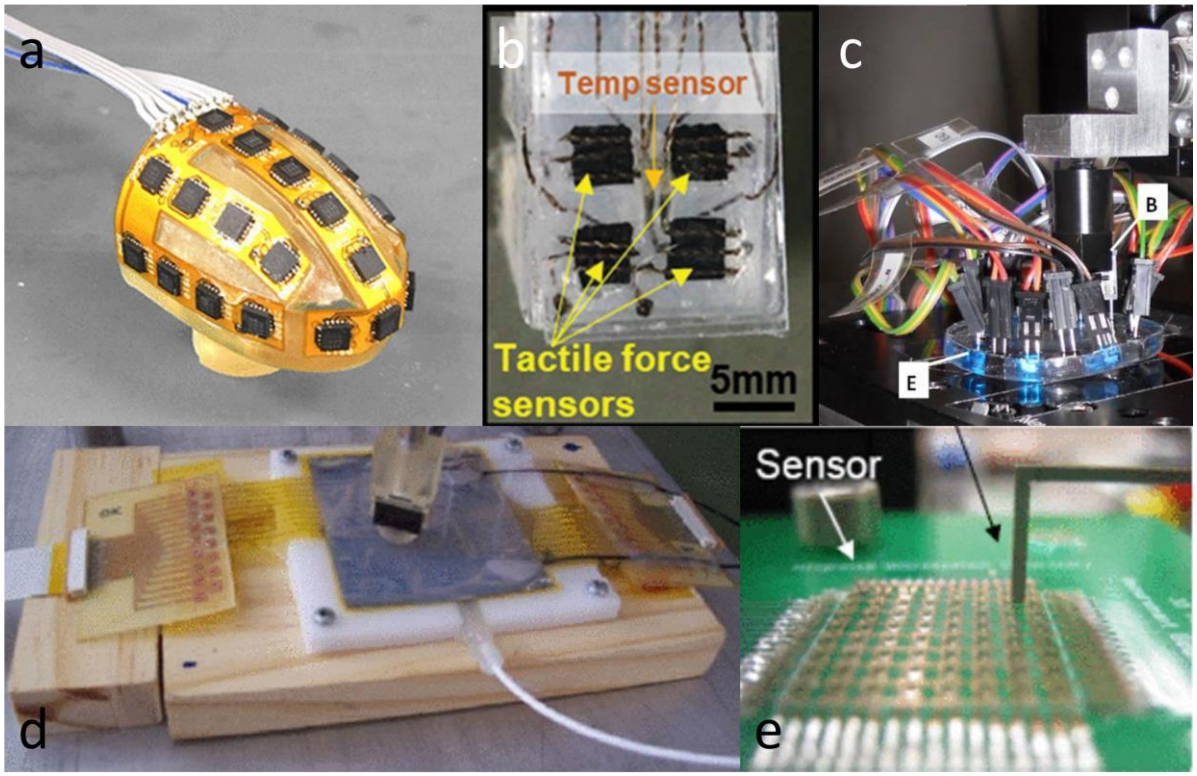

Figure 2.3 Tactile sensors developed recently showcasing problems with current approach.

a) uSkin fingertip [76] Copyright © 2018, IEEE, b) Human- Like Electronic skin with four tactile force sensors and a temperature sensor embedded in soft elastomer [77], c) Soft transparent Eskin for pressure sensing [78] d) Tactile sensor based on organic thin film transducer [79] Copyright © 2012, IEEE, e) Normal and Shear force flexible tactile sensor with embedded multiple capacitors [80] Copyright © 2008, IEEE.

All these issues have limited the number of dexterous robotic hands to incorporate tactile sensors [81]. The most well-known hands to implement tactile sensing are the GIFU hand [82], the MAC hand [83], the Obrero hand [84], Shadow hand [85]–

[87], Robonaut hand [88], Barret hand [89] and a few others [90]. Figure 2.4 presents robotic end-effectors equipped with tactile sensors.

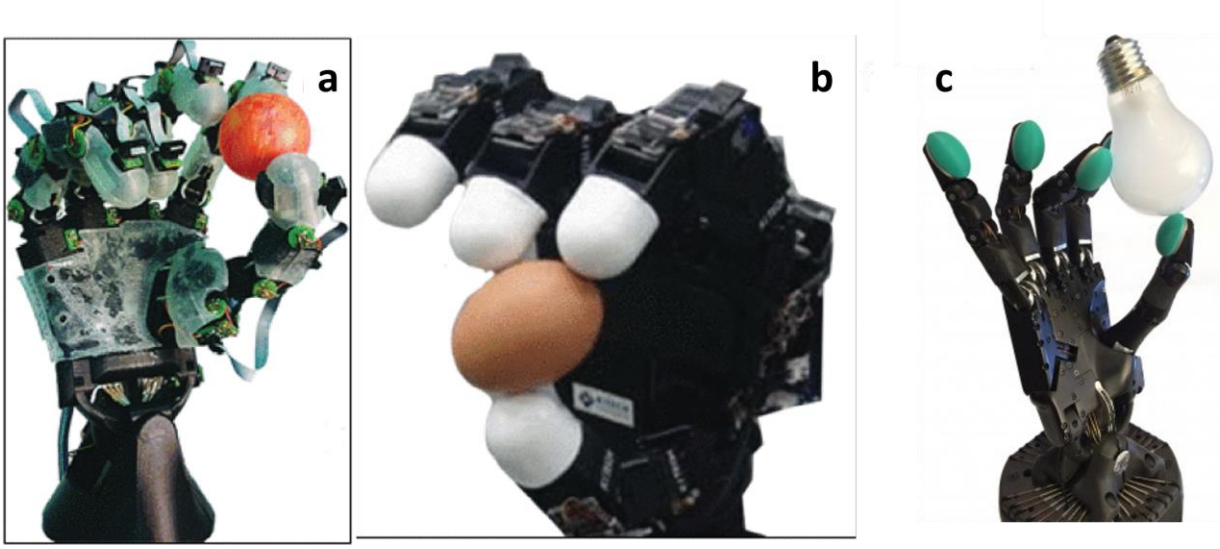

Figure 2.4 Robotic Hands utilising tactile sensing devices as feedback mechanisms.

Robotic hands enhanced with tactile sensors a) UB Hand VI [91], Copyright © 2013, IEEE, b) KITECH Hand [92], Copyright © 2012, IEEE c) Shadow Hand with SynTouch sensors [93].

Most of the tactile sensors developed in the recent years have not been integrated with robotic body parts, as the development of robotic parts is often costly, time-consuming and mechanically challenging. Based on the aforementioned, researchers often avoid developing their own platforms and either tested their devices in isolation (especially for lower extremities) or at best used already developed systems such as prosthetics or robotic hands and grippers [94]–[106]. Most of the tactile systems developed nowadays are based on an Eskin approach with high resolution and sensitivity, often avoiding the integration problems encountered by attachment to robotic systems.

Eskins have benefited from the advancement of flexible electronics with capabilities of bending and stretching, if need be, providing a significant advancement compared to rigid devices. Flexible substrates enable new fabrication methods for deposition of electronic components, electrodes, sensing materials and others, such as roll-to-roll processing, and 3D printing [107]–[113]. Recently, new works have incorporated thin-film transistors on a polymer substrate using graphene and other conductive materials, as part of the device, such as Field-Effect-Transistors (FET) [114]–[118]. Moreover, thinning devices have showed promising results with rigid materials able to bend by reducing the

thickness of the substrate, and as result reducing mechanical strain to the materials [119]–[124].

Eskins provide many benefits and can meet some of the requirements of prosthetic hands; however, as mimicking the sensory properties of skin while resembling its mechanical properties is challenging, there are currently no commercial prosthetic hands with tactile sensing capabilities. The reason for this is the electrical/mechanical performance of current tactile systems and the lack of proper propagation of tactile information to the wearer. Thus, many Eskins are now starting to be used in different applications, such as wearables, for pressure mapping, temperature and health monitoring devices and visual displays [125]. In the medical and dental field, implantable devices are also integrated with sensing and monitoring capabilities [126]. Some of the most recent Eskins also include energy generation capabilities, self-healing and multi-sensing modalities [127]–[132]. As more and more materials are explored, tactile sensors, in general, have increases their capabilities, in some cases even overpassing the human skin equivalent. Figure 2.5 provides an overview of the range Eskins applications that can be employed and highlights their strengths.

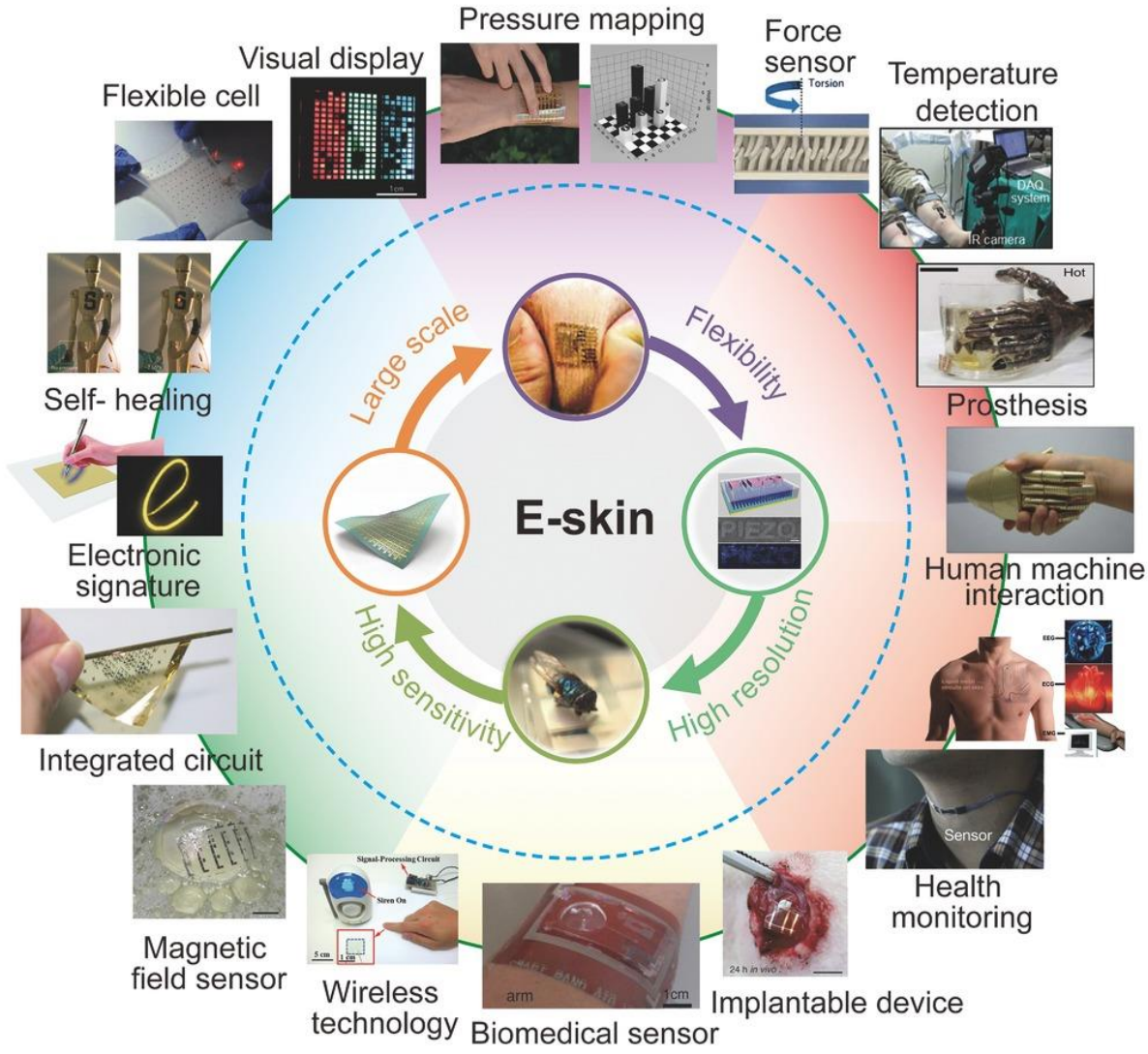

Figure 2.5 Electronic skin properties and applications in recent years [126].

This is only possible with materials that are now been explored. The next section discusses fabrication methods and materials in depth.

2.4 Fabrication methods and materials

New methods and materials have enabled more complex devices. Herein, the focus will be on the electrode and dielectric/sensing materials for fabrication of tactile sensors, as they are the most important parts of a transducer.

2.4.1 Electrodes

Research on tactile sensing has progressed beyond the old ways of fabricating electrodes via etching copper from a PCB. New fabrication techniques such as

screen-printing, roll-to-roll techniques, photolithography, electrodeposition, DIP-coating and many others are more compatible with the current requirements of tactile devices. This is thanks to the changing trend from inorganic materials, that are usually fragile and can have a permanent deform at low strain, to more mechanical compliant organic equivalents. Therefore, materials such as copper, silver and other inorganic materials do not receive the same attention as newly developed materials and composites. One of these newly developed materials is graphene, which has promising mechanical and electric properties [133]. Graphene has been used as an electrode but also as an active material in many applications, from tactile sensors to photovoltaic and energy storage devices [134]–[138]. Many works try to implement conductive polymers as electrodes. In many studies, polymer—poly(3,4-ethyl-enedioxythiophene–poly(styrenesulfonate) (PEDOT:PSS), has been used as an electrode or mixed with other materials to increase its conductivity or other mechanical or electrical properties [139]–[142]. Indium tin oxide (ITO) is another electrode used for tactile sensing, often valued for wearable applications due to its transparent nature [105], [143], [144]. AgNW and carbon nanotubes (CNTs) are other materials often used for electrodes [145], [146]. In the case of inorganic materials, a new approach to flexible electrodes is the deposition of electrodes on a pre-stretch substrate such as Polydimethylsiloxane (PDMS) then laminated with copper, silver or gold material [147], [148]. This technique is often used for interconnects rather than electrodes as they more often require higher electrical performance.

2.4.2 Active materials

Eskins have undergone rapid development to overcome new challenges. Polymer based composites are now used for the development of dielectric and sensing materials. Currently, a combination of organic and inorganic materials are used, as found in resistive, piezoresistive, piezoelectric and triboelectric devices. Devices developed nowadays can twist, bend and stretch with relative ease, with a minimum trade-off in sensitivity.

Piezoresistive transducers respond to lower pressures than previous devices by incorporating novel materials. Many have reported using piezoresistive sensors for strain measurements. Materials such as CNTs were used for strain measurements

[149]. Many devices use CNTs for their excellent conductivity and mechanical properties; these can be found in many applications not only in tactile sensing, but also as electrodes for rechargeable batteries [150]–[153]. CNT was also mixed with porous PDMS to create a soft piezoresistive sensor with a response of $0.033KPa^{-1}$ for a pressure range of 0-20 KPa [154]. Other materials used are Nanowires (NW) of different materials. NWs can grow at any length, depending on the desired application. Tactile sensing devices usually use semiconductor NWs, such as FET devices [155]–[158]. As an example, gold NWs on tissue paper were dip-coated and integrated on interdigitated electrodes to form a resistive device [159]. Another material type used for tactile sensors is conductive fillers embedded on soft elastomers. These materials are easy to use and are low-cost, usually containing carbon black and can be 3D printed. Other materials often used are metallic particles and CNTs [126], [160]–[162].

Capacitive sensors have also benefited from advancements in materials. The most common dielectric material used for capacitive sensors is PDMS films and researchers have tested many capacitive sensors using different PDMS thicknesses [163]–[166]. Most PDMS dielectric formation is done by spin-coating the material; the faster the rotation of the spinner, the thinner the dielectric material will be. The thickness of the dielectric often ranges from tenths of μm to mm. One study was able to fabricate a PDMS dielectric device with a thickness of 45μm with 3pF/N sensitivity [167]. Other materials that use spin-coated techniques are a poly(methyl methacrylate) (PMMA) solution, Ecoflex and others [168], [169]. Another method is drop-casting into a mould to obtain the desired morphology. Researchers used carbon-based silicone composite as a dielectric for a capacitive force sensor. [170]. The composite was mixed using ultrasonic dispersion and was afterwards degassed under vacuum, poured to a mould and cured under room temperature with a thickness of 0.5mm. The device sensitivity was 0.02536 %/Kpa with maximum hysteresis of 5.6% and a response time of 89ms at a pressure range of 0-700KPa. The device was demonstrated on a sock and insole wearable device and also demostrated as feedback to robotic fingertips.

Piezoelectric materials refer to materials that possess piezoelectric characteristics. The materials under mechanical force can generate electric charges due to the occurrence of electric dipole moments. This phenomenon

enables the conversion of mechanical stress to electrical signals. In general, piezoelectric devices have fast response times and relatively high sensitivity based on the piezoelectric coefficient (d_{33}). There are two types of materials used for such devices; inorganic and organic. Inorganic materials often exhibit a higher d_{33}, but they are often fragile and unsuitable for strain conditions. To combat this disadvantage, often composite materials based on polymers have been developed to increase their durability. A common material used for piezoelectric devices is PVDF, and is widely used in the literature [171]–[177]. A few preparation methods for forming piezoelectric devices are non-solvent induced phase separation (NIPS), thermal induced phase separation (TIPS), vapor-induced phase separation (VIPS), solution casting and electro-spinning [178]. Recently, oriented piezoelectric NWs are used to produce such devices. ZnO NWs, for example, used to produce a flexible sensor array that could map pressure with high sensitivity and resolution [159]. Table 2.3 presents studies of tactile sensors with the respective materials used and other performances.

Table 2.3 Tactile sensors and their performance. Adopted from [179]

Transduction Type	Materials	Sensitivity	Response/recovery time (ms)	Cycling numbers	Ref.
Piezoresistive	PDMS/SWNTs	1.8 kPa^{-1}	<10	67,500	[180]
Piezoresistive	PPy	133.1 kPa^{-1}	50	8000	[181]
Piezoresistive	PDMS/PEDOT:PSS/PUD	10.32 kPa^{-1}	200	-	[139]
Piezoresistive	Graphene/PU sponge	0.26 kPa^{-1}	-	10,000	[182]
Piezoresistive	PDMS/CNTs	15.1 kPa^{-1}	10	-	[183]
Capacitive	Alumina ceramic	3.5 MPa^{-1}	-	-	[184]
Capacitive	PDMS/air gap	0.7 kPa^{-1}	-	-	[132]
Capacitive	PDMS/Rubrene	0.55 kPa^{-1}	<10	-	[185]
Capacitive	Ionic conductor	10 MPa^{-1}	-	1000	[186]
Capacitive	Fluorosilicone/air gap	0.91 kPa^{-1}	<40	-	[187]
Piezoelectric	P(VDF-TrFE)	0.41 V Pa^{-1}	-	-	[188]
Piezoelectric	ZnO nanowires	2.1 μS kPa^{-1}	150	1000	[189]
Piezoelectric	Polypropylene	1MPa^{-1}	-	-	[190]
Triboelectric	PDMS/ZnS	6 MPa^{-1}	8.7	-	[191]
Triboelectric	PDMS/ITO	0.29 V kPa^{-1}	100	-	[192]

2.5 Additive Manufacturing and embedded sensors

Additive Manufacturing (AM) technologies, commonly known as 3D printing, is an emerging fabrication methodology, attracting interest across multiple disciplines. The field of 3D printing is experiencing exponential growth. In 2020, it was valued at 13.7 billion USD and by the end of 2026 is expected to reach 63.46 billion USD globally [193]. This relatively recent field of manufacturing has now been adapted to many industries, such as aerospace, automotive, medical & dental and consumer goods, to name but a few [193]–[202]. Figure 2.6 is a breakdown of the percentage of industrial sectors using 3D printing in their production [203]. AM has many attractive advantages compared to traditional fabrication methods (moulding/drop-casting, cutting, spin-coating etc.). 3D printing allows fast adaptation, reduces material waste, enables faster prototyping and above all provides unprecedented design freedom. This fabrication approach leads to new devices/products with arbitrary shapes, cavities and functionalities that are difficult to achieve with other fabrication methods. 3D printing can produce structures that are lightweight, due to the partial filling of the structure, with minor impact to overall strength of the part, or even higher strength in some occasions, due to fill patterns [204]–[206].

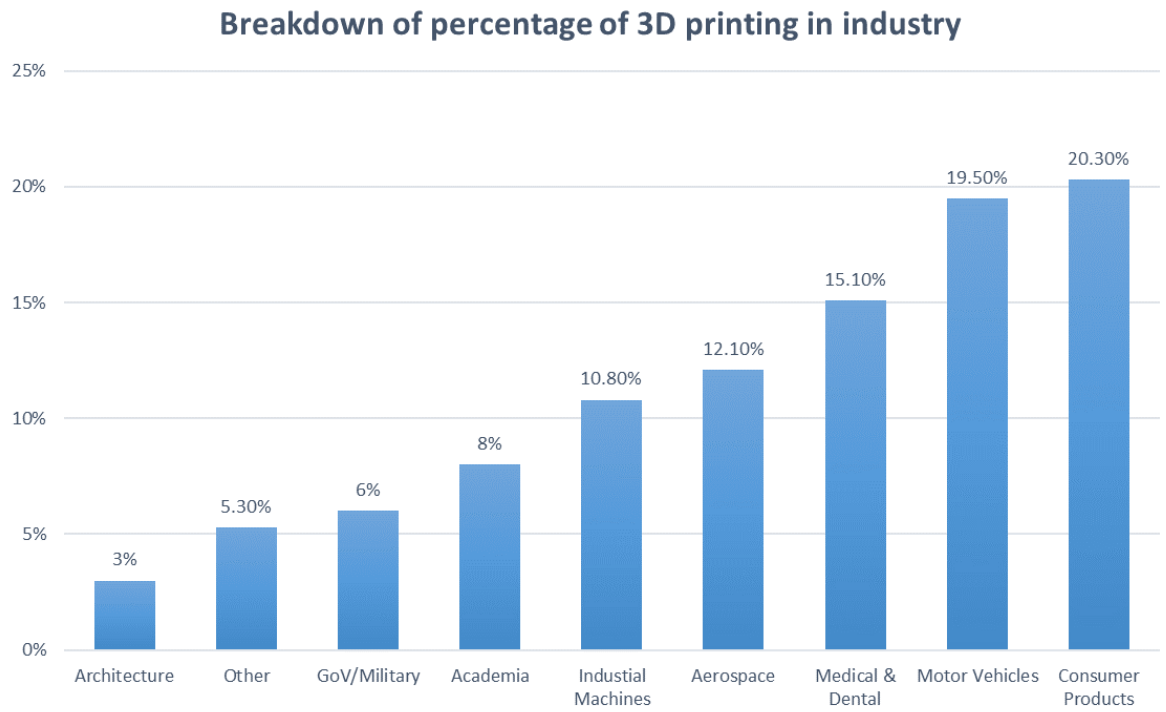

Figure 2.6 Breakdown of percentage of 3D printing use in industrial sectors. Adapted from [203].

3D printing consists of many technologies and processes for producing an object. Herein, a short description of the most used technologies for making smart devices will be presented. Lastly, we will present some of the latest works on the field of 3D printing for making intelligent systems.

2.5.1 Printing Techniques

3D printing has its roots in the late 1940s'and many different processes are established, depending on the materials used.. Each 3D printing methodology has advantages and disadvantages and, depending on the purpose of use, different methods can be employed. This section describes two of the most used AM technologies, based on the fabrication process. These are Laser-based processes and extrusion processes. There are three more processes (Adhesive, Electron Beaming and jetting processes) but they are not used as frequently [203].

2.5.1.1 Laser based 3D printing

This process uses a laser to melt, solidify or cure a material. This group could also be subdivided based on the way the material changes through the process. The

two processes are melting and polymerisation. In the first subdivision, the material is, usually, in powder form; as the laser melts the powder, a structure is formed where the laser passes. For the polymerisation processes, the material used is often a photosensitive resin; with the use of ultraviolet (UV) light, the resin cures and solidifies. Most common polymerisation processes are Stereolithography (SLA), Solid ground curing (SGC), Liquid thermal polymerisation (LTP), Beam interference solidification (BIS) and holographic interference solidification (HIS). In contrast, the melting processes are Selective laser sintering (SLS), Selective laser melting (SLM), Direct metal laser sintering (DMLS), Direct metal deposition (DMD), laser powder deposition (LPD) and selective laser cladding (SLC).

2.5.1.2 Extrusion printing

Extrusion deposition is the most used technique to deposit polymers on a 3D printer bed. This process is often done with the melting of polymers by a heated nozzle melting the polymer and depositing on the bed where it freezes back to solid state. The most well-known process is fused deposition modelling (FDM), also known as fused filament fabrication (FFF). This process uses a variety of thermoplastic materials such as acrylonitrile butadiene styrene (ABS), acrylonitrile styrene acrylate (ASA) nylon, polyetherimide (PEI), polylactic acid (PLA), thermoplastic polyurethane (TPU) to name but a few. Recently, a new technique, Direct Ink Writing (DIW), has been developed for cold extrusion [207].

DIW is critical for several technologies requiring precision of the materials deposited such as microfluidics, photonics, tissue engineering, sensors, flexible electronics and many others. The technology can utilise many different materials, from simple liquids to complex composites. This subsection of the extrusion printing method can be further divided depending on the method of deposition. Some of them are piston-driven, pneumonic or screw-based.

Figure 2.7 presents the working principle for laser-based 3d printing, FFF and DIW techniques.

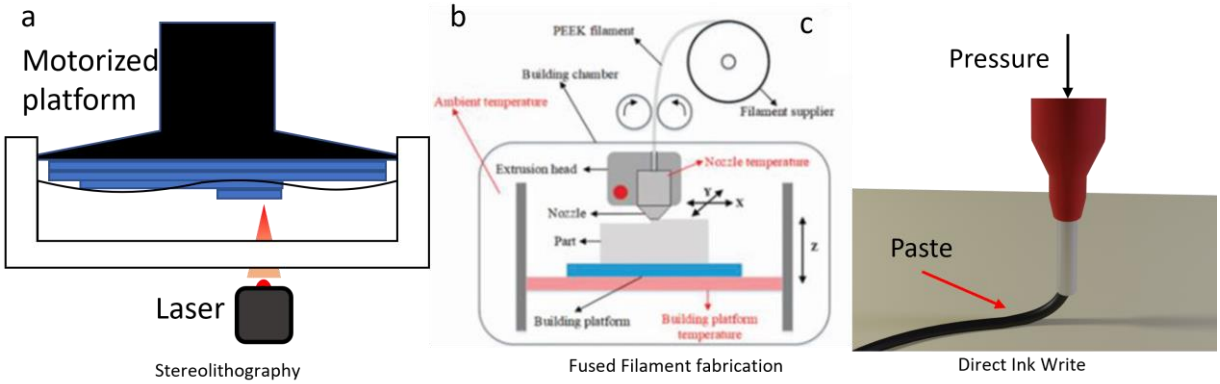

Figure 2.7 3D printing techniques

a) Stereolithography (SLA) 3D printing working principle. b) Fused Filament Fabrication methodology [208] Copyright 2018, MDPI. c) Direct Ink Write (DIW) working principle of based on pneumatic actuation.

2.5.2 3D printing and smart structures

Progress in the field is driven by the exploration of new materials/composites. The field of electronics is currently exploring the use of 3D printing in many applications. Both passive and active materials are used to make functional structures for various applications. Many works combine 3D printing techniques such as FDM and DIW to develop unique devices that traditional methods are unable to construct. A common characteristic of 3D printed devices is the intrinsic capabilities of multi-material printing of novel materials. This can result in devices fabricated with active elements and their packaging in one continuous step with a high level of automation.

2.5.2.1 Smart structures for advanced electronic devices using 3D printing

One of the first steps in the development of electronic components using 3D printing was the need to produce simple electronics. Basic structures such as fully printed capacitors, resistors and inductors have been demonstrated in the literature [209], [210]. Early works were fabricating those devices with a single conductive material such as copper-based filaments and conductive PLA composites. More complex devices are also possible with multi-material printing such as antennas, transistors, diodes, sensors, interconnects, supercapacitors, batteries and microelectromechanical (MEM) devices [211]–[220]. Many researchers have explored 3D printing techniques to form smart and intelligent devices such as electronic dice, wearable health monitoring systems, sensing

gloves etc. Figure 2.8 presents some of the devices fabricated using 3D printing techniques.

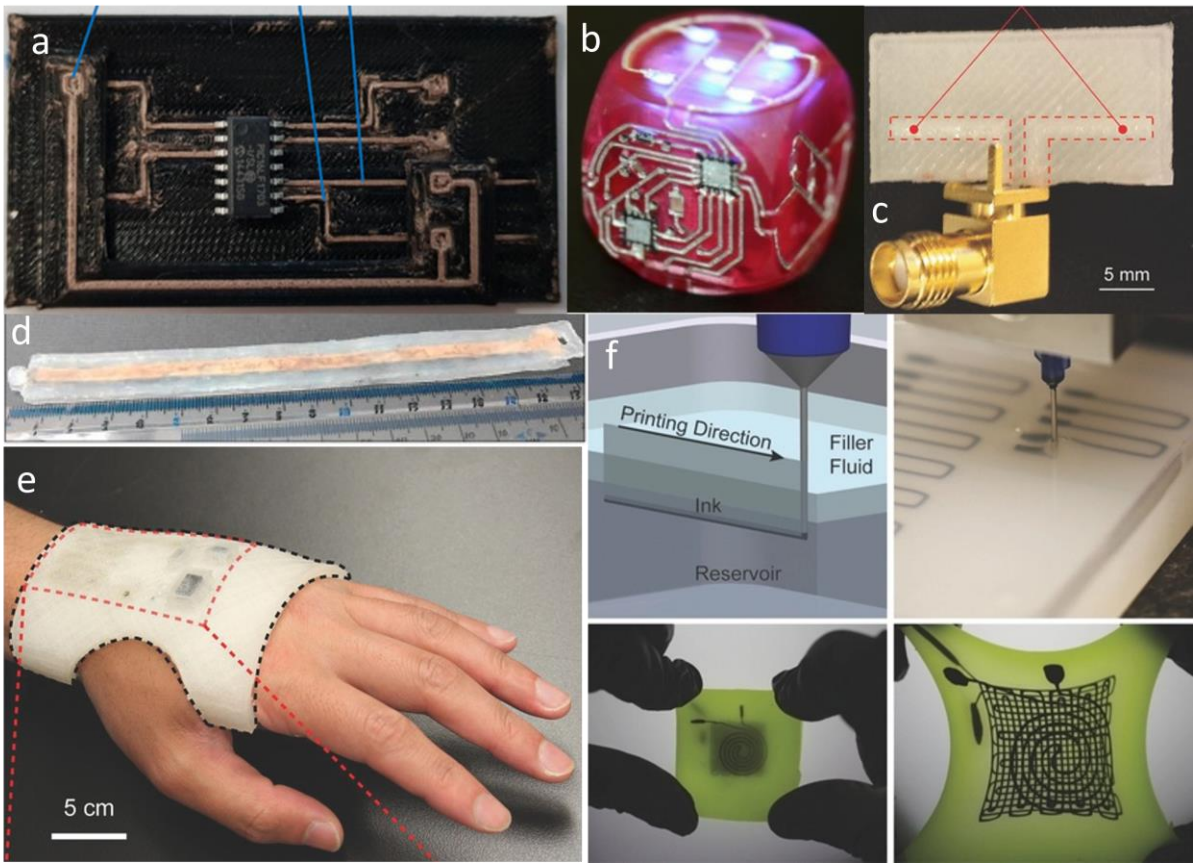

Figure 2.8 Examples of 3D printing used to make smart and intelligent structures.

a) 3D printed interconnects using conductive filament on flexible 3D printed substrate. [217] b) 3D printed rechargeable dice. [221] Copyright © 2014, IEEE c) Galinstan-based 3D printed dipole antenna. [219] Reprinted with permission from John Wiley & Sons Copyright © 2016, John Wiley and Sons d) Flexible 3D printed supercapacitor for wearable energy storage. [222] e) Smart glove with integrated liquid-state printed components and interconnects with IC chips in all three dimensions, various orientations, and multiple printing layers, delivering personalised system-level functionalities. [219] Reprinted with permission from John Wiley & Sons Copyright © 2016, John Wiley and Sons f) Embedded 3D printing process and realisation of a planar array of soft sensors and for strain measurements [223] Reprinted with permission from John Wiley & Sons Copyright © 2014.

3D printing manufacturing provides new freedom to fabricating soft functional materials. It can produce soft electronics that combine many fabrication techniques such as DIW with conductive and dielectric elastomers, while FDM can be used for packaging. With additional tools such as pick and place of surface-mount electronic components, 3D printers are a very attractive proposal for automation and industrial adaptation. Both passive and active electrical components are easily integrated to produce the desired electronic, sensing, communication and other parts required based on the desired application. Once

the electronic components are placed, they can be interconnected via printed conductive traces (either filaments or pastes). This can yield soft electronic devices that can find applications in a variety of areas such as wearables, soft robotics and biomedical devices [224].

For example, an electronic circuit was 3D printed using pick and place by suction, for the electronic components, and AgTPU material for the electric traces [224]. This resulted in a functional LED array able to be wrapped around a human finger. Moreover, 3D interdigitated micro-batteries were able to be fabricated by printing concentrated lithium oxide based ink using DIW [225]. DIW was also used with multiple materials to make a flexible supercapacitor. The materials were mounted on syringes and contained silicone paste, Ag paste, activated carbon particles and a gel electrolyte [222]. Ceramic materials can also be printed using AM techniques. Specifically, researchers were able to print an electrode membrane assembly (PEMA) prepared by depositing ceramic-polymer electrolytes directly over $LiFePO_4$ [226].

2.5.2.2 3D printed tactile sensors

AM techniques play a significant role in the advancement of sensing used for robotic applications. More and more works have explored the use of 3D printing for sensing modalities. These include, but are not limited to, strain, pressure, vibration and temperature [227]–[233].

Early 3D printed works for tactile sensors relied on embedding prefabricated or off-the-shelf tactile sensors and placing them in cavities of the 3D printing structure and printing on top of them in order to embed the sensing devices. Researchers have used 3D printers and were able to produce tactile sensors for anthropomorphic hands, insoles and grippers [234]. Some of the most common tactile sensors placed in cavities and embedded in devices are strain and pressure sensors such as Force Sensitive Resistors (FSR), capacitive sensor arrays and temperature sensors. Some works have also embedded the accompanying electronic components needed for measuring the sensor output, resulting in a standalone device.

Only recently, with the use of multi-printing materials, do we see a rise of intrinsic tactile sensors using 3D printing techniques. With the development of more sophisticated 3D printers, able to 3D print different materials, more complex designs can be realised. As an example, a multi-material and multi-nozzle 3D printer was able to print different rubber materials, with different young's modulus, in one print, resulting in a soft pneumatic actuated multilegged robot [235]. These advancements in 3D printing tools also have an impact on the fabrication of more intrinsic tactile sensors. For example, researchers were able to 3D print embedded sensors in a soft gripper finger utilising a DIW process. They made a curvature sensor, inflation sensor and a contact sensor in the finger using resistive based ink. The sensor ink is a conductive ionogel composed of the organic ionic liquid 1-ethyl-3-methylimidazolium ethyl sulfate (EMIM-ES) filled with fumed silica particles, which serve as a rheology modifier [236]. Furthermore, researchers were able to print stretchable tactile sensors using a combination of nanocomposite ink. The ink was derived by mixing submicrometer-sized silver particles within a highly stretchable silicone elastomer to form a resistive based sensor with compressive gauge factor of 180 [237]. Capacitive-based 3D printed sensors are also reported in the literature. Specifically, the most common capacitive-based 3D printed sensors use only the FDM approach with TPU filaments for dielectric and conductive TPU composites to form the electrodes [238]. Similarly, an integrated wearable resistive sensor array was fabricated with coaxial extrusion 3D printing for simultaneous pressure and direction sensing capabilities. The conductive material used was a conductive carbon grease, in the inner core of the printed trace, and the outer shell of the trace is a SE 1700 adhesive as the encapsulation layer resulting in a fibre formation. A capacitive sensor was formed as a row/column structure exhibiting a maximum sensitivity of 0.56 kPa^{-1} [239]. Table 2.4 compares different 3D printed tactile sensors developed recently.

Table 2.4 3D printed tactile sensing devices developed recently.

TRANSDUCTION METHOD	*MATERIALS*	*SENSITIVITY*	*RANGE*	*REF.*
CAPACITIVE	Carbon grease – adhesive	$0.56kPa^{-1}$ <2kPa	Up to 15kPa	[239]
RESISTIVE	Conductive ionogel	~25Ω/kPa	100 kPa	[236]
PIEZORESISTIVE	Silver particles/silicone elastomer composite	180 gauge factor	250kPa	[237]
RESISTIVE & CAPACITIVE	Ionically conductive ink composite/silicone	0.348 gauge factor	-	[240]
RESISTIVE	Carbon conductive grease	3.8 gauge factor	-	[223]
CAPACITIVE	Co-hydrogel, Aam/PEGDA and photo-initiator	$0.84kPa^{-1}$	3kPa	[241]
RESISTIVE	(TPU)/MWCNT filaments	1.5-3 gauge factor	-	[242]
CAPACITIVE	Carbon Black Ecoflex composite/Ecoflex BTO-Ecoflex substrate	-0.4 at 100% strain	100% strain	[243]
CAPACITIVE	Conductive hydrogel/polyethylene	$0.45kPa^{-1}$	1kPa	[244]

Most studies have presented 3D printed tactile sensors often in isolation or at best used as wearable applications. Figure 2.9 showcases the most recent works based on 3D printing sensors in the literature.

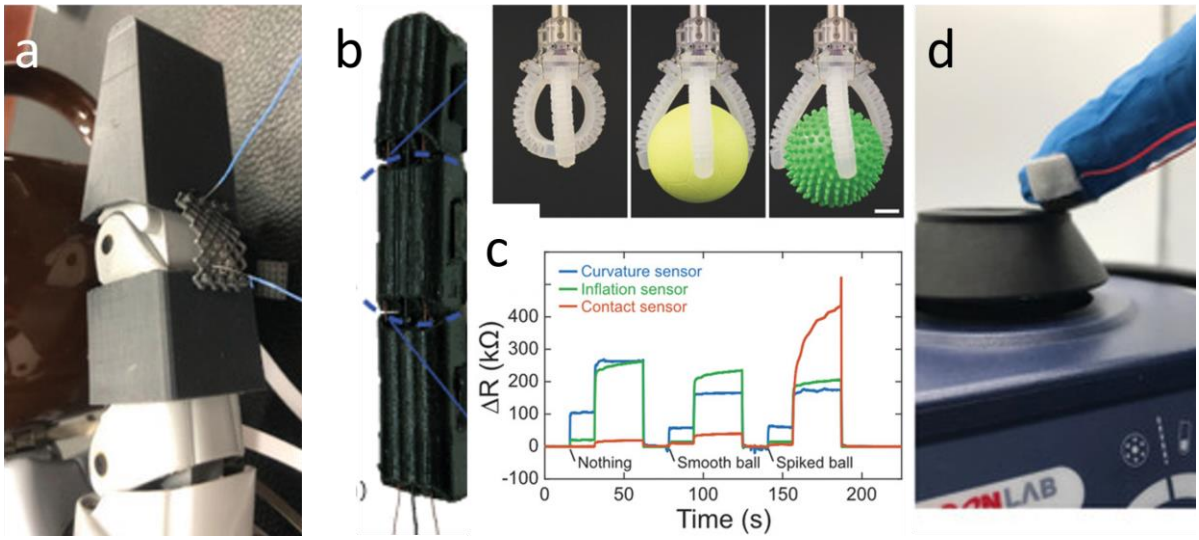

Figure 2.9 3D printed sensors recently developed.

a) 3D printed wearable Piezoresistive strain and tactile sensor on a robotic finger [245] Reprinted with permission from John Wiley & Sons Copyright © 2021. b) 3D printed finger with embedded strain sensors [246] Copyright © 2020, IEEE. c) Image showing a gripper holding nothing, a small ball, and a spiked ball [236] Reprinted with permission from John Wiley & Sons Copyright © 2018.

d) Stretchable piezoresistive sensor detecting dynamic vibration [247]. Reprinted with permission from John Wiley & Sons Copyright © 2018

The vast majority fail to present works with intrinsic use in robotic/prosthetic applications. One of the most common problems in the integration of 3D printing sensors and robotic parts is the combination of traditional FDM processes for making robotic parts and DIW processes for sensors. Often, to work, anthropomorphic robotic hands it requires complex large parts leaving, little to no space for embedded sensors and wiring.

2.6 Summary

The field of smart structures and robotics has progressed significantly over the last few years, with advancements in fabrication strategies, materials, and morphology. Pressure sensors have moved beyond fragile and rigid components that require multiple fabrication steps with manual alignment. With the introduction of organic-based materials, sensors and electronic devices are now soft, bendable and/or flexible. This brings robotics, prostheses, wearables and health monitoring systems to the next generation of devices, combined with the advancement of IoT technology and AI. Now, AM techniques have contributed to the formation of even more complex designs, materials, and unique structures, in the forefront of innovation.

This chapter initially outlined human skin modalities and transduction methods. Transducing methods used to realise artificial tactile sensors have been presented with their advantages and disadvantages, followed by materials and fabrication methods used to make them. Lastly, Additive Manufacturing has been introduced. A brief description of the different AM technologies, such as laser-based 3D printing and extrusion-based 3D printing, has been presented. 3D printing smart structures using novel composite materials have been included along with their unique realisation processes. 3D printing sensors using this novel fabrication processes have been presented and compared.

Even though tactile sensing and Eskins have been explored extensively, there is an unexplored potential for the use of 3D printing and tactile sensing for robotic

applications, novel materials, morphology, wiring and packaging. These well-known issues, where other fabrication processes are unable to provide solution, can be addressed with 3D printing. The following text presents a step towards this.

Chapter 3: Design of sensors, end-effectors, and peripherals

3.1 Introduction

Intrinsic or tightly integrated sensing, actuation, energy harvesting & storage, and computation into 3D structures could enable a new generation of truly smart and complex systems such as robots that have human-like dexterity, motor skills, and physical abilities that rely on feedback provided by specialised receptors in the body [248]–[250]. The field of robotics has strived to replicate human-like capabilities using large-area Eskins artificial muscles, computing devices, etc [251], [252] and are often placed on the external surface of the robot's body. These robots, however, often fail to execute intricate tasks that are easily conducted by humans. They also cannot be effectively used as current arrangements do not allow the synergistic working of sensors, actuation, and computation, such as the arrangements that exist in humans. To properly explore their full potential, next-generation robots require soft sensors embedded in the body to provide distributed touch and haptic feedback. This chapter presents a new approach to address the aforementioned issues, discussed in the literature, by intrinsically embedding sensors and electronics, developing 3D printed robotic/prosthetic parts that are robust, stable, and affordable.

Specifically, in this chapter a robotic end-effector with intrinsic tactile sensing fingertips and embedded read-out circuit is presented. The robotic part has also attached photovoltaic cells that are able to power the electronics and are covered with 3D printed transparent material for protection. The cells can also be used for proximity sensing. Finally, here an insole device with intrinsic sensing is also presented using this new methodology to further validate the approach and showcase the robustness of the devices.

3.2 3D printed Robotic Hand

This section, a robotic hand and wrist are presented with their mechanical and electronic parts. The overall design can be seen in figure 3.1. The hand resembles a five-fingered human-like hand with the thumb having two Degrees-of-Actuation (DoA) and 2 Degrees-of-Freedom (DoF). The rest of the fingers have 1 DoA and 3 DoF.

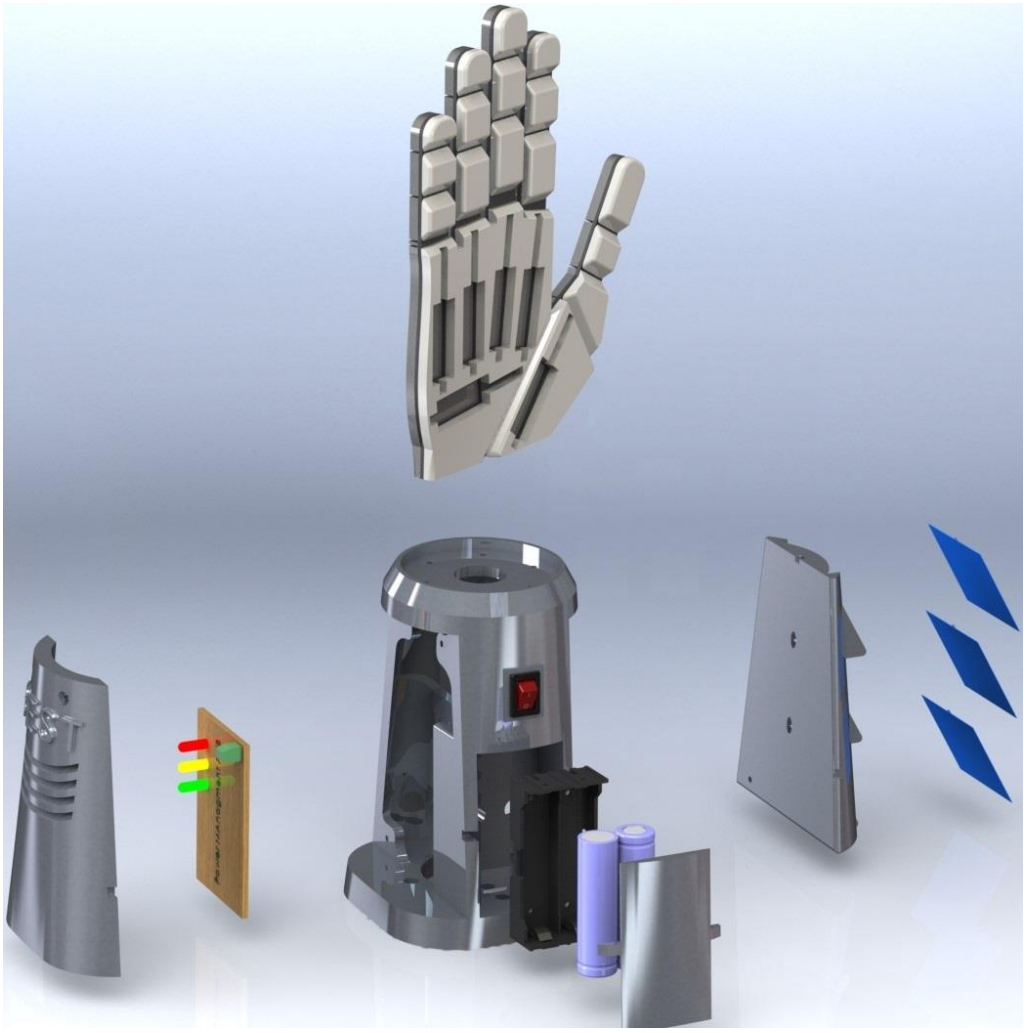

Figure 3.1 Overview of the Robotic hand/wrist.

Table 1.1 presents all the components found on the robotic hand and wrist including the electronics.

Table 3.1 Robotic Hand's Components

Component	Description	Amount
	Hand Parts	

Linear actuators	PQ12-63-6-R	6
Flex wires	Tendons	6
Nuts	M5	3
Bolts	M5	3
3D printing hand	Mechanical 3D printed structure	1
Wrist part		
Battery holder	Double 18650 Lithium Battery Holder	1
3D printed pieces	Wrist, Left & Right covers, Battery cover	4
Photovoltaic panel	193852 Monocrystalline Solar Cell, RSC-M125XL, Conrad	3
Battery	18650 Lithium Battery	2
Bolts	M3	4
Nuts	M3	4
Rocker Switch	Double Pole Single Throw (RS)	1
Power Management PCB		
MCU	PIC16F684E/P	1
Resistors	Various resistors for circuit operation	8
LED	green, yellow, red LED for power level monitoring	3
Diode	Voltage drop	2
Capacitors	Various capacitors	5
Inductor	22mH	1
Control PCB		
MCU	PIC16F88-E/P	1
Capacitors	Stabilising the signal	2
Diode	Voltage drop	1
Bluetooth	DSD TECH HM-10 Bluetooth 4.0 BLE iBeacon UART Module	1

3.2.1 Design of the robotic hand

The robotic hand was a collaborative effort between me and Dr. William Navaraj. The 3D printed hand was designed to utilize the capabilities of multimaterial 3D printing offered by state-of-the-art 3D printers with a layered architecture to ensure easy printability without requirements for any support structure. The palm area of the hand has six slots for six PQ12-63-6-R microlinear actuators (two actuators for the thumb and four for the rest of the fingers). The hand was fabricated using three different 3D printing materials (Figure 3.2). The hand is segmented into three sections: bottom, middle, and top, and was printed in a layered fashion. The first layer is PLA (of 4 mm thickness) followed by a second layer of ABS (1 mm thickness). The adhesion between ABS and TPU is much higher

than TPU and PLA. Hence, the thin layer of ABS was used, followed by the TPU which forms the third layer. This is followed by a fourth layer of ABS, lastly the final layer was a PLA material. The multimaterial printing was possible as the printer used has the capability to print three materials from its three nozzles. This layered arrangement utilizes the rigidity of PLA/ABS as a skeletal support structure, whereas the elasticity of TPU is used to achieve flexion for the fingers' joints. The fingers are actuated via a tendon mechanism. The tendons were connected to the distal phalanges and were pulled through slots in the hand via microlinear actuators to achieve the desired flexion. During extension, the linear actuator is released, and the joints get back to the normal state as the TPU reverses back from its elastic deformed bent state. This structure can be classified as an adaptive under-actuated tendon mechanism where the fingers can bend easily with a single actuator used by each finger. Furthermore, the phalanges have been designed with gaps to embed the electronics related to intrinsic touch sensors.

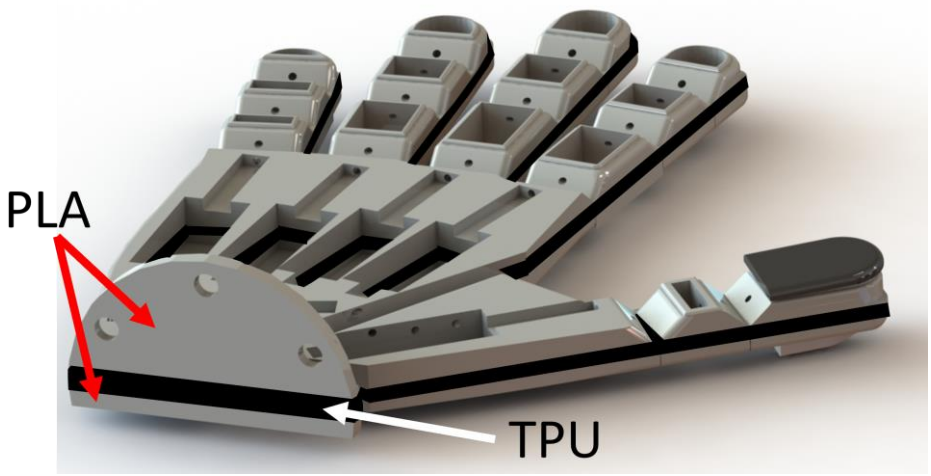

Figure 3.2 The 3D printed hand
CAD design of the hand with the smart sensing phalanx. [253].

3.2.2 Design of the wrist

The wrist has a cylindrical-based shape with an average diameter of 100 mm and total a height of 170 mm. The wrist is segmented into 4 total bodies: Core structure, left and right cover and the battery door cover. The wrist is housing all the necessary electronics for the proper operation of the hand. At the front of the

wrist, a cavity is located for housing two 18650 Lithium-Ion batteries. The output of the batteries is connected to a rocker switch and from the switch a PCB is powering the motors and the rest of the electronic components. The right side of the wrist was designed for mounting the 3 solar panels at an angle of 60^{o}. The left side of the wrist is housing the PCB used for controlling the hand. The bottom of the wrist has a cylindrically shaped cavity for further integration to robotic arms. Figure 3.3 shows the entire integrated system.

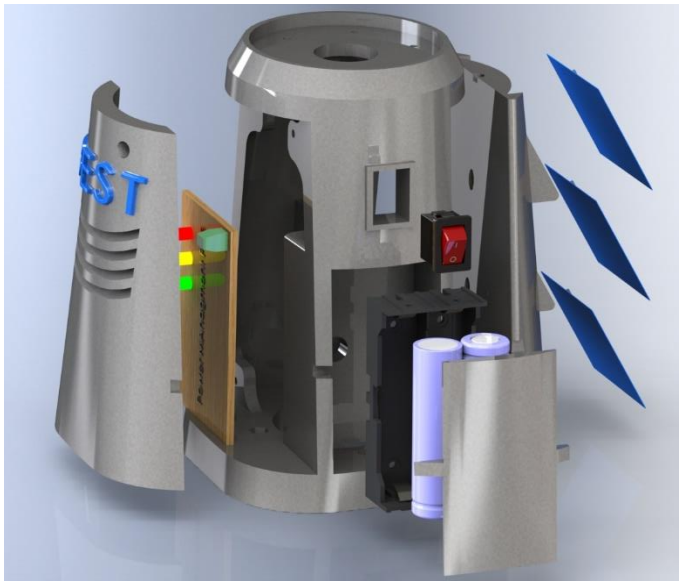

Figure 3.3 Robotic Wrist

3.3 Tactile Sensors

3D printing is widely used as a quick way to transform a design concept to the physical world. The field of AM allows printing of several types of polymers, including soft and bendable materials. While 3D printing allows an easy way to develop complex mechanical 3D structures, it does not inherently allow these mechanical parts to have any sensing capabilities. However, in applications such as robotics and prosthetics, 3D printed structures with sensory capability are much needed [254].

3.3.1 Embedded capacitive sensors for robotic hands

3.3.1.1 3D printed Phalanx with embedded pressure sensor

This part is adapted from:

M. Ntagios, W.T. Navaraj, R. Dahiya, "3D Printed Phalanx Packaged with Embedded Pressure Sensor", IEEE Sensors Conference, 2018, Copyright © 2018, IEEE.

This part of the thesis presents an early adaptation for using 3D printing method to develop a robotic finger with embedded capacitive touch sensors. The concept has been demonstrated by designing and printing the distal phalanx of a finger with soft material.

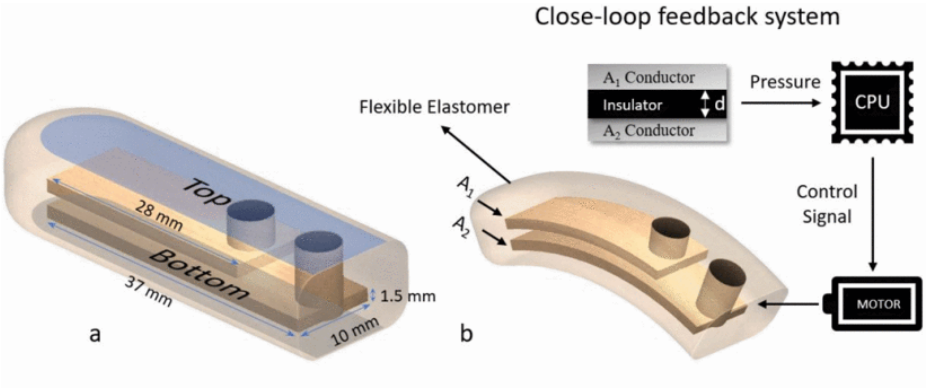

Figure 3.4 (a) CAD design of the distal phalanx. (b) Phalanx in a bending condition. [254] **Copyright © 2018, IEEE**

The finger design closely resembles the average prosthetic distal phalanx of the human index finger with dimensions of 48mm ×16mm ×10mm. The phalanx structure is designed to have two cavities, which, when filled with conductive materials, lead to the formation of a parallel plate capacitor inside the phalanx. These cavities are designed and located at the bottom half of the device with each of them being 1.5 mm thick and 10 mm wide. The bottom cavity is 28 mm long and the top cavity is 37 mm, as shown in figure 3.4. The separation between the cavities is 200 μm, which defines the thickness of the dielectric material between the two plates of the embedded capacitor. The two holes at the one end of the phalanx allow access to the two cavities and these are plugged after filling up the cavities with conductive materials.

3.3.1.2 Robotic Hands with Intrinsic Tactile Sensing via 3D Printed Soft Pressure Sensors

As the previous study showed promising early results. As a next step, a thorough investigation of the 3D printing approach was conducted. 3D printing could also

be used for the deposition of the electrodes for a higher level of autonomous fabrication. The packaging and the transducer part can be fabricated simultaneously in the fingertips of the robotic hand. To this extent, this section describes the development of a complex 3D intelligent structure using innovative designs and multimaterial additive manufacturing technology. The distal phalanges of the 3D printed thumb presented herein have inherent soft capacitive sensor and embedded electronics. Figure 3.5 presents the intelligent fingertip with the embedded electronics and sensor tightly integrated into the distal phalanx of a robotic hand showcased for the first time.

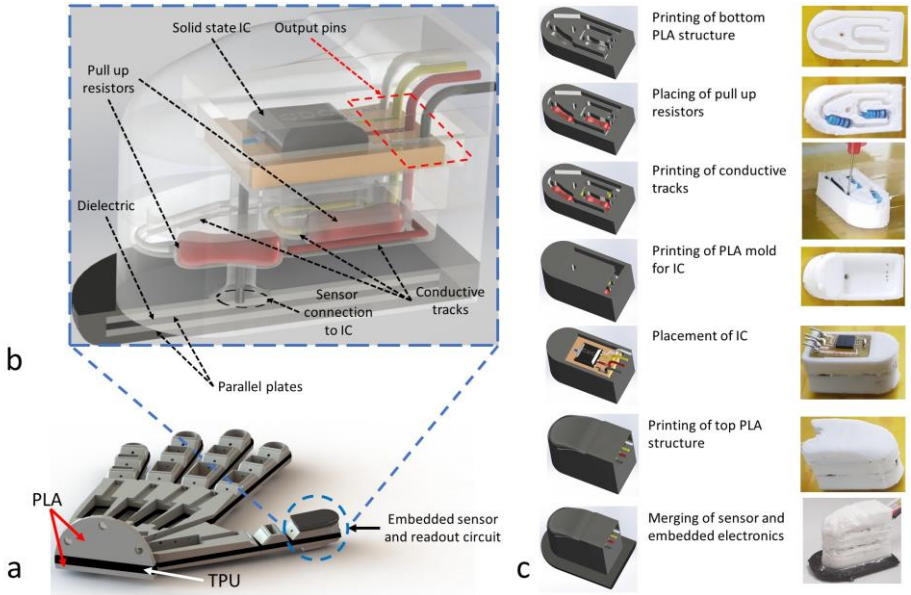

Figure 3.5 The 3D printed hand with intrinsic tactile sensing

a) CAD design of the hand with the smart sensing phalanx having a soft capacitive touch sensor and an embedded readout circuit. b) CAD design of the interior structure of the phalanx. c) Fabrication steps for the 3D printed phalanx.[253]

For the capacitive sensor, TPU and two-part rubber (Ecoflex) are used as dielectric materials. Silver paint, conductive PLA composite and a graphite ink, are used as electrodes of the capacitive structure and explored to develop five different variants of the sensors using a modified 3D printer, which is capable of extruding conductive ink, metal paste, and polymers, presented in section 6.1.

The full design of the intrinsic touch sensor is shown in Figure 3.6a. The simple design makes it easy to fabricate the embedded capacitive pressure-sensing phalanx using the different combinations of materials. In some way, the architecture of the phalanx imitates the human distal phalanx which consists of

the bone with soft tissue and skin. The design resembles this pattern with a rigid base made from black PLA, the conductive and the dielectric elements mimicking the soft tissue, and the top layer of the TPU 3D printing filament (Young's modulus of 12 MPa) resembles the elastic properties of the human skin with Young's modulus of 5–20 MPa [255]. The embedded capacitive pressure-sensing phalanx has two computer-aided design (CAD) model variations to compensate for the different fabrication techniques required for the two dielectric materials.

The embedded capacitive pressure sensor is 19.6 mm wide, 2.6 mm thick, and 28 mm high. The phalanx structure has five parts: base structure, bottom electrode, dielectric, top electrode, and top polymer layer. A mould for the bottom electrode is designed on top of the base structure and filled with the conductive material for the formation of the capacitive sensor. Each electrode is 14 mm wide, 0.5 mm thick, and 19.2 mm high. The distance between the bottom electrode and the surrounding walls of the base structure is 0.3 mm. Similar to the bottom electrode, the top electrode has a separation distance of 0.3 mm from the surrounding walls. This offset/gap prevents the 3D printer nozzles from colliding into the existing fabricated structure during printing. There are two access points in the 3D printed phalanx, one for each electrode of the capacitive-sensing element. The overlapping surface area of the two parallel plates is 250 mm^2 and the dielectric thickness between them is 0.5 mm. Figure 3.6b shows the fabrication processes of the two variations and the performance of the system is presented in the section 5.3.2.

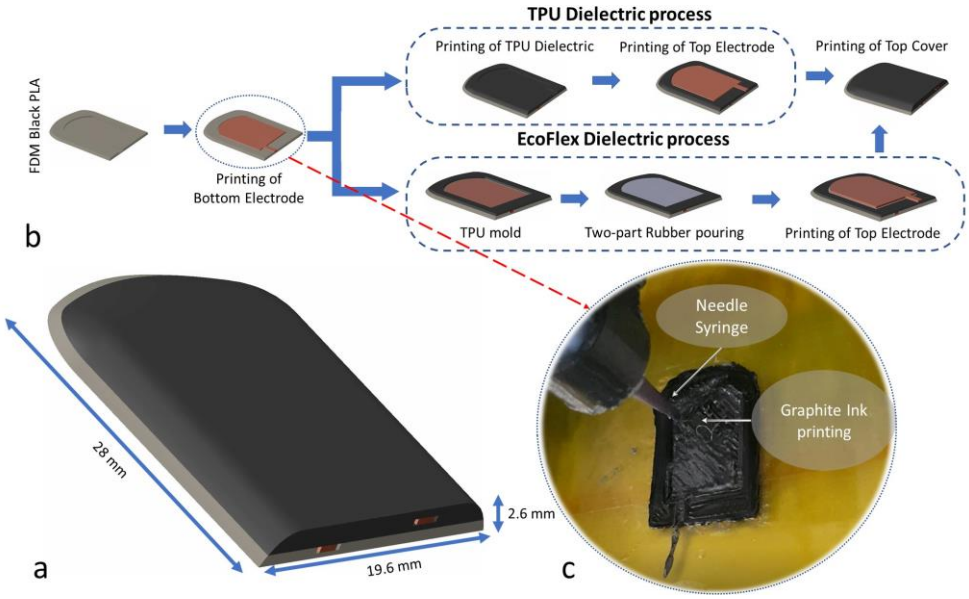

Figure 3.6 Design of intrinsic capacitive fingertip.

Capacitive pressure-sensing part of the phalanx showing a) the complete structure of the phalanx, b) the fabrication procedure of the TPU and two-part rubber dielectric, and c) the graphite ink printing using the modified desktop 3D printer capable of cold extrusion.[253]

3.3.1.3 Increasing Resolution

This part is adapted from:

M. Ntagios, P. Escobedo, R. Dahiya, "3D Printed Robotic Hand with Embedded Touch Sensors", IEEE Flexible and Printable Sensors and Systems Conference, 2020, Copyright © 2020, IEEE

Besides the amount of applied force to a fingertip, tactile systems require also the need to understand the point of contact. To this end, the following expands the previous work by increasing the number of sensors for locating the point of contact of a force exerted to the fingertip. The touch or pressure sensors were fabricated by 3D printed electrodes using copper-based conductive filament and a two part-rubber as the dielectric. The sensitive fingertip was tested with dynamic and static stimuli, explained in section 5.3.3.

The thumb fingertip has two soft embedded capacitive pressure sensors, used as a feedback system to understand the distribution of an applied force on top of the distal phalanx of a robotic hand (Figure 3.7). The sensing phalanx resembles the human fingertip of the thumb with two soft capacitive sensors located inside, as

shown in Figure 3.7b. The entire device is 20 mm wide, 30 mm long and 8.3 mm thick. The overlapping areas of the parallel capacitive sensors are 163.24 mm^2 with a dielectric thickness of 1 mm. The capacitive sensors have a 2.5 mm distance between them and are located at 5.8 mm depth inside the highest point of the fingertip. The parallel plates are 0.5 mm thick with an offset of 0.25 mm from the walls of the designated cavities to eliminate the chances of bridging with each other during the fabrication process.

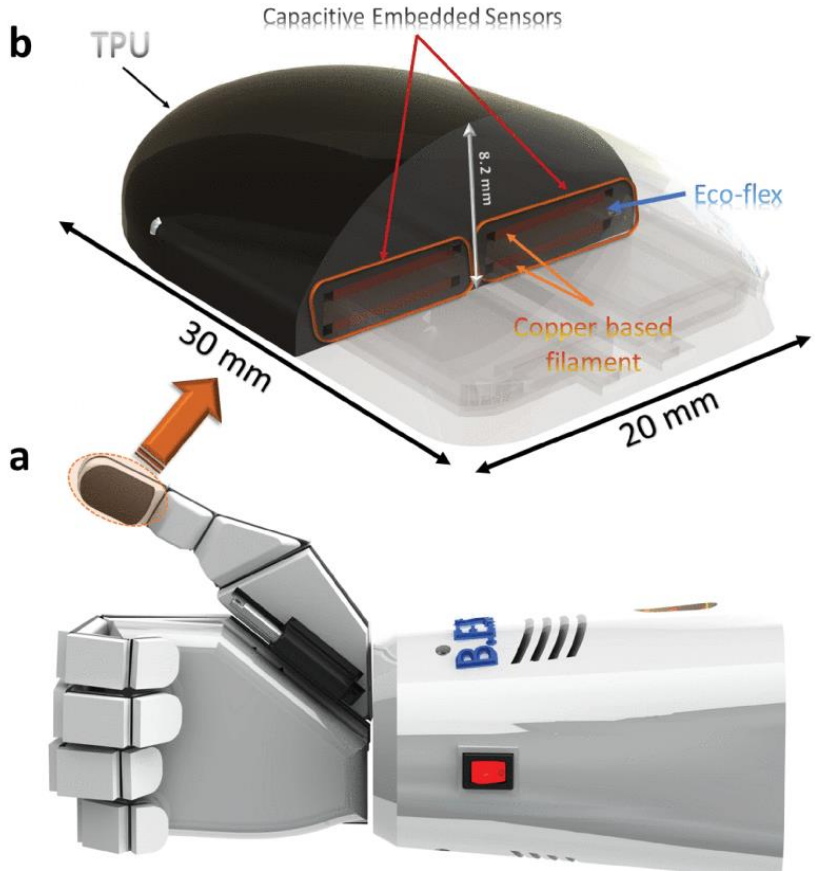

Figure 3.7 a) CAD Design of robotic hand with fingertip having embedded soft capacitive sensors. b) Cross-Sectional view of the soft sensing fingertip. [256] **Copyright © 2020, IEEE**

3.3.2 Intrinsic tactile sensors for gait analysis

To further showcase the adaptability/flexibility and robustness of multimaterial 3D printing, a 3D printed soft and flexible insole with intrinsic sensing capabilities is presented. A soft, flexible, and low-cost capacitive pressure-sensitive insole developed using resource-efficient single-step 3D printing method, is presented. The insole is developed using elastomeric materials with the soft and robust sensors that can bend and twist without altering its performance. The insole is

designed to have four sensing zones to capture the pressure information from the entire contact area.

The device was designed to resemble a human foot using state-of-the-art CAD software. The size of the insole resembles a size 4 UK shoe. The limiting factor to the insole design was the build area of the used 3D printer (Ultimaker S5). The insole's design was done to accommodate four embedded pressure sensors. The four sensors are capacitive pressure sensors fabricated with two different techniques - 3D printing and drop-casting. A total of 8 holes are designed at the side of each capacitive plate, for the wire bonding, while the device was entirely fabricated using the 3D printer without the need of any other fabrication tool.

The insole is 225mm long from heel to toe, from side to side it is 87 mm long and the thickness is 10.5mm. Each electrode has thickness of 1.4mm and the dielectric has thickness of 4mm. The toe sensor covers an area of 3,356 mm^2, the left and right sensors cover an area of 2,855 mm^2 and 2,482 mm^2 respectively and the heel sensor covers about 2,100 mm^2. Figure 3.8 presents the design and dimensions of the sensorised insole for anthropomorphic robotic and wearable systems. The characterization results can be found in the following section 5.4.

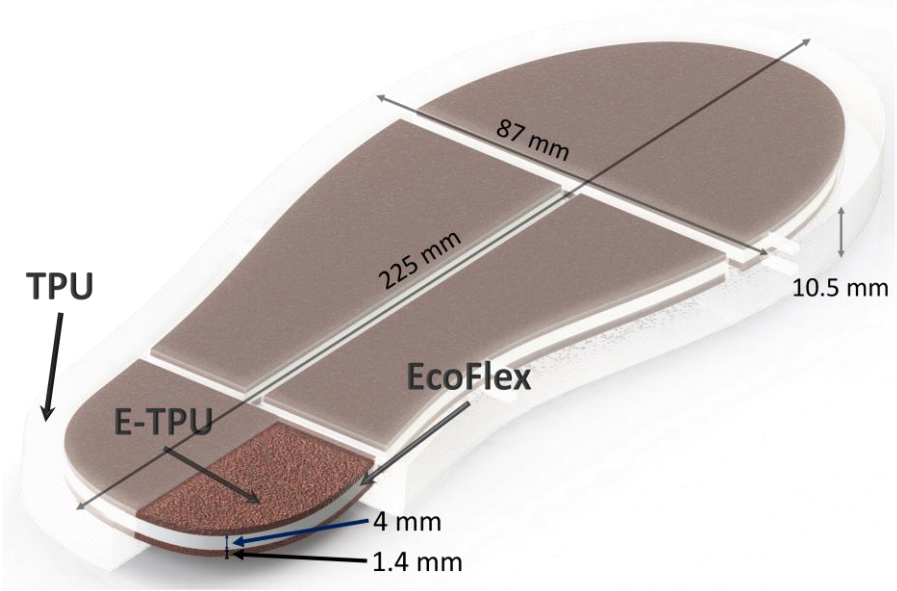

Figure 3.8 View of the internal structure of the sensorised pressure sensor insole for anthropomorphic robotics[257]

3.3.3 Packaging of piezoresistive tactile sensors

As capacitive readout electronics require relatively long time to read the capacitive value, a piezoresistive device and electronic components were embedded in the distal phalanx of the thumb for faster response. Piezoresistive sensors are ideal for vibration conditions as they can read faster than capacitive readouts.

Here a fabricated piezoelectric sensor for vibrotactile feedback for robotic/prosthesis is present. The sensor was provided from Dr. Oliver Ozioko as a collaborative work towards enhancing tactile sensing in robotics [258]. The fabricated sensing layer was systematically embedded in a fingertip. Figure 3.9 shows the scheme utilized for embedding one of the soft piezoresistive sensors into the fingertip of the 3D-printed hand as a proof of concept. First, a CAD model (Figure 3.9a1,a2) of the required fingertip was designed to fit into the custom 3D-printed hand. The CAD model was designed to fit into the cavities of the distal phalanx of the thumb (Part A). In the interior of the design, channels connecting to the basic electronic components required for reading the resistance value of the sensor, are located. The piezoresistive sensor (Figure 3.9a3) was encapsulated by the second part of the model (part B). The designed models for part A and part B were then printed separately with rigid and soft materials, respectively (Figure 3.9a1,a2). Part A was printed with PLA using a nozzle of 0.4 mm diameter, 100% infill, and 0.1 mm layer height. The nozzle and the heated bed temperatures were 200 and 60 °C, respectively. In the core of part A (Figure 3.9a1), there is a cavity designed for embedding a resistor that is needed to read the value of the piezoresistive pressure sensor. To achieve this, the Gcode was modified to pause the print around the 100th layer. At this point, the resistor was placed in the cavity and the printing was resumed.

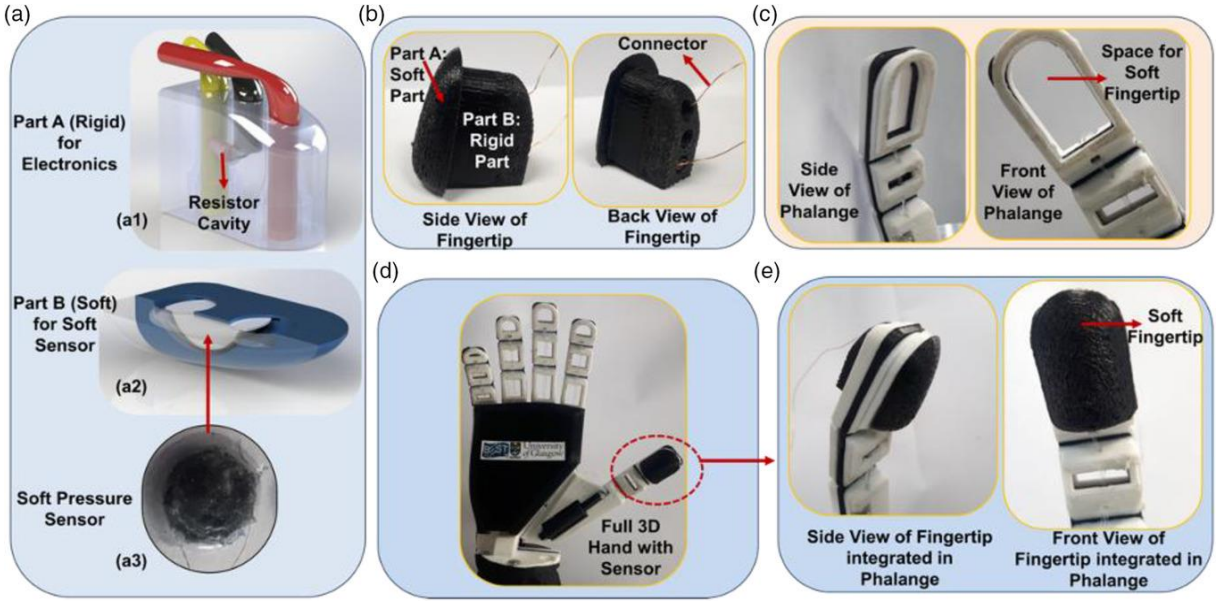

Figure 3.9 Embedded piezoresistive tactile sensor

a) 3D Model of the fingertip and soft piezoresistive sensor; b) the fabricated 3D-printed fingertip with embedded sensor; c) Phalange of the custom 3D-printed hand with provision for integrating the sensorised fingertip; d) full custom 3D-printed hand with the sensorised fingertip attached; e) zoom in of the integrated fingertip. [258]

Part B (Figure 3.9a2) was printed with TPU (NinjaFlex, NinjaTech) at a temperature of 235 °C with a 60% infill. TPU is a flexible elastomer highly suitable for replicating the stiffness and elasticity of the skin. In this case, the GCode was also modified to pause at the 27th layer for the placement of the sensor. After embedding the sensor, the printing flow rate was tuned from 100% to 99% to reduce the infill line width to further improve the compressibility. Finally, the two parts were glued together with Epoxy and attached to the robotic hand (Figure 3.9e).

3.4 Robotic hand with embedded sensors and energy harvesting capabilities

This section was adopted from:

M. Ntagios, P. Escobeto, R. Dahiya, "3D printed packaging of photovoltaic cells for energy autonomous embedded sensors" IEEE Sensors Conference,2020, Copyright © 2020, IEEE

Prosthetic and robotic systems require an extensive amount of energy to operate. Motors and electronic components draw considerable amount of power. In the case of powered prosthesis, batteries have a limited time of operation, usually around an hour before the batteries are depleted. The current battery technology is not sufficient for use in prosthesis, in a practical manner. Energy density and capacity are not up to the task for a prosthetic hand to be used consistently as batteries need to be changed constantly and add to the prosthesis weight.

To ensure that the sensing, actuating, and computing units on such devices are powered for a significant amount of time, the robotic hand designed in the previous section 3.2 was integrated with photovoltaics. Photovoltaics emerge as the most suitable solution due to energy harvesting capabilities, as they can generate power for the various sensing/electronic components in robotics and other related applications. Solar cells are also the optimum solution for prosthetics/robotics due to their low weight. The lightweight, fewer parts and the ease of implementation of such devices are extremely attractive for robotic applications. Unfortunately, the most efficient commercial solar cells are extremely fragile to be used with robots operating in an unstructured environment. They may break or crack due to impact if the robots collide with objects around. To prevent such undesirable situations, a packaging arrangement is necessary to protect the solar cells. In this regard, 3D printed package with transparent materials has been explored here.

An experimentation of 3D printed covers for solar cells and evaluate the effect of the printed structures on the performance of the photovoltaic device, is presented. Three 3D printed covers were fabricated with different thicknesses and tested to see the effect of the thickness of the material on the energy generated by the solar cells. The covers were 3D printed from a transparent PLA filament. All covers were printed with the same 3D printer and settings. From the results, we identify the trade-offs between thickness, structural integrity, and energy harvesting, and are presented in section 5.6. The system can be seen in Figure 3.10.

Figure 3.10 3D printed hand with Energy harvesting cells.

a) 3D printed robotic hand with three photovoltaic panels. b) 1mm thickness covers attached on the top to reduce wear and tear.[259] Copyright © 2020, IEEE

3.5 Summary

This chapter presented the design approach used in the development of smart systems with intrinsic sensors, embedded electronics and energy harvesting devices. Several sensors presented in this chapter are fabricated using AM techniques, while prefabricated sensors were also used and embedded in the robotic parts resulting in more robust and tightly integrated smart systems. The fabrication processes and performance of these systems can be seen in Chapter 5. The overarching goal is to develop smart systems with high complexity and 3D printing can facilitate the production process. This design approach can be expanded not only to robotic/prosthesis end-effectors but also to the overall anthropomorphic robotic bodies. Beyond robotic application, the design approach can be adapted in many other fields such as wearables, smart devices for IoT and healthcare to name but a few.

The following chapter describes the electronics used for these systems, thus covering the designing aspect of the smart structures developed throughout the thesis.

Chapter 4: Electronics and embedded electronics using 3D printing

4.1 Introduction

Different electronic circuits were designed and developed, to control the robotic system and read the tactile information from the various sensors. This chapter presents the electronic circuits used throughout the development of the systems in chapter 3. All electronic designs were made using Eagle (Autodesk) software, an electronic design automation software (EDA). As a first step, the schematics for the electronics were drawn, followed by the fabrication of the PCB.

4.2 Electronics and electronic components for robotic hands

The 3D printed robotic hand presented in section 3.2 has two PCBs, one for power management and another for controlling the hand's movement.

4.2.1 Power management unit

The first PCB developed for the robotic hand was a power management circuit. The robotic hand is using two lithium-ion batteries in series resulting in an input voltage of 8.4V (fully charged) to 7.4V (depleted). The robotic hand is actuated via six PQ12-63-6-R microlinear actuators requiring an input voltage of 6V. The PCB designed here, drops the voltage from the batteries to a constant 6V for high current operation, as the motors can draw, at worst case scenario, 3 Amps. To step down the voltage a step-down converter is used (LMR 14050, Texas Instruments). At the same time, a microcontroller (MCU) (PIC16F684) is used and powered by the batteries. A diode drops the 6V output of the step converter to 5.2V and powers the MCU. The MCU is responsible for monitoring the voltage level of the battery pack. Three LEDs are used and driven by the MCU for visual

indication. Figures 7.1 and 7.2 in the Appendix present the schematic and PCB layout of the power management module.

4.2.2 Controller PCB circuit

The output of the power management circuit is then connected to a second PCB. The output of the power management PCB is connected via pins to the motors' power lines. Meanwhile, a diode is also connected in series to the power line to drop once again the 6V input to a 5.2V output and powers a second MCU (PIC16F88). The MCU is responsible to drive the motors using 6 Pulse Width Modulation (PWM) pins. The MCU is also connected to a Bluetooth module and transfers data between the MCU and an external device (tablet/smartphone). Figures 7.3 and 7.4 in Appendix present the schematic and PCB layout of the control circuit.

4.3 Embedded electronics for intrinsic sensing devices

Electronic circuits often require a large amount of space, especially for complicated systems such as robotic hands. Dexterous robotic hands, especially, use a number of motors and mechanical parts to actuate their fingers, wrist, etc. Due to that, electronics need to be even more tightly integrated into the body of the robot. Towards that, this section presents a tightly packed readout circuit embedded in the distal phalanx of the thumb of the robotic finger in collaboration with Habib Nassar as collaborative effort towards 3D printed interconnects. The sensor, able to read pressure, is capacitive based and was presented in section 3.3.1.2. To read the capacitive value a Capacitive to Digital Converter (CDC) (AD7747, Analog Devices) was used. The Integrated Circuit (IC) can read data from one of the plates and the second can be grounded. The IC reads the capacitive value and transmits the data to a MCU via Inter-Integrated Circuit (I2C) communication protocol. The I2C protocol requires two pull-up resistors for the data and clock lines. The size of the fingertip allows to fit the CDC and pull-up resistor in a stacking configuration for vertical integration. The pull-up resistors are embedded between the CDC and the sensor. Vertical 3D printed conductive lines connect the IC with the pull-up resistors and sensor. The IC was, firstly, soldered on a small break-out PCB due to small size pads (0.25m). That was

necessary as 3D printing in such resolution was not possible. The breakout board has pins to connect the IC to the MCU. Figure 4.1 shows the schematic of the embedded circuit.

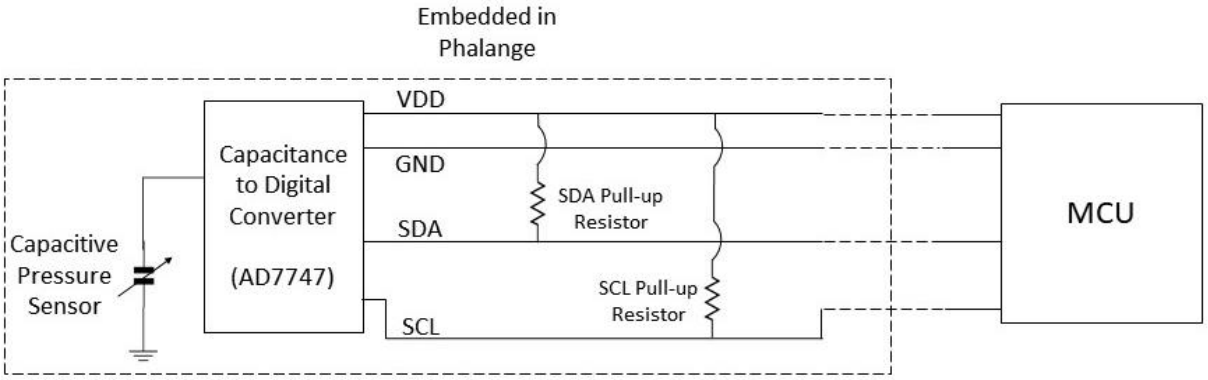

Figure 4.1 Schematic of embedded electronics in the robotic fingertip.[253]

4.4 Readout circuits for tactile sensors

4.4.1 Robotic hand capacitive sensors readout circuit

All capacitive sensors for the fingertips use similar readout circuits as explained above. As the thumb fingertip of the robotic hand has embedded the readout electronics the rest of the digits were measured using CDCs mounted on a PCB. The PCB was fabricated and assembled to demonstrate the capability of the variety of sensors, mounted on the hand. The schematic of the system and the fabricated PCB dedicated to the capacitive readout electronics is presented in figure 4.2. The system uses a microcontroller to communicate with several CDC ICs via I2C communication protocol, similar with the above section 4.3. An I2C multiplexer (MUX) is used to communicate with the several CDCs, due to the fact they have the same I2C address. This arrangement was done to expand to multiple sensing fingertips. The CDCs convert the capacitance value from the sensors to digital data and transmit back the data to the MCU. The microcontroller transits the data via Universal Asynchronous Receiver/Transmitter (UART) protocol to Universal Serial Bus (USB) converter. A Personal Computer (PC) receives the data and displays them on a LabVIEW program. The CDC converters have two inputs for capacitive sensors and can operate in a single-ended or differential mode.

In this thesis, both modes were used. The single-ended mode was used to read the values of the sensors in section 3.3.1.1. The differential mode was used for the work described in 3.3.1.2 as each fingertip has two embedded sensors and, in this way, it is used to estimate the contact point of the force without the need of a large array of sensors.

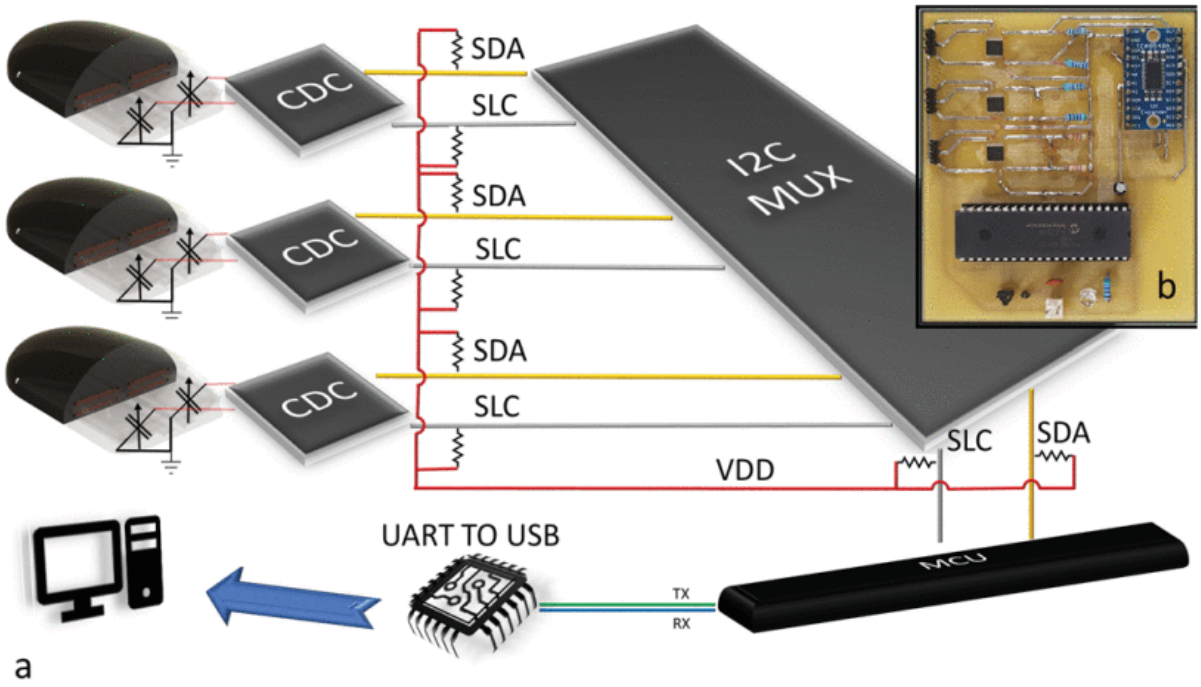

Figure 4.2 a) Schematic of the system b) Fabricated PCB for reading capacitance value and transmission of digital data. [256] **Copyright © 2020, IEEE**

4.4.2 Robotic hand piezoresistive sensor readout circuit

For the piezoresistive sensor presented in section 3.3.2, a simple voltage divider circuit was designed. The resistor used for the readout circuit was embedded, in a similar manner as the resistors in the previous section 4.3. The 3D printed fingertip with the piezoresistive sensor has three pins, as can be seen in figure 3.9a. One pin is connected to the ground, the second is for suppling 5V, and the third is the output of the voltage divider circuit. The output of the voltage divider is connected to an Analogue to digital converter of an MCU (Atmel SAM3X8E ARM Cortex-M3). The MCU is connected to a PC via a USB cable. A Graphical-User-Interface (GUI), based on LabVIEW, was designed to present the data captured by the MCU. Figure 7.5 in the Appendix shows the robotic hand with the sensorised fingertip being pressed while the data are presented in the LabVIEW GUI.

4.4.3 Insole electronic readout circuit

In section 3.3.2, an insole design was presented. Herein the electronics involved in reading the capacitive values, are presented, in a similar approach as the previous capacitive sensors. Once the device characterization was completed (see section 5.4), one of the tested devices was further used for feedback during walking. For this, the device was integrated with a CDC IC chip (FDC1004-4, Texas Instruments). The IC is connected to four capacitive sensors in a single ended configuration with grounded electrodes. The IC is connected to a microcontroller (Atmel SAM3X8E ARM Cortex-M3) using I2C communication protocol and the microcontroller is connected to a PC via a USB connector (Figure 4.3a). A custom-made C-sharp program (via visual studios) was made to represent the data captured from the IC as a GUI program. The GUI presents the data in two ways.

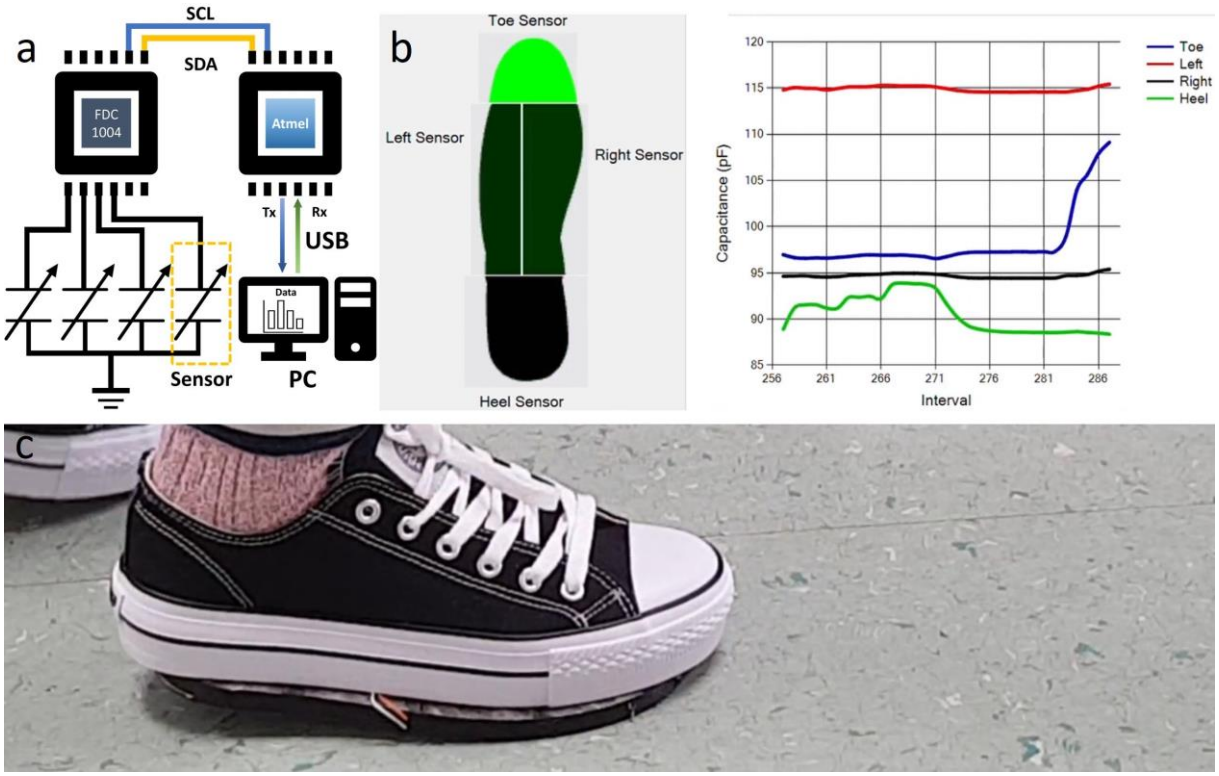

Figure 4.3 Demonstration of 3D printed insole under load.

a) electronic circuit schematic of the system. b) GUI created to represent the data received from the microcontroller. c) sensorised insole under load and connected to external electronics for capacitive measurement.

The GUI on the top left side of the screen has an insole shape image segmented in four parts that represent the area of the respected sensor. At the start, the image area is black and represents no pressure applied to the specific sensor. As

pressure increases, the pressed part of the insole starts to become green and, with an increase in pressure the intensity of the green color further increases. On the right is the graph displaying the capacitance for each sensor. The graph updates in real-time thus providing a better understanding of the history of each sensors' response. Figure 4.3b shows the GUI of the system and figure 4.3c is a snapshot of the device being pressured upon and the response is provided via the GUI.

4.5 Summary

Intelligent systems require numerous electronic components and sophisticated circuits to operate. Particularly, robotic systems with a high number of actuating parts leave electronic circuits limited space. As dexterous hands implement complex mechanical parts and many actuators, there is not enough space for the required electronics and readout circuits to be implemented with traditional techniques. Embedded electronics in the core structure of the robotic parts are essential for such systems. Embedding electronics and 3D printed interconnects using AM technique can provide the tools needed for utilising the available space located in the mechanical body of the robot. This approach can be expanded to other areas, not just robotics, such as food packaging for monitoring the quality of products, in pipelines with embedded electronics and sensors for monitoring flow and materials.

This chapter presented the electronics used in robotic systems, such as readout electronics for tactile sensors and the electronics involved with the robotic hand. Meanwhile, it presents the embedded electronics used for the development of smart and intrinsic tactile sensing fingertips.

Chapter 5: Packaging and Performance

5.1 Introduction

Multimaterial printing enables complex designs and structures to be fabricated in a layer-by-layer manner. This provides the designing tools to fabricate intrinsic and tightly integrated sensing, actuation, and computation into 3D structures for a new generation of devices and systems. The multimaterial 3D printing techniques, used in this thesis, offer advances over current AM strategies. Previous works have mainly focused on the printing of relatively thin and planar structures. Considering this, multimaterial printing for making tactile feedback mechanism for robotic hands with the embedded electronics and sensors in 3D space has not been explored in depth. The approach offers the ability to realize different types of structures without the need for expensive equipment, large-scale modifications, or expensive materials. AM allows for easily customizable designs and on-site/on-demand production while reducing material waste, energy consumption, and prototyping time. AM technique has the potential for simultaneous multimaterial printing of conductive or photosensitive materials and polymers, resulting in smart structures. This chapter presents the fabrication process and the performance of the systems described in chapter 3.

5.2 Fabrication of robotic parts and assembly

The robotic hand's design was presented in the above section 3.1. The robotic hand was printed with a CubePro Trio 3D printer (3D Systems), able to mount three different filaments. The printer has a large print volume (275mm x 265mm x 240mm) for printing relatively large structures. The printer was mounted with PLA, ABS and TPU filaments for the fabrication of the hand. The printing temperatures were 180 ^{o}C, 200 ^{o}C and 210 ^{o}C for PLA, ABS, TPU respectively. The entire structure was printed at 100% infill with layer height of 0.2mm.

The wrist of the hand was printed using Ultimaker S5 with a printing volume of 330mm x 240mm x 300mm. The printer has two nozzles for printing different materials, but for the wrist only one nozzle was used and was mounted with white PLA material. The printing temperature was set to 200^{o}C at 70mm/s speed with 15% infill resulting in approximately 20 hours print with a total weight of 300 g. The entire assembled system weighs less than 800g. This is an additive benefit of 3D printing as majority of robotic end-effectors weight usually above 1 kg and the data processing are done externally from the hand.

5.3 Realization and performance of sensorised fingertips

5.3.1 Fabrication and performance of embedded pressure sensor using 3D printing

The design of an early study in embedded sensors was presented in section 3.3.1.1. Herein, the fabrication process and performance are presented. The 3D printer used is CubePro Trio 3D Printer. The printer was mounted with a TPU filament for printing the fingertip. The system was set to print with 70µm layer height. The FDM printing resolution is 200 µm. The extrusion temperature was set at 216^{o}C. With these settings, the printing duration of the phalanx was 50 mins. The result was a high compressible and bendable structure without any deformities or the need for supporting structure. Figure 5.1a shows the interior of the sensorised phalanx and Figure 5.1b the complete printed structure [254].

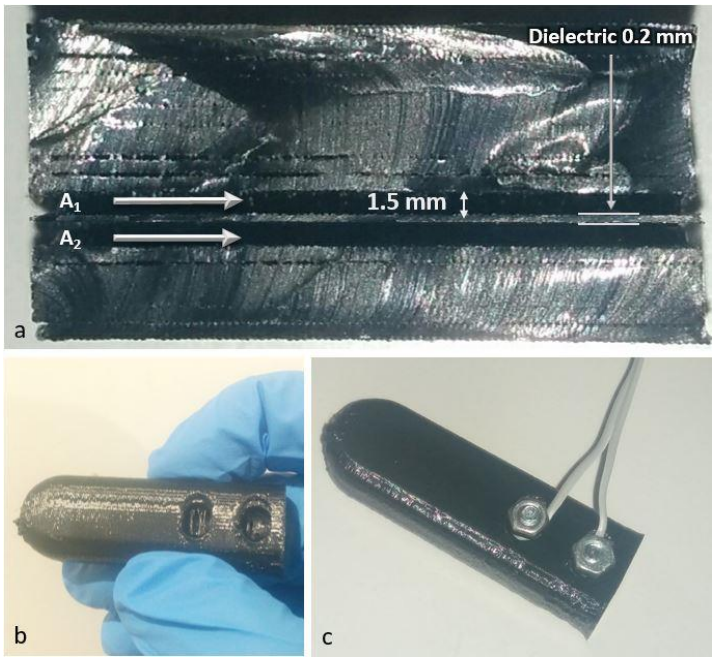

Figure 5.1 (a) 3D printing of the phalanx using FDM technique; (b) the 3D printed phalanx; (c) the phalanx with embedded capacitive touch sensor [254]**. Copyright © 2018, IEEE**

Once the device was fabricated, the steps related to the formation of the capacitive sensor were initiated. The capacitor's parts comprise of two cavities of the printed structure and one layer of the flexible TPU material, which acts as the dielectric. The separation distance between the two plates is 0.2 mm under no load. As pressure is applied to the device the gap between the cavities decreases.

Once the device was printed, the conductive material was injected into the cavities using a syringe. The syringe was inserted into the cavities and a commercial silver conductive paste was injected. The use of silver conductive paste was mainly due to its simplicity of use and high conductivity. After injecting the silver ink, two wires were inserted inside the cavities for wire bonding. After this, the cavities were plugged to prevent spilling of the conductive material, as shown in figure 5.1c. The paste was cured for 1 hour at 80°C, and after it was exposed to ambient air for 12 hours.

The device was tested under various loads and the change of capacitance was measured accordingly. An FSR of known characteristics was placed underneath the device to record the applied force. The bottom surface of the device and the FRS were in contact, while two plastic plates were secured above and below the system. The top plate was applying force downwards towards the setup. The changes in the capacitance were recorded with an LCR meter while a digital

multimeter was recording the resistance of the FSR as the ground truth. Figure 5.2 presents the data captured from the experimentation.

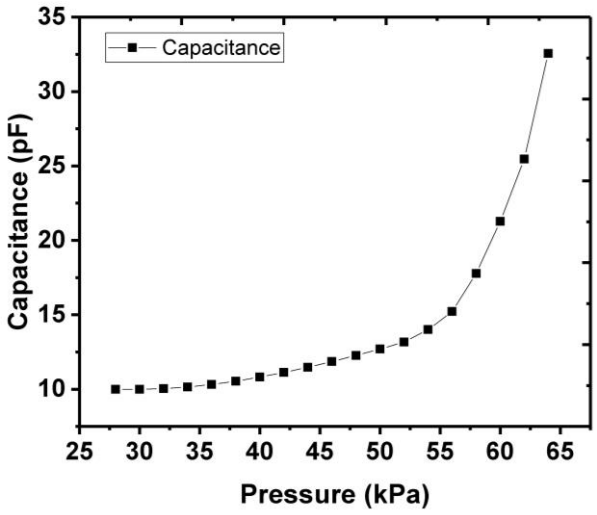

Figure 5.2 Capacitance change with respect to pressure applied on the 3D printed phalanx. [254]**. Copyright © 2018, IEEE**

The capacitance of the device increases with an exponential rate as the pressure increases. The sensitivity of the sensorised phalanx has a linear dependency, with an average sensitivity of 0.025 kPa^{-1} in the range of 20 kPa up to 52 kPa. The sensor did not show response to pressures below 20kPa, which was due to deformation of the cavities before there a deformation of the dielectric material, occurred. The increase in sensitivity can be related to the porosity of the dielectric due to the direction of printing (vertical printing). The device after applying pressure above 70kPa was shorted. This sparked a further investigation in the printing approach of the dielectric and material choices. These problems are resolved in the following section.

5.3.2 Fabrication & performance of intrinsic tactile sensors

In section 3.3.1.2, the design of the intrinsic tactile sensor was presented. Herein the fabrication process and the performance are presented. The problems mentioned above were resolved in this section. The fabrication direction of the dielectric was changed from vertical to horizontal, resulting in a bulk structure without pathways for the conductive material to short the device. Three conductive and two dielectric materials were mismatched, resulting in the

formation of 5 variants of the sensor. The deposition of each electrode/dielectric material required different fabrication techniques.

The three conductive materials used for the formation of the parallel capacitance plates are a commercially available silver conductive paint (RS Components 186-3600, having resistivity (ρ) = 0.001 Ω cm), a commercially available conductive PLA filament (proto-pasta CDP11705, ρ = 15 Ω cm), and an in-house formulated graphite-based ink (ρ = 2.6 Ω cm).

The ink was formulated by Dr. Abhilash Pullanchiyodan in an organic solvent-based system. Initially, 0.5 g of Triton X-100 (Sigma Aldrich) and 0.35 g of polyethylene glycol (Sigma Aldrich) were dissolved in 9.0 mL of terpineol (Sigma Aldrich) solvent by magnetic stirring for 30 min. After that, the binder ethyl cellulose (0.15 g, Sigma Aldrich) was added, and the mixture was stirred for 1 h. Finally, 4.0 g of graphite powder (Sigma Aldrich) was added, and the mixture was continuously stirred for 6 more hours to obtain a well-homogenized stable ink. The electrical resistivity of the developed ink was measured using a four-probe method on the printed pattern. After stirring, the graphite ink was used to fill the syringe connected to the extruder for paste extrusion. The internal diameter of the nozzle used to extrude the paste was 0.51 mm with the printing layer height set to 0.25 mm and the print speed set to 3 mm s^{-1}. After the printing process, the print bed was heated to 60 °C and a hot air gun was used at 100 °C to dry the composite for 2 h.

The reason for the use of these conductive materials is their printability using a commercially available paste extruder (DISCOV3RY 2.0 system, Structur3D Printing) with the 3D printer presented below in section 6.1.

The first dielectric material used to form the capacitive sensor was a two-part silicone rubber (Ecoflex 00-30, Smooth-On, Inc) that has high elasticity with Young's modulus of 27.24 kPa and a dielectric constant of 2.8. The preparation of the material can be found in the Appendix A. This material can withstand high temperatures, which is a requirement as FDM process deposits liquid plastic. The second dielectric used was a flexible TPU (NinjaFlex 85A, NinjaTek) 3D printing filament, with a tensile modulus of 12 MPa and a dielectric constant of 3.57. The sensor's response was investigated based of these materials.

Three devices for each type were fabricated from the combinations of these materials. In addition, a sixth type of the device was fabricated with TPU, as the dielectric, and conductive PLA to form the parallel plates of the capacitor. However, the higher temperature required for the extrusion of TPU, compared with conductive PLA, resulted in the mixing of the dielectric and conductive materials while printing and prevented the formation of the transducer.

To fabricate the sensing devices, an open-source desktop 3D printer (RepRap Ormerod 2) was customized to be able to extrude conductive pastes (see section 6.1). Figure 3.6c shows the deposition of the graphite ink as an electrode for the formation of the transducer. In all variations, the base structure was fabricated using the traditional FDM method. The electrodes of the capacitive sensor were fabricated with different techniques, depending on the material used. For example, the silver adhesive paint was applied with a brush, the conductive PLA was deposited using the traditional FDM process, and the graphite ink was deposited using the paste extrusion setup added to the 3D printer.

The TPU flexible filament material used as a dielectric was deposited from the original FDM extruder of the modified 3D printer. In contrast, the two-part rubber was prepared separately with the parts mixed in a 1:1 volume ratio. The rubber was poured on top of the bottom electrode and the excess material was removed with a flat tool. The adhesion of both the two-part rubber and the graphite ink with the other printable materials was found to be poor and the FDM deposition of materials on top of them was not possible. To overcome this problem, a thin layer of Kapton film was placed on top of the dielectric to enable FDM printing. After the deposition of the top electrode, the full encapsulation of the sensing element was done via FDM printing. Figure 3.6b shows the fabrication process and figure 5.3 presents one device from each variant.

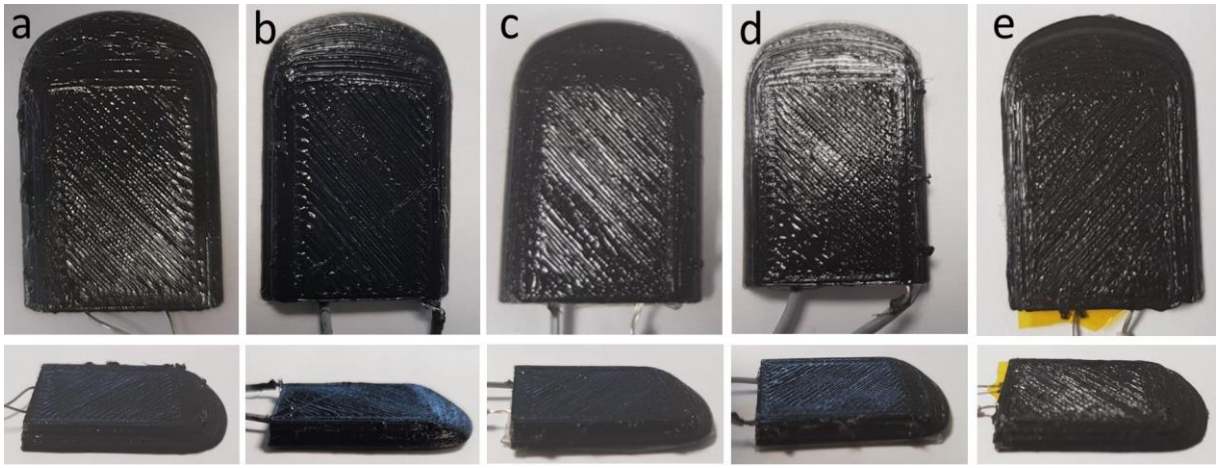

Figure 5.3 3D printed devices with sensor structures comprising:

a) silver paint with two-part rubber dielectric, b) silver paint with TPU dielectric, c) graphite ink with two-part rubber dielectric, d) graphite ink with TPU dielectric, and e) conductive PLA with two-part rubber dielectric. [253]

For each type of sensor, a set of three devices was fabricated and characterized. Once the sensors were fabricated, the characterization process followed. The devices were placed on a load cell and force was applied on the top via an actuator controlled by a LabVIEW program. The capacitance was measured using an LCR meter. The five different fabricated intrinsic capacitive pressure-sensing phalanges, namely Ecoflex-silver (Eco-Ag), Ecoflex-graphite (Eco-Grp), Ecoflex-conductive PLA (Eco-PLA), thermoplastic polyurethane-silver (TPU-Ag), and thermoplastic polyurethane-graphite (TPU-Grp), are shown in figure 5.3a–e. All five devices were tested for their sensing capabilities and Table 5.1 summarizes the average sensitivity and linearity, in the entire tested range, of all the types and the amount of drift for all sensors.

Table 5.1 Specifications of the five types of sensors

	Eco-Ag			Eco-Graphite			Eco-PLA			TPU-Ag			TPU-Graphite		
Sensitivity [kPa^{-1}]	0.002115			0.001214			0.00218			0.000651			0.003		
Linearity	0.80			0.33			0.99			0.58			0.93		
Drift ($\times 10^{-4} min^{-1}$)	S1	S2	S3	S1	S2	S3	S1	S2	S3	S1	S2	S3	S1	S2	S3
	5.6	1.9	0	-10	7	6	8	18	4	1.6	2.1	-0.6	3.6	21	2.1

Figure 5.4 shows the average relative change of capacitance of each type with respect to increasing pressure from 0 Pa to 50 kPa.

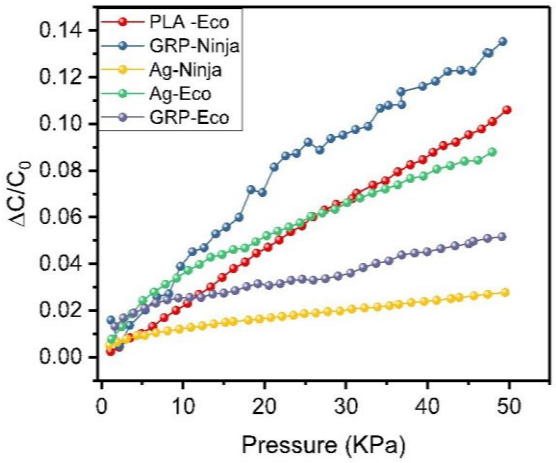

Figure 5.4 The average change in the relative capacitance of the five printed sensing devices with increase in pressure [253].

It is clear from the figure that all types show an increase in capacitance with an increase in applied pressure. However, the rate of change in capacitance in each type is not the same. Figure 5.5 shows all the characterizing results of all the devices besides the Eco-Ag.

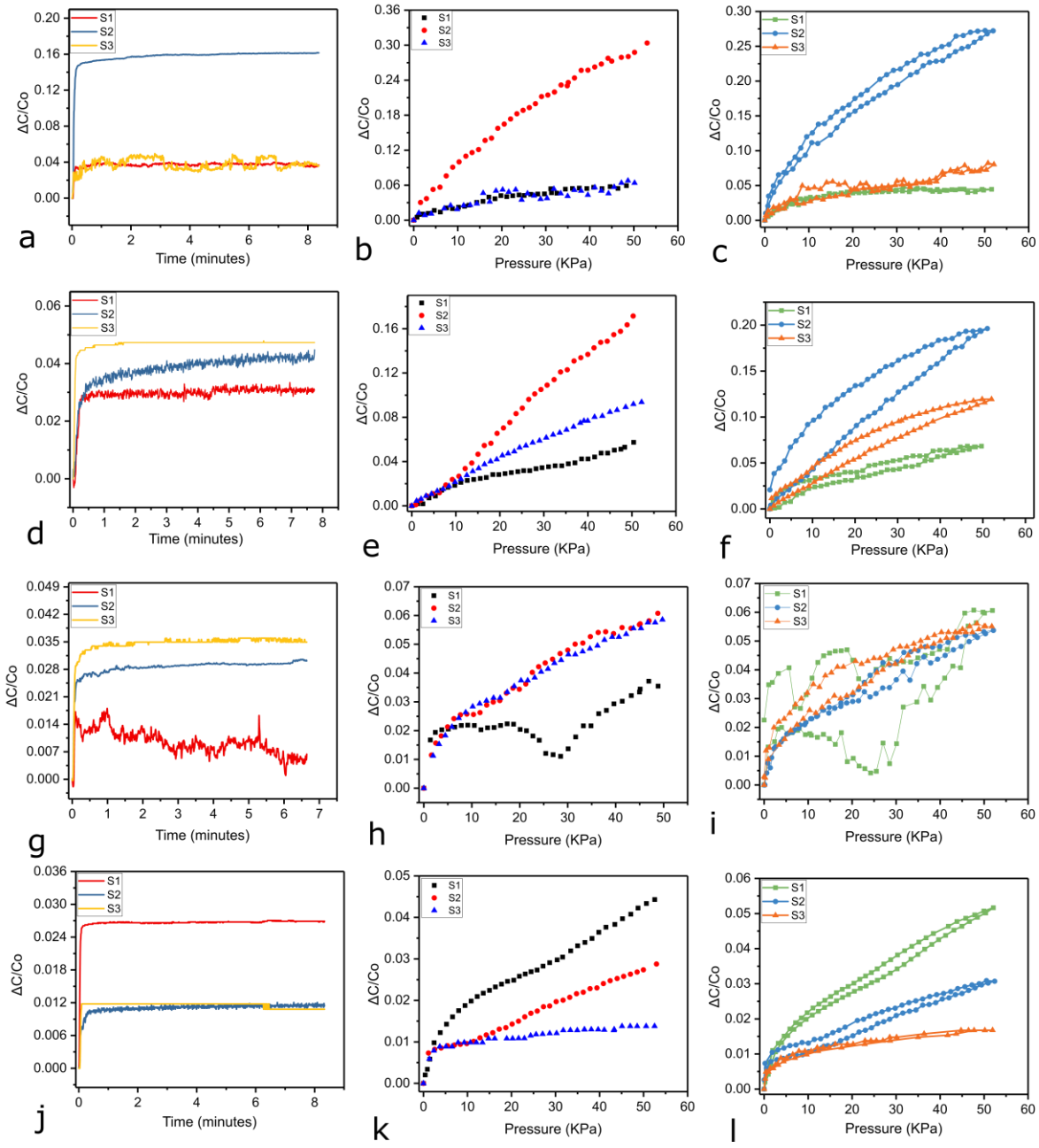

Figure 5.5 Response of each device under different conditions.

a-c) TPU-Grp devices under constant load, relative change of capacitance over pressure and hysteresis. d-f) Eco-PLA devices under constant load, relative change of capacitance over pressure and hysteresis. g-i) Eco-Grp devices under constant load, relative change of capacitance over pressure and hysteresis. j-l) TPU-Ag devices under constant load, relative change of capacitance over pressure and hysteresis. [253]

All devices were tested under a constant pressure of 20 kPa for 8 min. The devices were also tested for hysteresis from 0 kPa to 50 kPa. Finally, the devices were tested for their dynamic cycle response with increasing pressure (0–50 kPa) and Figure 5.6 shows the cycling testing for one sensor of each type besides Eco-Ag.

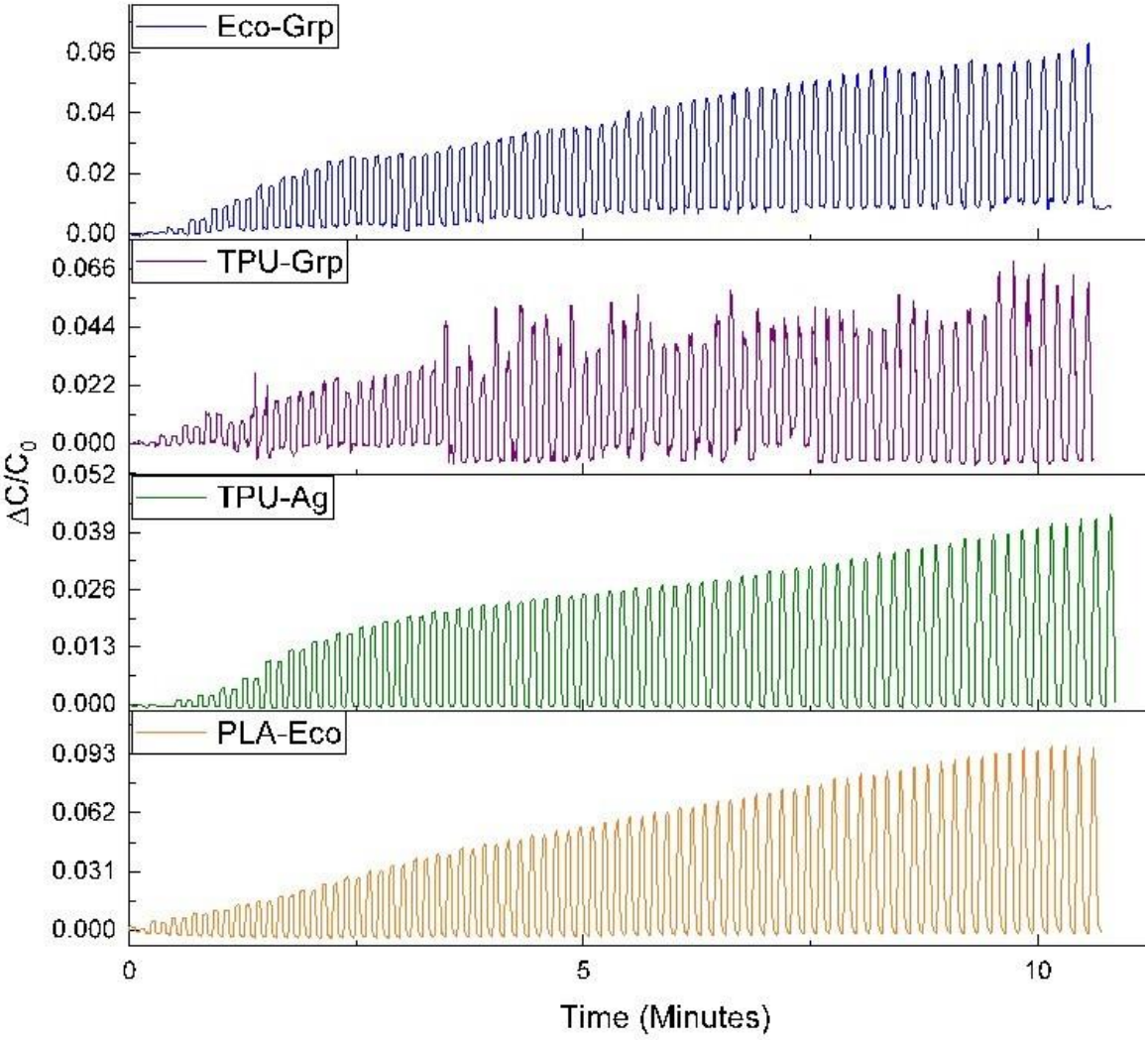

Figure 5.6 Dynamic response of various samples.[253]

Among the tested types, the TPU-Grp devices, on average, showed the highest sensitivity (0.00309 kPa^{-1}) in the tested pressure range from 0 Pa to 50 kPa. The linearity was found to be 0.932.

The Eco-PLA devices were found to have an average sensitivity of 0.00218 kPa^{-1} and the linearity of the devices is 0.99 in the entire tested range, with a significant deviation in sensitivity among them. Another detriment of this type is that all devices showed the highest amount of hysteresis compared to other devices of the other types, specifically in the range of 10 –30 kPa.

In contrast, the Eco-Grp showed irreproducible results. One of the devices showed instability in all characterization tests. Two of the devices showed an increase in capacitance over time under a constant load, while the third one showed an

unstable response with a general trend of decreasing capacitance. This is due to the fragility of the electrode. The graphite while dry can easily crack under any stress. While the material under no load shows good electrical characteristics, but under small amount of force shows a lot of cracks. The average sensitivity of all devices was found to be 0.00121 kPa^{-1}. There are two linear regions, one from 0 to 14 kPa with sensitivity of 0.00256 kPa^{-1} and a second from 14 to 50 kPa with sensitivity of 0.000721 kPa^{-1}. From hysteresis testing, all devices show hysteresis but not in the same pressure region. The first device showed hysteresis in the entire tested range with the second showing hysteresis in the 25–35 kPa range and the last showing hysteresis in the 10–25 kPa range. Due to the aforementioned issues, this type of sensor was found to be unreliable for the current application.

The devices formed by the TPU and the silver show minor drift. The response of each device varies significantly and the average sensitivity for the entire range was found to be 0.00065 kPa^{-1} and showed the lowest sensitivity. Two devices exhibit hysteresis in two different pressure ranges: the first in the range of 25–35 kPa with the second in range of 10–25 kPa.

The Eco-Ag devices exhibit superior performance among the rest of the devices, capable of reliably sensing pressures as low as 1 kPa. All three devices showed high stability and reproducibility in their response. All devices showed insignificant drift for over 8 min of constant pressure. High sensitivity was observed up to 10 kPa at 0.00374 kPa^{-1}, whereas for pressures above 10 kPa, the sensitivity of the devices dropped to 0.00134 kPa^{-1} with linearity of 0.996. The Repeatability and reproducibility of the sensors were major factors for choosing this type to integrate with the embedded readout circuit. Figure 5.7a shows one of the three Eco-Ag devices' relative change in capacitance over time with an increase of pressure every second cycle (from 0 Pa to 50 kPa) for over 100 loading and unloading cycles.

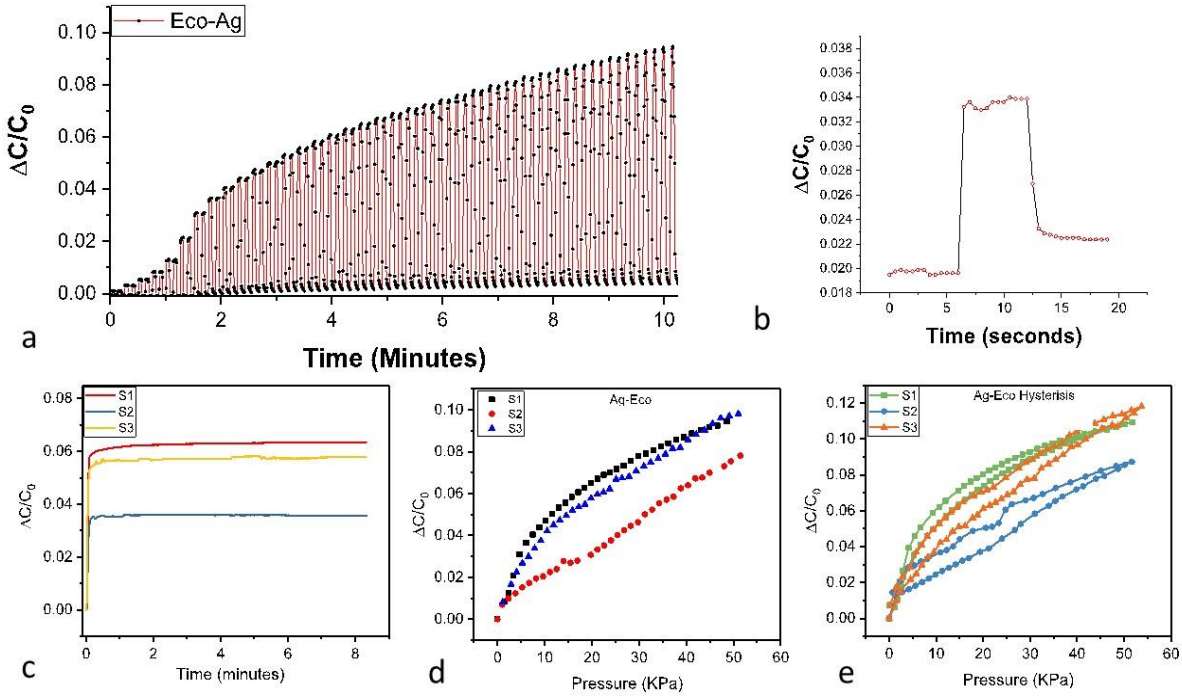

Figure 5.7 Ag-Eco performance

a) Dynamic response of one of the Eco-Ag sensing devices over time with increasing pressure. b) Relative change in capacitance of the Eco-Ag sensing device with respect to time during one of the loading-unloading cycles. c) Response of all three sensors under constant load. d) Relative change in capacitance with increasing pressure. e) Hysteresis curve of the tested devices. [253]

It was noted that all the devices showed similar response trends, as well as excellent stability and repeatability in the tested range. Similar testing was conducted for the rest of the devices.

Figure 5.7b shows the relative change of capacitance response of one of the Eco-Ag devices under loading and unloading with respect to time. This test can be segmented into three phases: pre-load, load, and unload phase. The sensor in the pre-load condition was subjected to a static load of 6.6 kPa. Then, the pressure was increased to 18 kPa for a short period of time, indicating the load phase. The sensor's response time to a sudden change in pressure is in the order of a hundred milliseconds. Then, the pressure was reduced back to the previous level during the final unload phase. The device's response is, again, in the range of a few hundred milliseconds with minor deviation before and after the load phase. The devices were tested under constant pressure and all of them showed minor deviation over time (Figure 5.7c). Figures 5.7d and 5.7e show the relative change of capacitance over an increase in pressure and the hysteresis of each fabricated device for this variation. All three sensors have similar behaviour with good reproducibility. From the above, we conclude that the two-part rubber with the

silver adhesive paint had superior performance in comparison to the rest of the fabricated devices.

The TPU-Ag devices showed the lowest sensitivity on average. This was the main factor for discarding this type as a tactile feedback sensor. This can be attributed to the elastic modulus of the TPU as it is almost two orders of magnitude higher than that of EcoFlex.

The graphite ink devices when combined with the TPU dielectric are less reproducible, despite their higher average sensitivity. The large deviation and unusual behaviour in sensitivity of each graphite-based device compared to the silver-based devices may be due to the formation of microcracks in the graphite-printed film, which tends to propagate with the application of higher amounts of pressure. This can be observed from hysteresis and cyclic tests for both graphite-based devices. The two devices with low sensitivity made from TPU and the graphite ink have an average sensitivity of 0.00145 kPa^{-1} a comparable sensitivity to the TPU-Ag devices. Nonetheless, the graphite ink could be used to develop interconnections between the sensor and the readout circuit, where chances of deformation or cracking are low. This will be a low-cost interconnect which can be used in an automated 3D printing process.

Similarly, the phalanges fabricated from the graphite ink and the two-part rubber (Eco-Grp) have low sensitivity (0.001214 kPa^{-1}). As mentioned earlier, the graphite ink starts to crack even under small amounts of pressure. In one of the devices, this effect can be seen clearly in the hysteresis of the device. This effect can be seen in both variations of the graphite-based devices. As a result, the sensors containing the ink were discarded for the use in the robotic/prosthetic hands as tactile sensors.

Eco-PLA variation shows good response in terms of sensitivity with an average of 0.00218 kPa^{-1} and a linear response in the entire tested range. The devices showed good stability, but they also showed the highest hysteresis.

The superiority of the Eco-Ag devices over the rest of the devices is due to the material properties of the silver adhesive and the two-part rubber. The surface roughness of the silver was compensated by the capability of the two-part rubber

to surround the adhesive and establish a strong bond between them. Moreover, silver did not show a paste-like behaviour, such as graphite ink, after curing. The silver adhesive paint, even as a fragile material after curing, showed exceptional robustness in the packaged phalange.

To demonstrate the potential of the presented approach for robotic hands with intrinsic tactile sensing, five modular sensors based on the Eco-Ag variation were printed and mounted on the distal phalanges of a 3D printed prosthetic hand. The PCB used for the demonstration was presented in section 4.4.1 to read out the data from the sensors and transmit the data to a computer via a USB cable. A LabVIEW program was designed for the representation of the data captured from the integrated circuits on the PCB. Figure 5.8a–e shows the 3D printed hand with integrated soft capacitive sensors. On the right side of the figures, the graphs represent the real-time response of the sensors on the five distal phalanges. As pressure is applied on them, the capacitance increases, and this change can be observed from the graph.

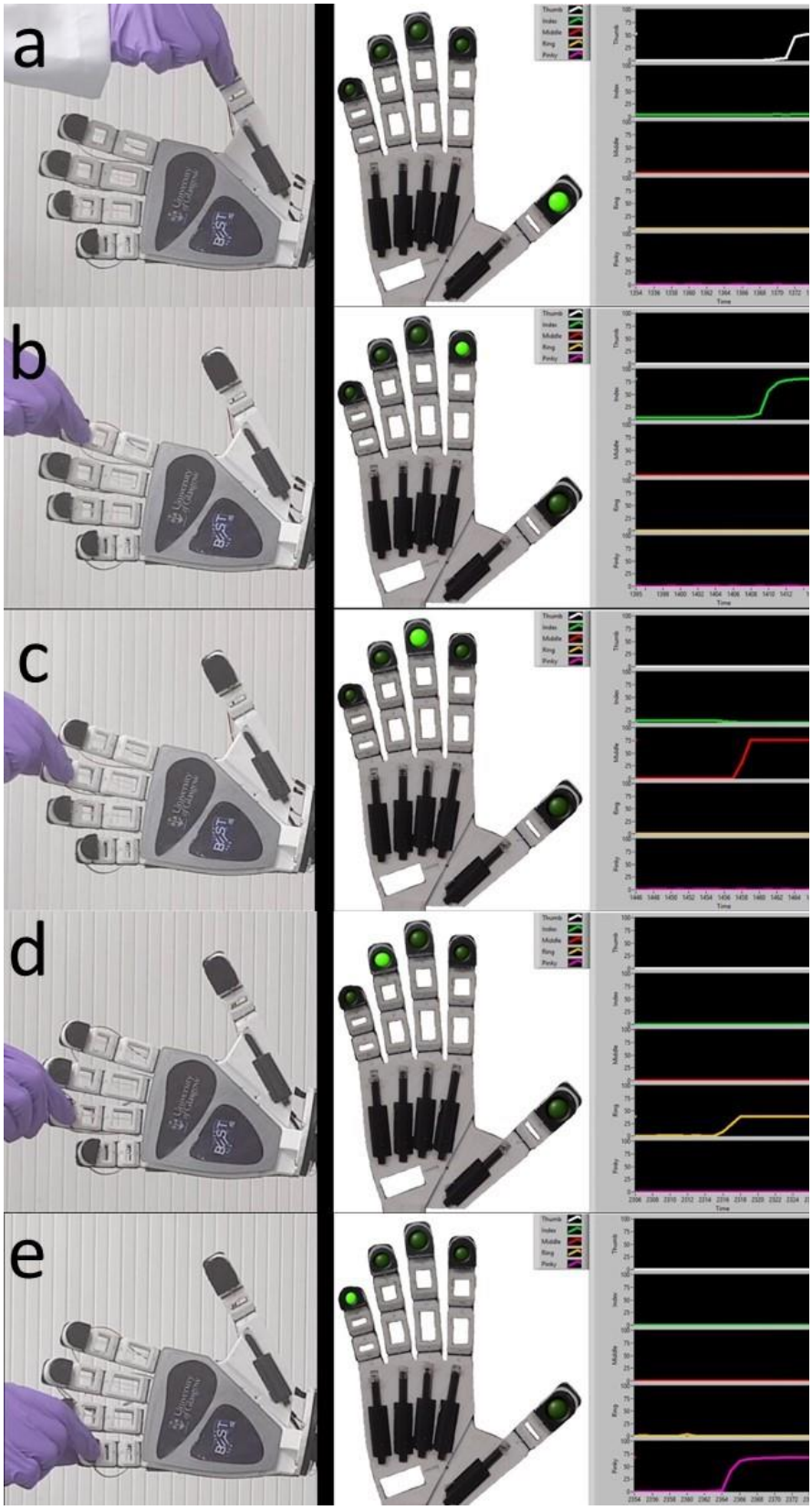

Figure 5.8 Modular-embedded capacitive pressure-sensing distal phalanges (a-e) on a robotic hand responding to pressure stimuli shown via LabVIEW. [253].

Even though this is a progress towards smart and intelligent sensors with embedded electronics, issues arose. The main issues are driven by the paste

extrusion system. The material flow seemed to be inconsistent, and extrusion of the material was difficult to control. To overcome those issues a novel extrusion system is needed. Chapter 6 presents an attempt towards a novel 3D printing extrusion system.

5.3.3 Realization & characteristics of soft touch sensor

As the DIW extruder system was used in the previous section showed inconsistencies, we explored other conductive filament materials that are more flexible than PLA. In this section, we explored new materials and attempted to design and fabricate more sensors in one phalange. The objective was not only to be able to read pressure information but also to be able to estimate the point of contact on the robotic hand.

The design of the fingertip was presented in section 3.3.1.3. The device has two capacitive sensors in a parallel-plate configuration. The 3D printing materials used in this study are chosen for their bendability and softness. The electrodes of the capacitive sensors are made from copper-based composite filament (electrifi, Multi3D) and the dielectric material was formed by a two part-rubber material (Ecoflex 00-30). The rest of the fingertip was fabricated using TPU filament (NinjaFlex, NinjaTek). The electrifi filament has shown good electrical characteristics.

All fabrication steps took place on an Ultimaker S5 3D printer. The printer was mounted with the TPU filament on the first nozzle and Electrifi on the second. The device was printed with 0.2 mm layer height and printing speed of 15 mm/s from the two 0.4 mm diameter nozzles. The infill of the TPU was 45% and the conductive filament was 100% with printing temperatures of 230°C and 150°C respectively. The 45% infill of the TPU was found to allow some compressibility to further enhance the grasping capabilities of the fingertip. The entire fabrication process took approximately 3 hours including curing and wire bonding.

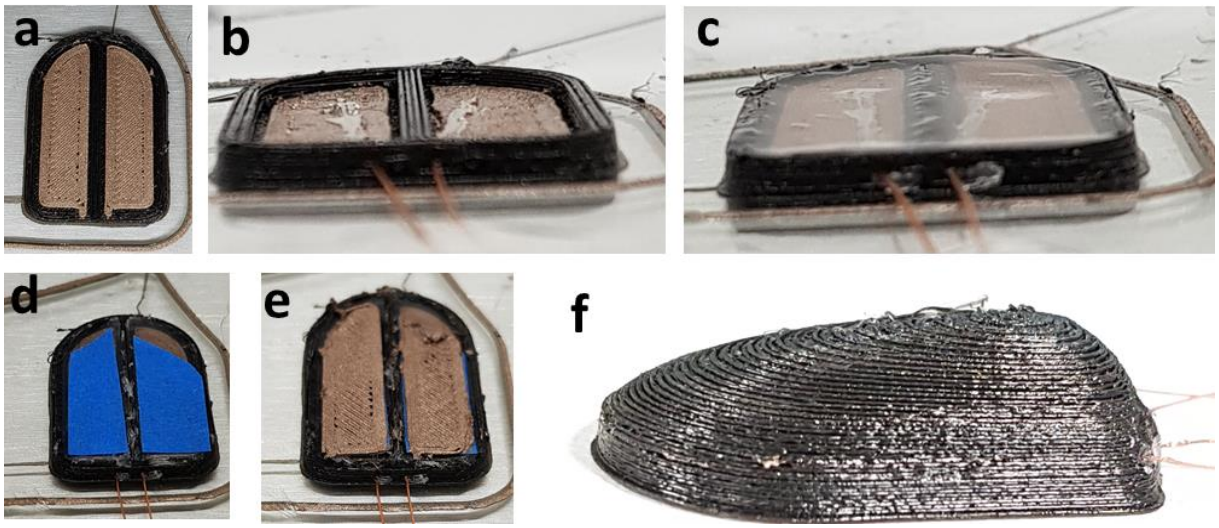

Figure 5.9 Fabrication steps of the soft capacitive sensing fingertip

a) bottom electrodes. b) Formation of the cavity for the dielectric. c) electrode-dielectric structure. d) adhesive tape on top of the dielectric. e) Deposition of the top electrodes. f) Soft-embedded capacitive pressure sensing fingertip. [256] Copyright © 2020, IEEE

The fabrication started with the printer depositing TPU in a layer-by-layer method. On the third printed layer, the second nozzle mounted with the conductive filament started the deposition of the bottom electrodes of the device. The Gcode was modified to pause on the 4th layer of the print to allow the wiring of the electrodes (Figure 5.9a). Once the wire bonding was done the print was resumed until the 10th layer, where the printer formed the two cavities dedicated to the dielectric material (Figure 5.9b). The two part-rubber was mixed in a 1:1 ratio and stirred for 15 mins. The mixture was poured on top of the cavities and cured for 20 minutes, thus forming the electrode-dielectric structure (Figure 5.9c). Once the dielectric was fully cured, a blue scotch masking tape (RS Components) was cut with the shape of the electrodes and placed on top of the dielectric. This step is required to enable the printing of the conductive material on top of the dielectric as the adhesion between the two-part rubber and the filament is poor (Figure 5.9d). On the 13th layer, the printer was paused for the last time for the wire bonding of the top electrodes (Figure 5.9e) and once completed the print was resumed. Figure 5.9f shows the fabricated device.

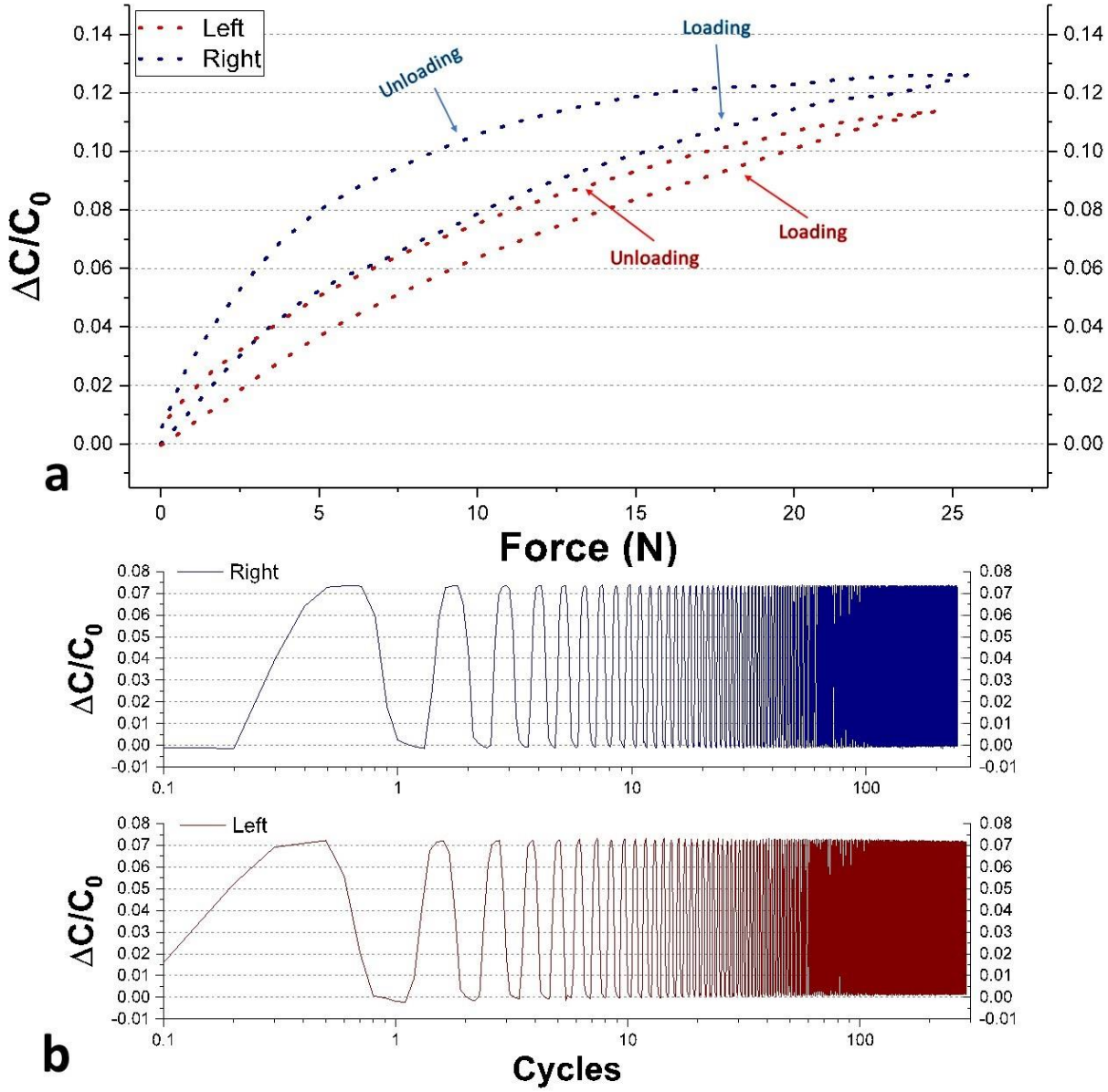

Figure 5.10 Experimentational results of the soft tactile sensor.

a) Relative change of capacitance with respect to static force. b) Relative change of capacitance of the two sensors over time. [256] Copyright © 2020, IEEE

The sensor system was tested under static and dynamic condition. Figure 5.10a shows the relative change of capacitance with respect to force for the two sensors. The devices were examined under linear loading, up to 25 N, and linear unloading, down to 0 N. From that experiment, the hysteresis graphs were obtained for the two sensors. Likewise, the sensors were loaded and unloaded from 0N up to 15 N for more than 200 cycles at a frequency of 1 cycle/s. The results revealed that both transducers have similar response and have high repeatability. Figure 5.10b presents the relative change of capacitance with respect to cycle.

The left sensor has a nominal capacity of 3.933 pF while the right sensor is 4.471 pF. The sensitivity of the left sensor is 0.005523 N^{-1} with linear fit of 92.2% for the entire test range (0 N-25 N). The right sensor showed similar characteristics with sensitivity of 0.00657 N^{-1}, but slightly less linear response with linear fit of 64%. The right sensor showed slightly higher sensitivity, but in contrast it showed a slightly larger amount of hysteresis. These variations could be due to minor imperfections related to dielectric deposition, as the drop-casting process could cause uniformities. Due to the comparable responses of the two sensors, their integration on a robotic hand does not require any sophisticated hardware compensation.

Once the entire system was assembled a custom-made LabVIEW program was developed to present the data captured from the sensors. Figure 5.11 presents the fully functional system and the response captured and presented in a custom-made LabVIEW program. In Figure 5.11a the right side of the fingertip was gently pressured and on the top right side of the figure, a gauge type indicator shows the additional percentage capacitance of the right sensor over the left sensor. Figure 5.11b presents the fingertip pressed on the left side and the response of the system. The positive value represents the extra percentage capacitance of the right sensor over the left, while the negative value represents the extra percentage capacitance of the left sensor over the right one. This can be used for estimating to point of contact of a force on the finger.

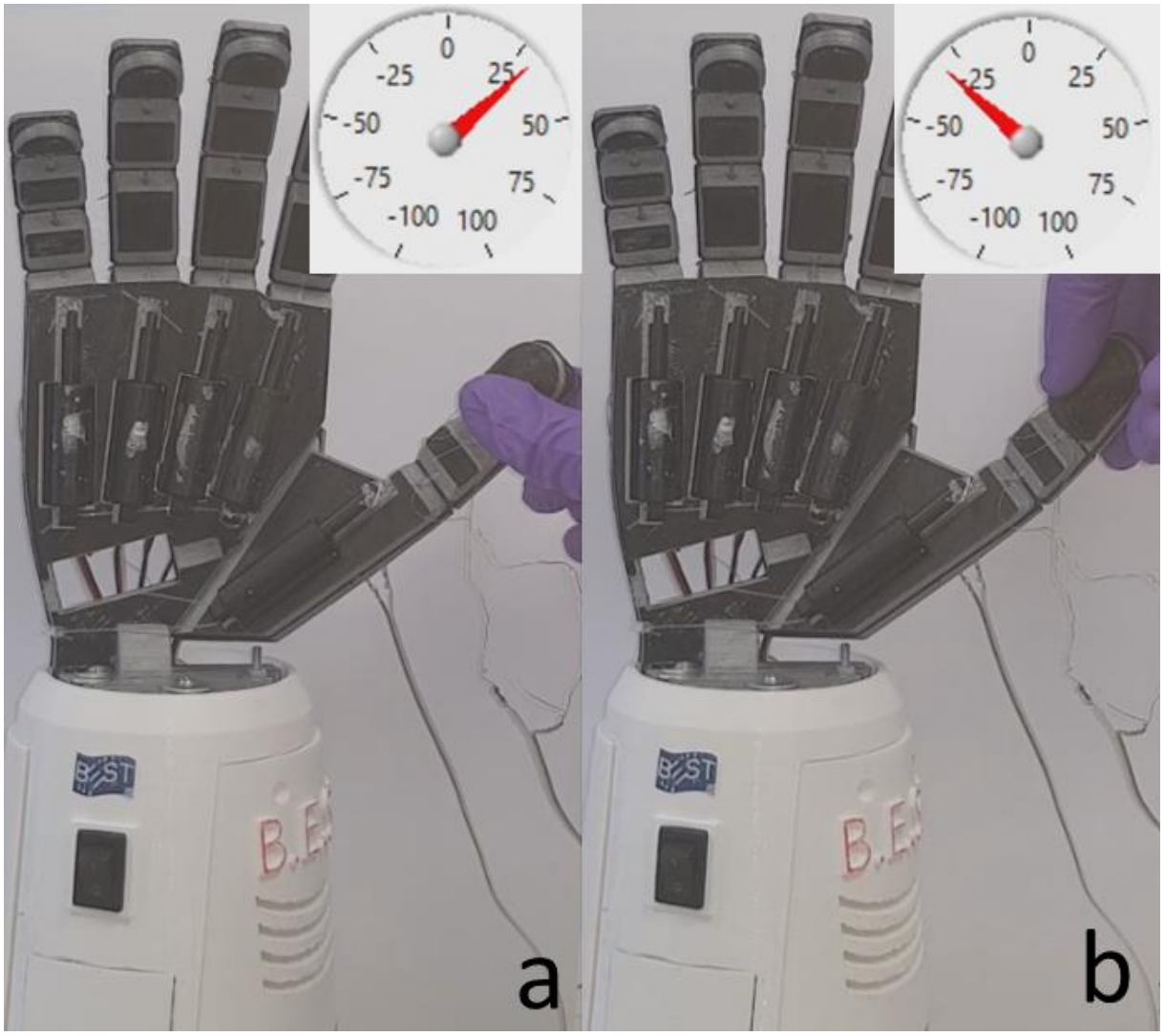

Figure 5.11 Robotic end effector with soft embedded pressure distribution sensors and the response of the system presented by a custom-made LabVIEW program.

a) force applied on the right side of the fingertip and presenting the percentage change in capacitance over the left sensor. b) force applied on the left side of the finger-tip and the response and presenting the percentage change in capacitance with respect to the right sensor. [256] Copyright © 2020, IEEE

This work presents a novel approach to estimate the point of contact of a force for robotic applications. The fingertip showed good performance especially in terms of repeatability and durability. The low percentage infill for the TPU encapsulation material allows some compression of the fingertip like human skins.

Nonetheless, the drop-casting method of the dielectric for tactile sensors of this scale is an issue as the accuracy of the method is based on the person's skills rather than a closed-loop system. In addition, the conductive material used in this study can be considered costly and has limited flexibility therefore a better material is needed for better reliability.

5.4 Manufacturing and characterization of insoles

Even though drop-casting is a non-ideal method for developing dielectric materials, for larger scale structures the deviation from device to device would be insignificant. In this section, a conductive TPU based filament is used as electrode that is more cost-effective and flexible, an ideal material to withstand extreme forces and strain. In that regard, an intrinsic insole for gait analysis is presented. The design of the insole was previously introduced in section 3.3.2.

5.4.1 Fabrication

The pressure sensitive insole was developed using a multimaterial 3D printing system. The capacitive sensors were 3D printed using the Ultimaker S5, a 3D printer capable of printing two materials in the same print. The first material was a TPU. The second was a conductive thermoplastic filament, PI-ETPU (Palmiga-PI-ETPU 95-250 Carbon Black). The PI-ETPU filament was used to fabricate the electrodes of the capacitive sensors and the TPU was used as an encapsulation material for the sensors. Ecoflex 00-30 (Smooth-On) was used in 1:1 ratio to form the dielectric layer of the capacitive sensors.

The printer was mounted with two 0.4mm nozzles with the TPU material attached to the first nozzle and the PI-ETPU on the second nozzle. The slicer software used was Cura 4.7.1 (Ultimaker). The following are the optimized printing parameters. The layer height was 0.2mm, speed was set to 25 mm/s for both materials, the printed temperature for the TPU was set to 240 ^{o}C and 250 ^{o}C for the PI-ETPU and the temperature of the bed was set to 45 ^{o}C. The infill for the TPU was set to 85% and for the PI-TPU was set to 95%. The file that generated the instruction for the printer (gcode) was modified to include pauses at layers 21, 38, 41. The total time for printing one device was about 18 hours on average for three devices.

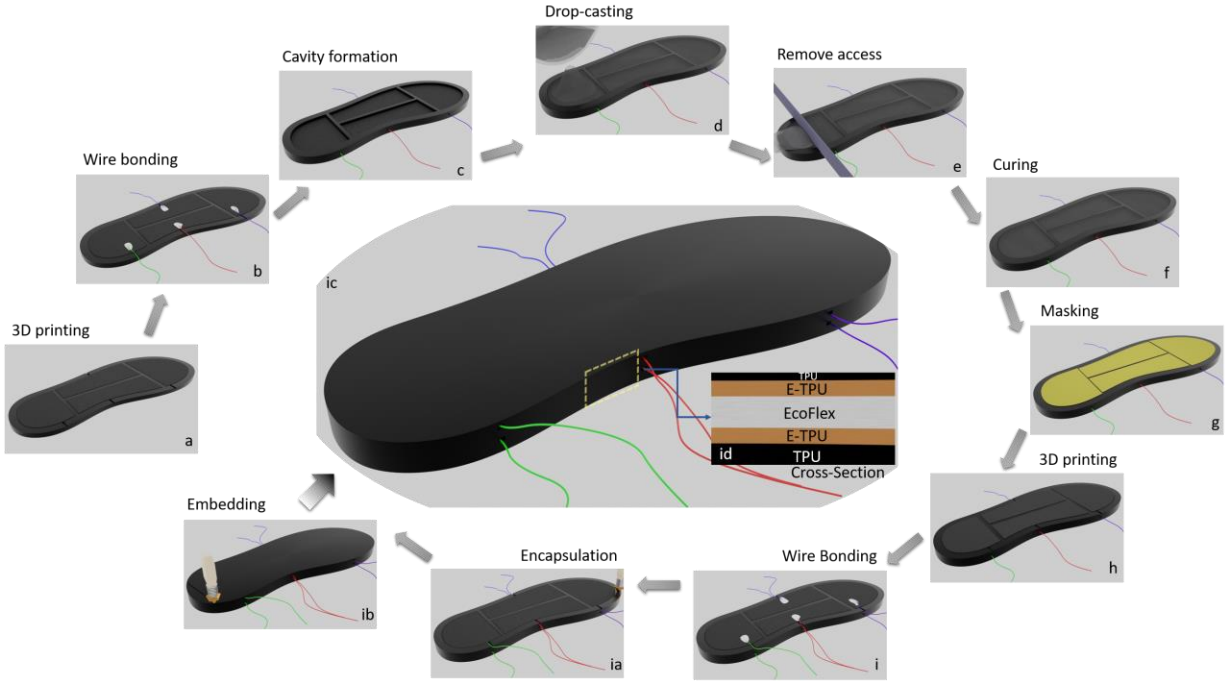

Figure 5.12 Fabrication process of the 3D printed embedded capacitive pressure sensors insole[257].

a-ib) Fabrication steps for 3D printing the insole. ic) Final depiction of the pressure sensing device. id) Cross-Section presenting the different materials.

Initially, the print started with the deposition of TPU on the bed of the printer. The printer at layer 18 started the deposition of the bottom electrodes. At layer 21, the printer was paused to allow access to the bottom electrodes for wire bonding. Thin wires were placed on top of the electrodes and a small amount of silver paint (RS Pro Silver Conductive RS186-3600, RS Components) was applied on top of the area where the wire and the electrode were touching, to reduce the conduct resistance, and left for some time to dry. Figure 5.12b shows the result of this process. Once the wires were secured and the paint dried, the printing process was resumed. At layer 38, the printer was paused again to form a cavity with a depth equal to the thickness of the dielectric. Once the printer was paused, the material needed for the soft dielectric layer between the two printed electrodes of the capacitor, was prepared. For this, the Ecoflex was prepared separately in a beaker, and it was poured at 1:1 weight ratio, then part A and part B were mixed vigorously for about 20 minutes. After, the beaker was placed under vacuum for about 10 minutes to remove all bubbles from the mixture. The mixture, then, was removed from the vacuum, it was drop-casted on the cavities of the capacitive sensors to form the dielectric layer. The excess amount of

material was removed by scraping the entire device leaving an even level plane with the rest of the print. The device was left to cure for about an hour. Once the dielectric was completely cured the area of the dielectric was covered with a thin masking tape (RS Pro 60° paper masking tape, RS Components). This is due to poor adhesion of PI-ETPU with Ecoflex as direct deposition of PI-ETPU was found to be challenging. Once the process was completed, the print resumed until layer 41. Once the printer reached that layer the system was paused, and the wire bonding of the top electrodes was carried out (Figure 5.12i). The same process was followed as the bottom electrodes for wire bonding. After this the printing of the last layers of the device was carried out. The outcome of this fabrication process was a flexible, soft, and highly bendable structure (Figure 5.13a-b). The 85% infill of the TPU material allows the structure to be softer than a 100% solid TPU structure. This makes it more attractive for wearable applications such as in walk monitoring systems as it absorbs impact more gradually than a solid block.

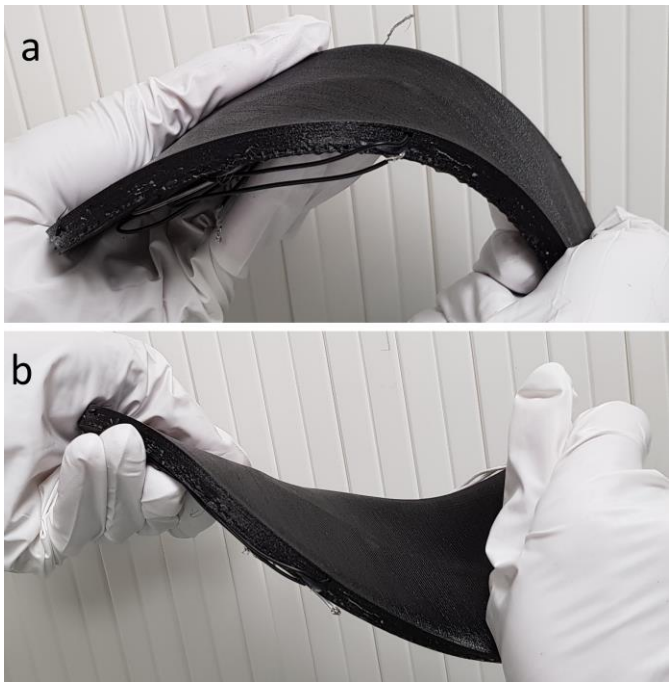

Figure 5.13 a) Fabricated 3d printed capacitive pressure insole under bending condition. b) Sensorised insole viewed while twisted[257].

5.4.2 Characterization of sensing insole

Three separate insoles were fabricated for characterization. From those three fabricated insoles, the toe sensors were characterized and compared with each other under three different testing conditions. The first set of experiments was to

determine the response of the sensors with respect to the applied pressure. Secondly, they have been tested for a prolonged cycling response, to confirm the reliability and robustness of the sensor during actual use when frequent force is expected. Lastly, the devices were tested for their time response.

The capacitive transducers were characterized for their response with respect to different magnitudes of force. The devices were tested under increasing and decreasing amounts of the applied pressure. The toe sensors were tested up to 300kPa pressure with a step of 30kPa. This covers a much wider range of forces than the devices may experience during use. Even at extreme pressures, the sensors did not alter their functionality. Figure 5.14 presents the relative change of capacitance with respect to the applied pressure for all three devices. It can be observed that there are two linear regimes of the sensor's response. The first linear region is from 0 - 60kPa with sensitivity of 2.4 MPa^{-1}. The second range is from 60kPa to 300kPa, for which the sensitivity was found to be 0.526MPa^{-1}. The sensors exhibit an average maximum hysteresis of 9.57%. The highly sensitive range is due to the deformation of the softer elastomer (e.g., dielectric material). The second range is mostly due to the deformation of the encapsulation material. The TPU material, that encapsulates the transducer, can deform at a different rate from the softer elastomer, thus, the transducers do not saturate at low forces, extending the measuring range of the device.

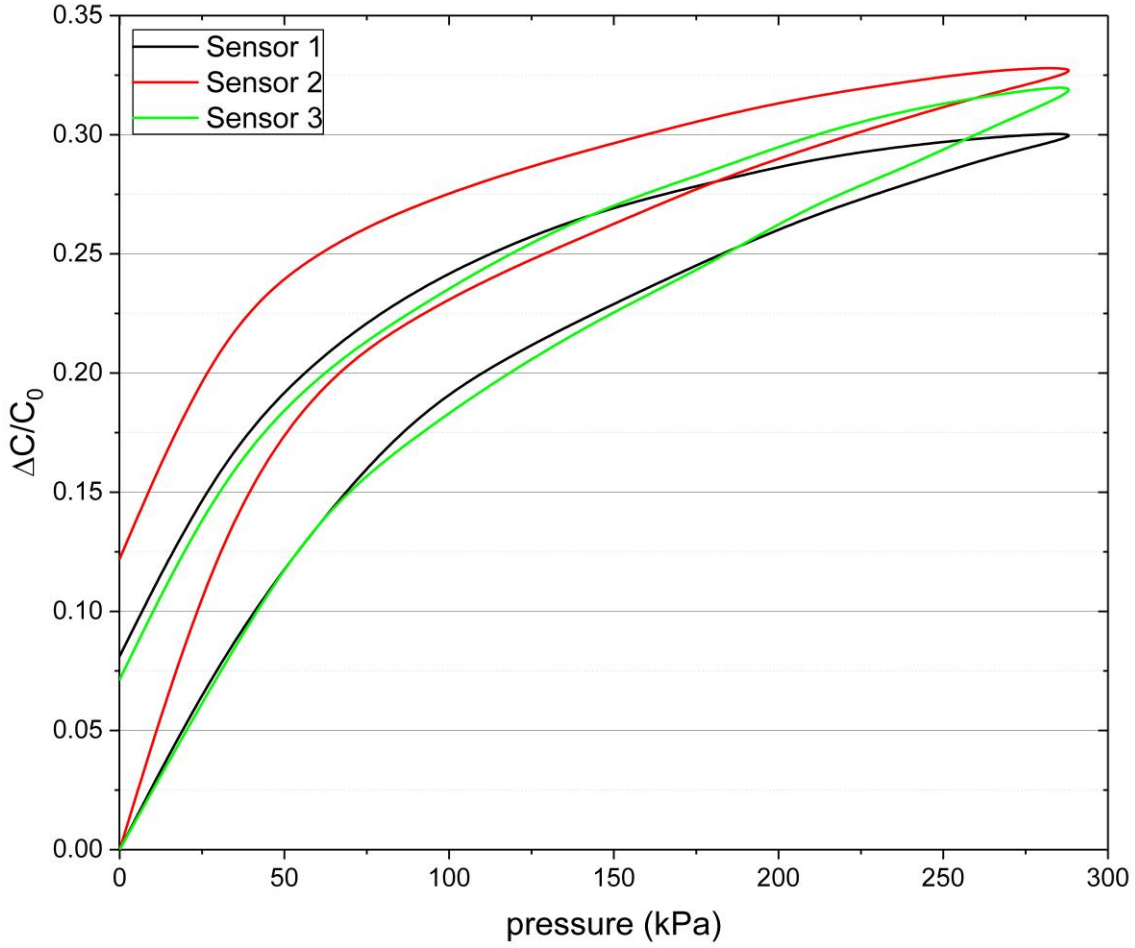

Figure 5.14 Relative change of capacitance with respect to pressure of the three-3D printed capacitive tactile sensors insoles[257]**.**

Next, the three sensors were tested for long-term stability of the response. All sensors were applied with pressure of 30kPa for 1000 cycles. Each device was tested for 2 hours, and 46 minutes and each cycle lasted for 5 seconds of applied force followed by 5 seconds relaxed state i.e., no force applied. Figure 5.15 presents the relative change of capacitance for each cycle for all three sensors. All three devices have similar responses with negligible change from cycle to the next cycle. This provides the necessary reliability for the potential use of tactile sensing in robotic applications where accurate pressure information is needed during prolonged use in harsh terrains.

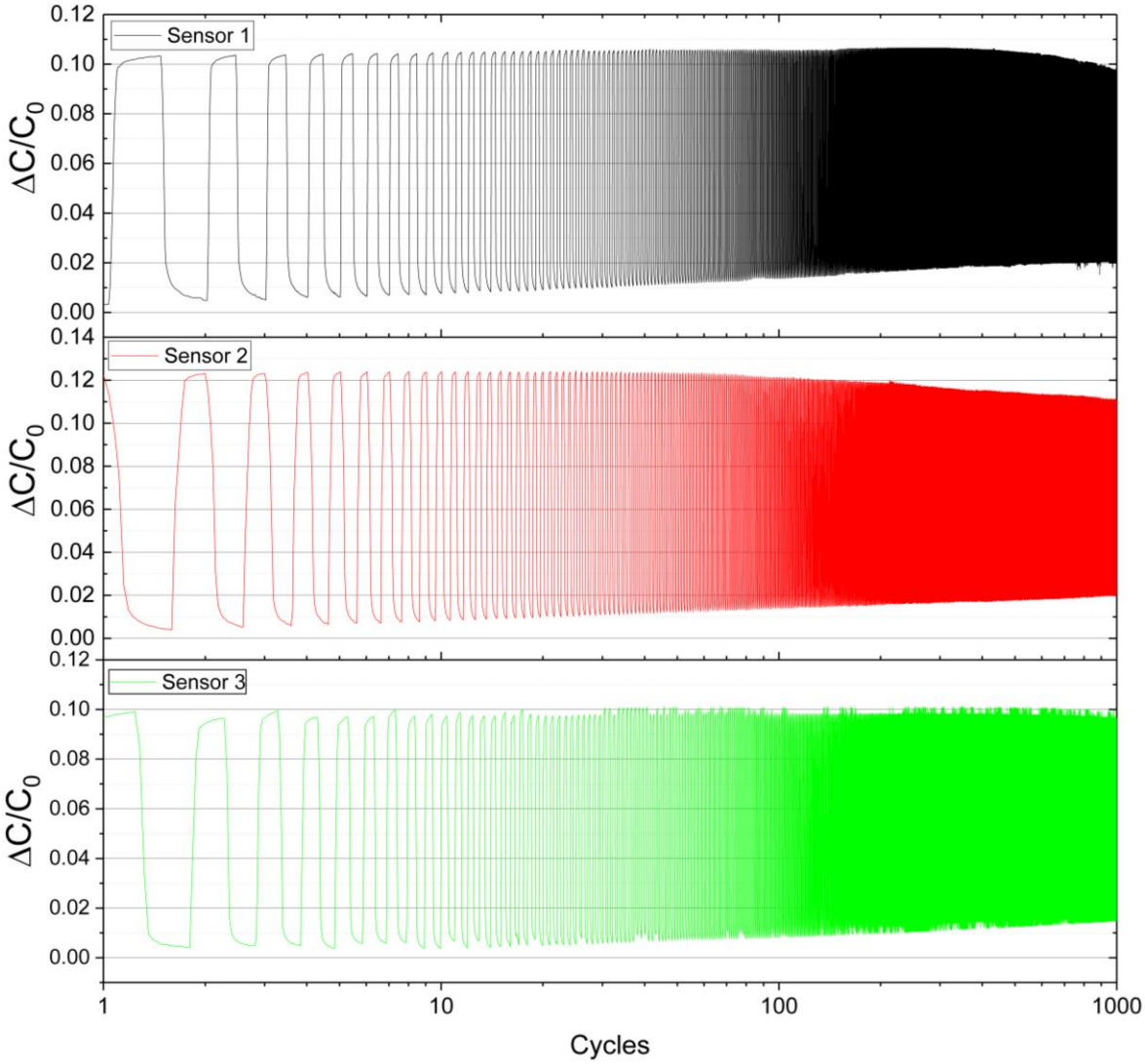

Figure 5.15 Cyclic performance of three devices for 1000 cycles at 30kPa of pressure[257].

Last set of experimentation was to see the time it takes for the sensors to respond to the changes in applied force. The sensors at the beginning were not under any stress. Then a load of 20kPa was applied for a long period and the capacitance of the devices were continuously measured. Once the sensors had a constant (or saturated) response, the applied force was suddenly removed to measure the response time. Figure 5.16 presents the results of the measurements. All devices had similar response. The average response time of the sensors to reach 90% of the applied force value was found to be 3 seconds and the time to reach 98% was slightly over 1 min. For decreasing load, the sensors average time response from 0 to 90% was found to be 25.5 seconds with a total of 2 minutes to reach the 98%. Table 5.2 summarizes the results of the experimentation. The difference in response times at the time of applying force and its removal, is likely due to the

viscoelastic effect of the Ecoflex resulting in an increase time response of the device when forces are released.

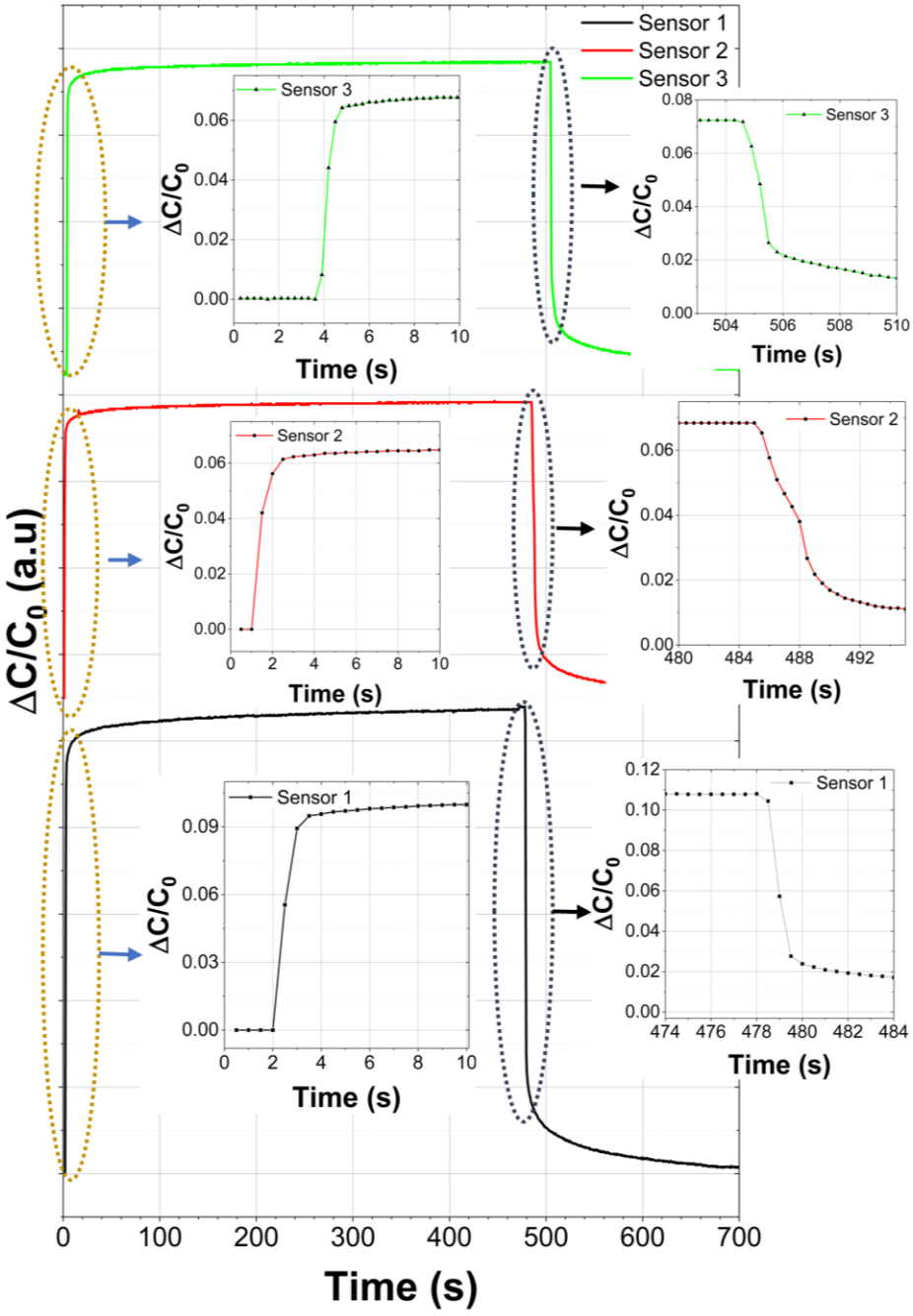

Figure 5.16 Response of the 3D printed insole over time with a sudden increase and decrease of the load[257].

Table 5.2 Time response of 3D printed insole

Direction	Time to reach 90% (s)	Time to reach 98%(s)
Increasing force	3.2	107
Decreasing force	25.5	170

To further evaluate the 3D printed capacitive sensing insole, all sensors in one insole were characterized under different conditions. Two sets of experiments were conducted: The first was to characterize the sensors with respect to applied pressure up to a maximum load of 1000N. As the surface area of each sensor differs slightly, the corresponding pressure response for each sensor differs as well. The response of the sensors from one insole is given in figure 5.17. The right sensor exhibits sensitivity of 0.854 MPa^{-1} for the entire pressure range while the left section exhibits sensitivity of 1.065 MPa^{-1} and the heel sensor's sensitivity is 0.867 MPa^{-1}.

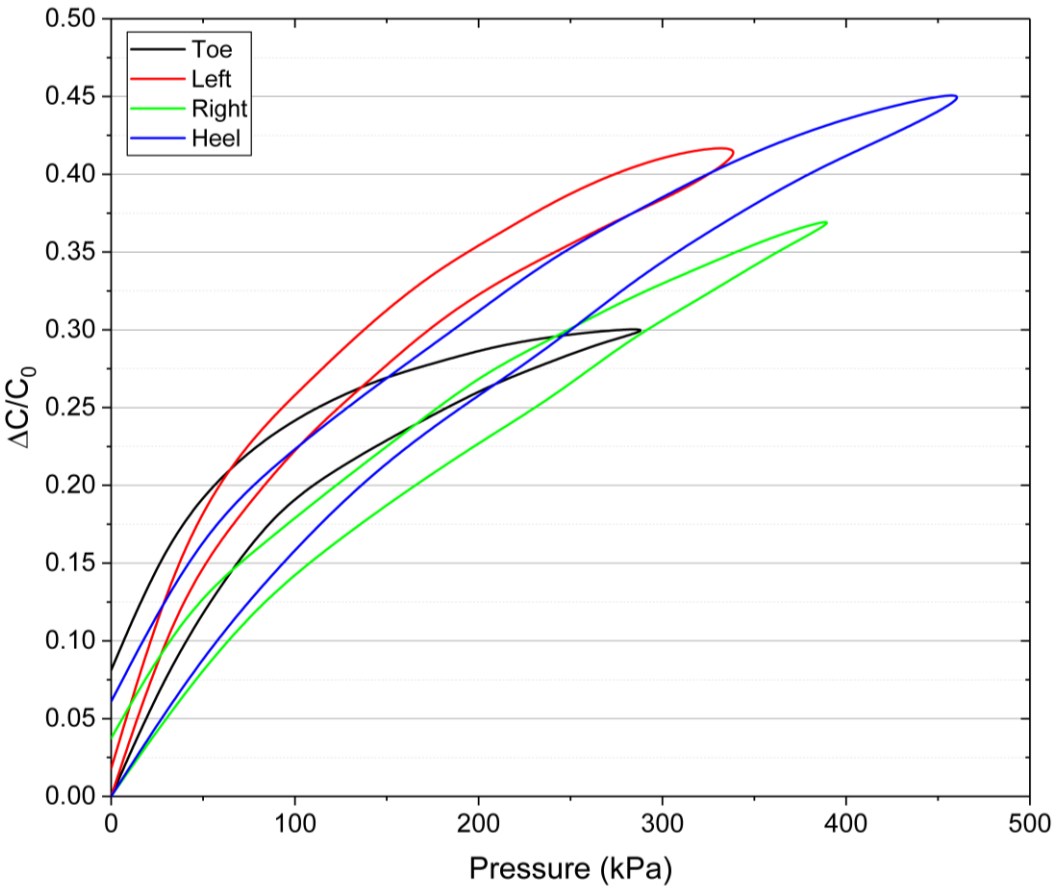

Figure 5.17 Relative change of capacitance with respect to pressure for all four sensors in one of the 3D printed insole[257].

Furthermore, the insole was tested under different bending conditions and the response of each sensor was recorded. In this experiment one of the insoles was placed in such a way that only the front and back of the device were touching the test set up, as shown in the inset in figure 5.18.

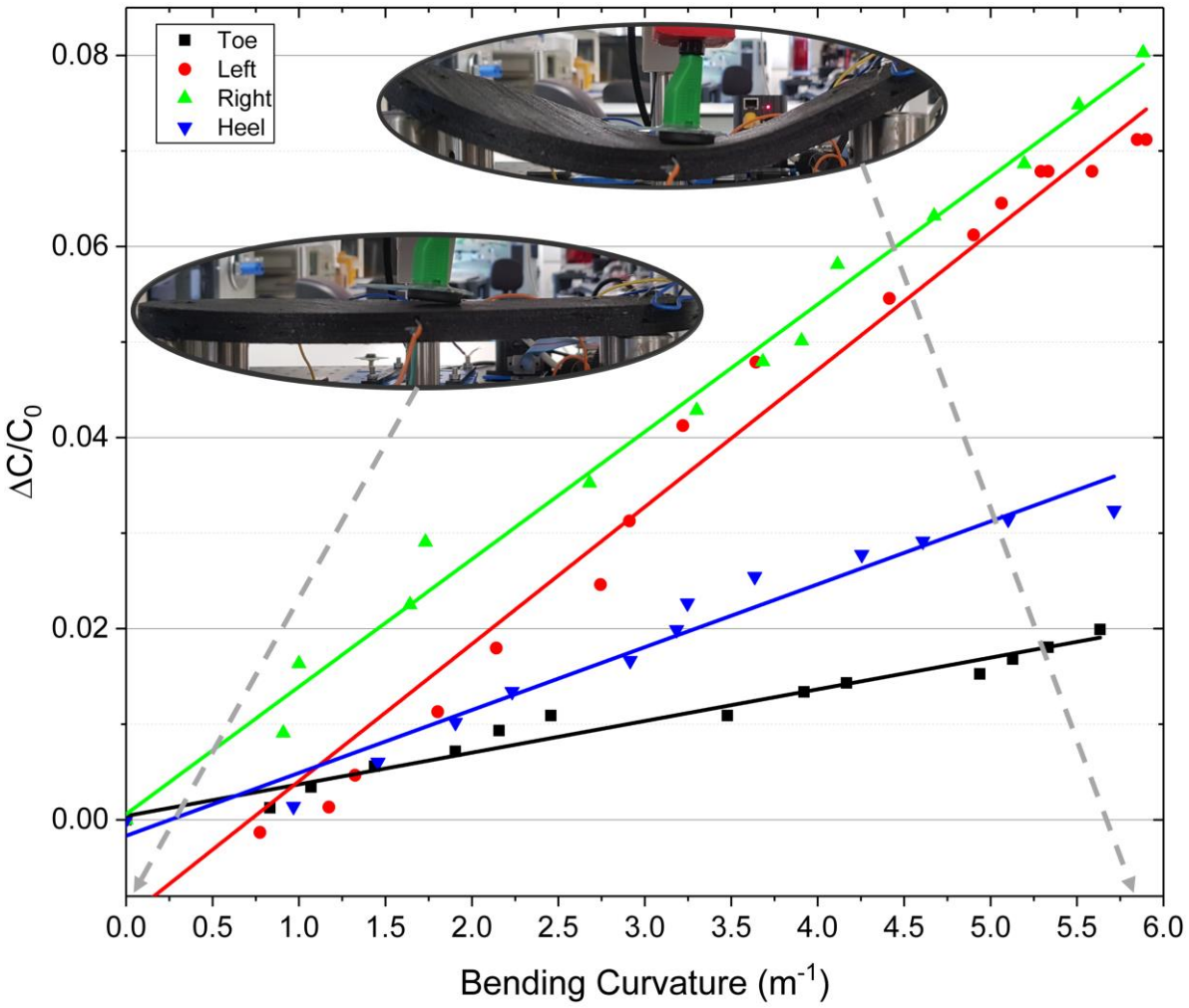

Figure 5.18 Relative change of capacitance with respect to bending curvature for all four sensors in one of the 3D printed capacitive sensing devices[257].

A linear motor was placed above the centre of the device and was able to bend the device at specific intervals. The maximum bending curvature that the device experienced was 5.6 m^{-1}. Figure 5.18 shows the relative change of capacitance with respect to bending curvature. All sensors exhibited linear response. The sensitivities for the right and the left sensors were 0.0133m and 0.0143m respectively. The toe and the heel sensors exhibited a lower sensitivity of 0.003m and 0.006m, respectively. The different sensitivities of these sensors are due to the geometrical/dimensional differences, as the sensors in the centre are longer than the ones at heel and toe.

The 3D printed insole was also tested under different temperatures to observe the potential response variation in outdoor conditions. The device, at first, was left overnight in a cold environment at a temperature of 11°C and then was placed at room temperature (23°C). The output of the toe sensor was monitored with an infrared non-contact digital thermometer and the temperature and capacitance of the device was monitored constantly and logged. Once the device reached room temperature, a heat gun was placed above the device at a 30 cm distance, and it was set to 100°C at the maximum air flow. The device started to heat, and the temperature and response of the sensor were continuously monitored. The maximum temperature the device experienced was 29°C. Figure 5.19 shows the relative change of capacitance with respect to temperature and at the same time the response to pressure for comparison. The sensor shows a liner response with temperature with a sensitivity of 0.0023°C^{-1}. This shows that the relative change in capacitance due to temperature variation of 18°C is equivalent to the 15kPa of applied pressure.

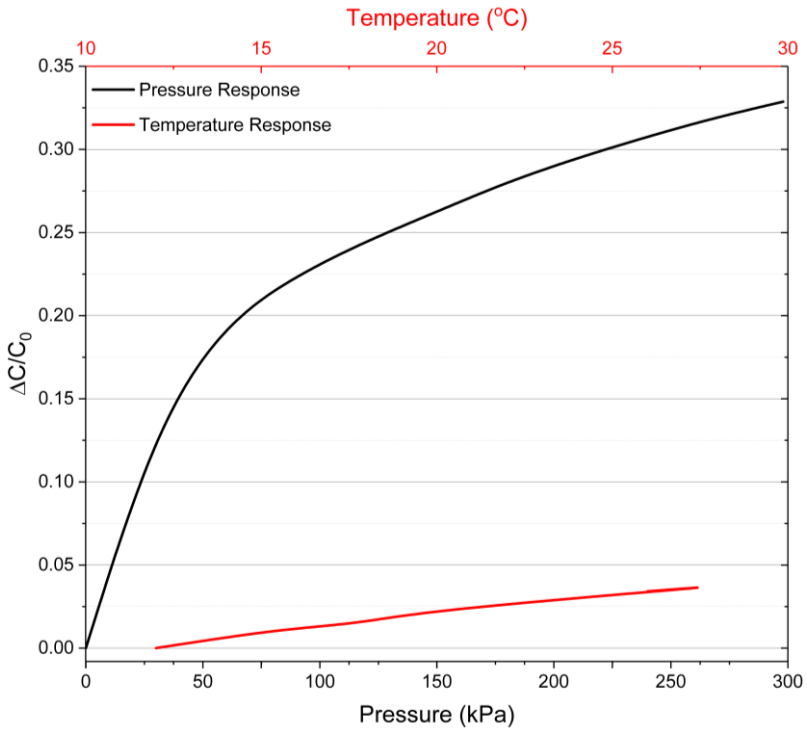

Figure 5.19 Relative change of capacitance with respect to temperature and pressure of the toe sensor[257].

Table 5.3 compares this work with respect to other similar works reported in the literature. From the table is clear the sensors in the 3D printed insole provide a higher sensitivity than some works reported in the literature.

Table 5.3 Comparison of 3D printed insole with previous works reported in the literature[257]

Materials	Sensitivity	Range	3D printed?	Ref.
Gold thin films-Silicone rubber	0.4 MPa^{-1}	160kPa	No	[260]
MWNT/PEDOT:PSS-Porous PDMS	1.12 MPa^{-1}	1400kPa	No	[261]
Conductive PDMS-Ecoflex	0.42 MPa^{-1}	1200kPa	Yes	[262]
Gold-Ecoflex	0.48 MPa^{-1}	250kPa	No	[263]
Silver cloth-cotton cloth	0.95 MPa^{-1}	200kPa	No	[264]
ETPU-Ecoflex	**2.4 MPa^{-1}**	300kPa	Yes	This Work

5.4.3 Demonstration of gait analysis

The device was tested for gait analysis under walking conditions. The sensorised insole was securely placed under a shoe and the wearer walked at a normal pace. The real-time data captured with GUI for three steps of the right leg is shown in figure 5.20. From the data, there is a clear view of the walking pattern of the individual and can see the repeatability of the response.

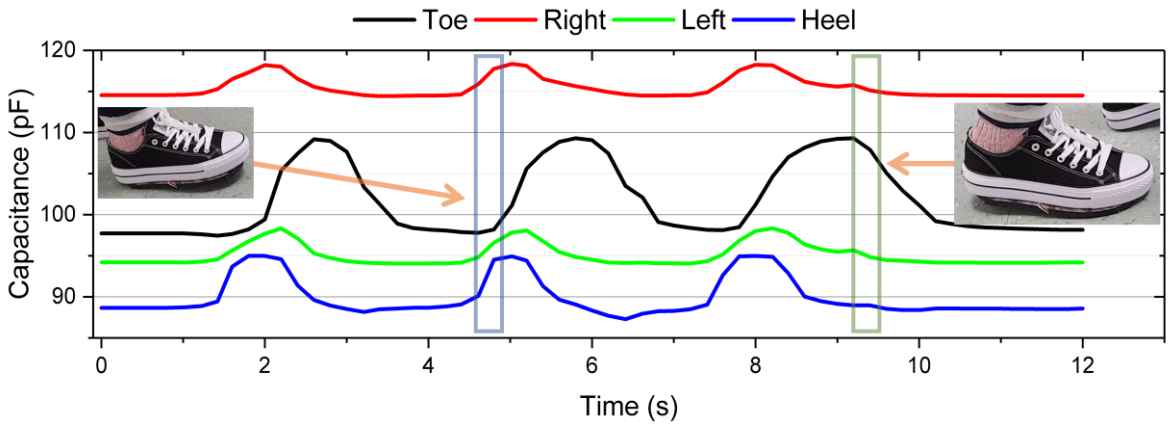

Figure 5.20 Shoe integrated with the 3D printed embedded capacitive sensorised insole used for gait analysis, presenting the data capture from the MCU in real-time over three steps of the right leg[257].

This section presented an extremely durable pressure sensing insole for gait analysis with the use of 3D printing. The intrinsic insole was 3D printed using different materials and showcases good performance. Nonetheless, the sensor has a relatively high response time making it difficult for use in extreme dynamic conditions.

5.5 Performance of piezoresistive sensors and frequency response

To combat this issue, piezoresistive sensors often have a better response time compared to capacitive sensors. To overcome the issues in the previous section, this thesis adapted piezoelectric sensors for dynamic response.

5.5.1 Characterization

The piezoresistive tactile sensor design and formation process were described in section 3.3.3. Herein, a brief introduction to the performance of the sensor is presented. The piezoresistive device (SensAct) was made by Dr. Oliver Ozioko and it is presented here for better clarity of the systems' capabilities. Figure 5.21a shows the loading and unloading characteristics of four fabricated piezoresistive sensing elements using a contact force between 0 and 12 N. Considering all four sensors in Figure 5.21a, the sensors have a mean variation of ΔR/Ro ≈ 70% around 5 N, with a standard deviation approximately 8.9%. Figure 5.21b shows the cyclic loading of the four fabricated sensors with a force of 3 N. This resulted in an average resistance variation of ΔR/Ro ≈45% with a standard deviation of ≈3.2% and a response time of ≈149 ms. More details about the device characteristics can be found in [258].

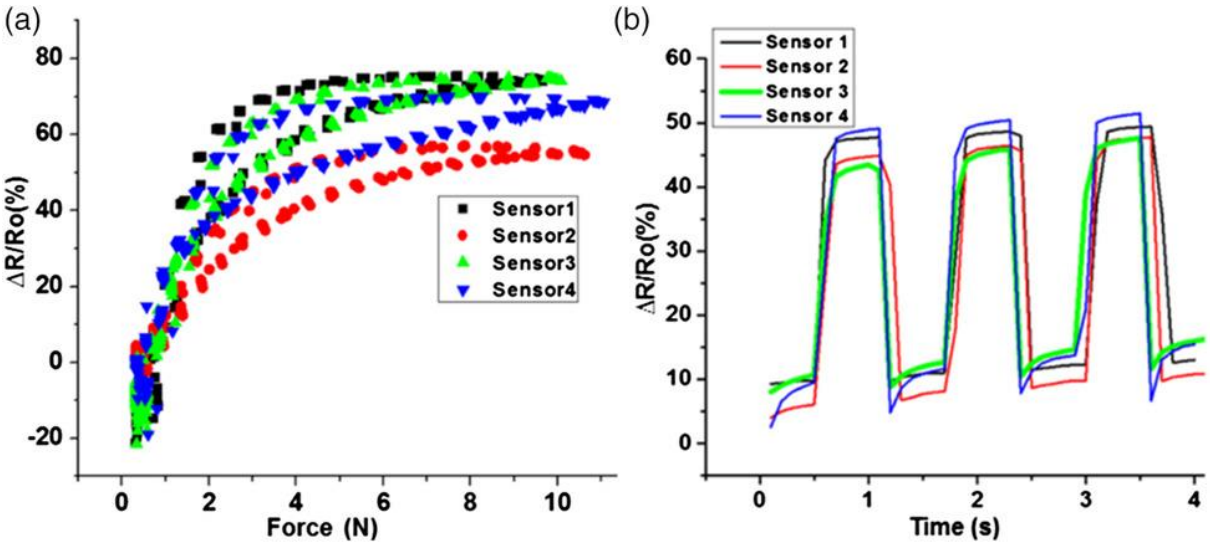

Figure 5.21 a) Loading and unloading characteristics for the four fabricated piezoresistive sensing layers; b) cyclic loading of the sensors using 3 N force at 0.8 Hz. [258]

5.5.2 Time-domain and frequency domain response

The SensAct device was embedded in a 3D printed fingertip of a robotic hand as explained in section 3.3.3. After that, the device was demonstrated to capture the response of the sensorised fingertip as shown in Figure 7.5 in the Appendix. From figure 5.21b, the sensor's response under cycling testing shows to have variation between different cycles, but a significant fast time response, ideal for exploring the possibility to identify different vibrotactile stimuli. To that end, two different stimuli were acting upon the device to observe the difference in the response of the device in the frequency domain. The first was a cycling pressure with a frequency of 0.5 Hz. In the second case, a cardboard box was sliding on the device at a slow pace. Figure 5.22a presents the binary data for time domain and frequency domain response of the device for the first stimuli, while figure 5.22b shows the binary data for time domain and frequency domain for the second case.

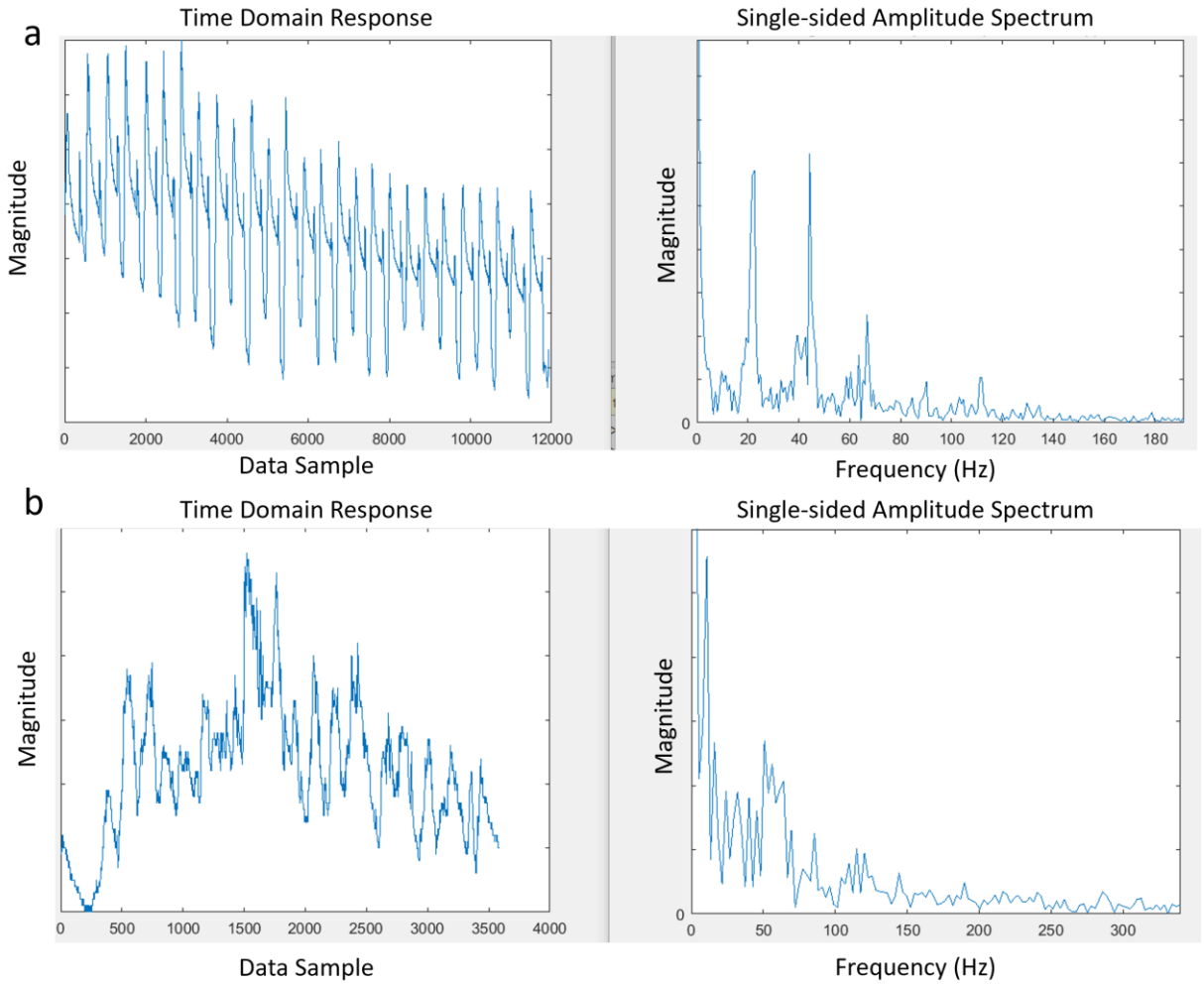

Figure 5.22 Time and frequency domain response of the SensAct sensorised 3D printed fingertip

a) Response of a cycling response at frequency of 0.5 Hz b) Sliding of a cardboard box

A Fourier Transform was used to obtain the Frequency Domain response of the device. This can alleviate the need for the capacitive sensors to have an extremely fast response as this type of devices can act as the fast-adaptive receptors for artificial skins, while capacitive sensors can act as the slow adaptive receptors.

5.6 Performance of embedded photovoltaic cells

As all these sensors and devices require energy to be provided to them to operate. This thesis suggests an alternative solution to the energy needs of smart structures. To this endeavour energy harvesting devices were explored to provide the necessary power to the systems. As current technology of photovoltaics implements fragile materials, the need to protect them from external hazards is necessary. Herein, 3D printed covers for protecting solar cells are presented with

different thickness. The cells are integrated on the robotic hand and the design was presented in section 3.4.

5.6.1 Energy harvesting device

For this section, a commercial photovoltaic device (193852 Monocrystalline Solar Cell, RSC-M125XL, Conrad) was used to harvest the energy from the incident solar electromagnetic waves produced from a high illumination office lamp. The light source is a 4 W LED lamp with color temperature (CCT) of 4500 K and Color Rendering Index (CRI) higher than 80 RA according to manufacturer specifications (model LT-T15, Aglaia, California, USA). The cell has an efficiency of up to 17.8%. The panel has dimensions of 50x50 mm^2, with nominal voltage of 0.5 V, nominal current of 0.77 A, and short circuit current of 0.85 A.

5.6.2 Fabrication of the covers

All covers were printed with Ultimaker S5 3D printer. The printed covers were printed with the following settings for consistency of the results. The infill was set to 100% with a line filling pattern. The layer height was set to 0.1 mm. The printed temperature was set to 200°C with a printing speed of 40mm/s. Slower printing speeds, in general, provides better adhesion between layers, which is desired for solar panel covers.

Firstly, we printed a small 3D-printed plastic part with a small cavity where the photovoltaic panel could be secured safely. This small base part was printed with a black PLA filament. This structure was necessary to keep the experimentation consistent from cover to cover. The covers were printed from a transparent PLA material. Even though the material is transparent after the printing process the parts looked more translucent than transparent. After the fabrication process, the parts were placed above the base structure and tested.

5.6.3 Characterization setup

Firstly, the base structure with the photovoltaic panel were placed on a flat surface without any cover (Figure 5.23a). A high illumination lamp was directly illuminating the structure from above at 10 cm. Then we recorded the output of the solar cell using 4-wire measurements with a Precision Source/Measure Unit

(SMU) B2912A (Keysight Technologies, Santa Clara, CA, USA). The 4-wire measurement scheme eliminates the voltage error caused by the test lead residual resistance so that only the voltage drop across the device under test (DUT) is measured. The Keysight B2900A Quick I/V Measurement Software was used to automate the sweep measurements by connecting the SMU unit to a PC through USB. Afterwards, we covered the device with the 1mm thickness translucent PLA 3D printed part and recorded again the output of the device. This was followed by 2mm and 5mm thickness covers (Figure 5.23b,c). Lastly, we covered the device with a thick black cloth that absorbs most of the visible light and recorded the performance of the photovoltaic panel. Figure 5.24a presents the recorded I-V curves of the device under no cover, 1mm, 2mm, 5mm thickness covers and completely covered. Figure 5.24b presents the power generation of the device under the five conditions mentioned above with respect to voltage.

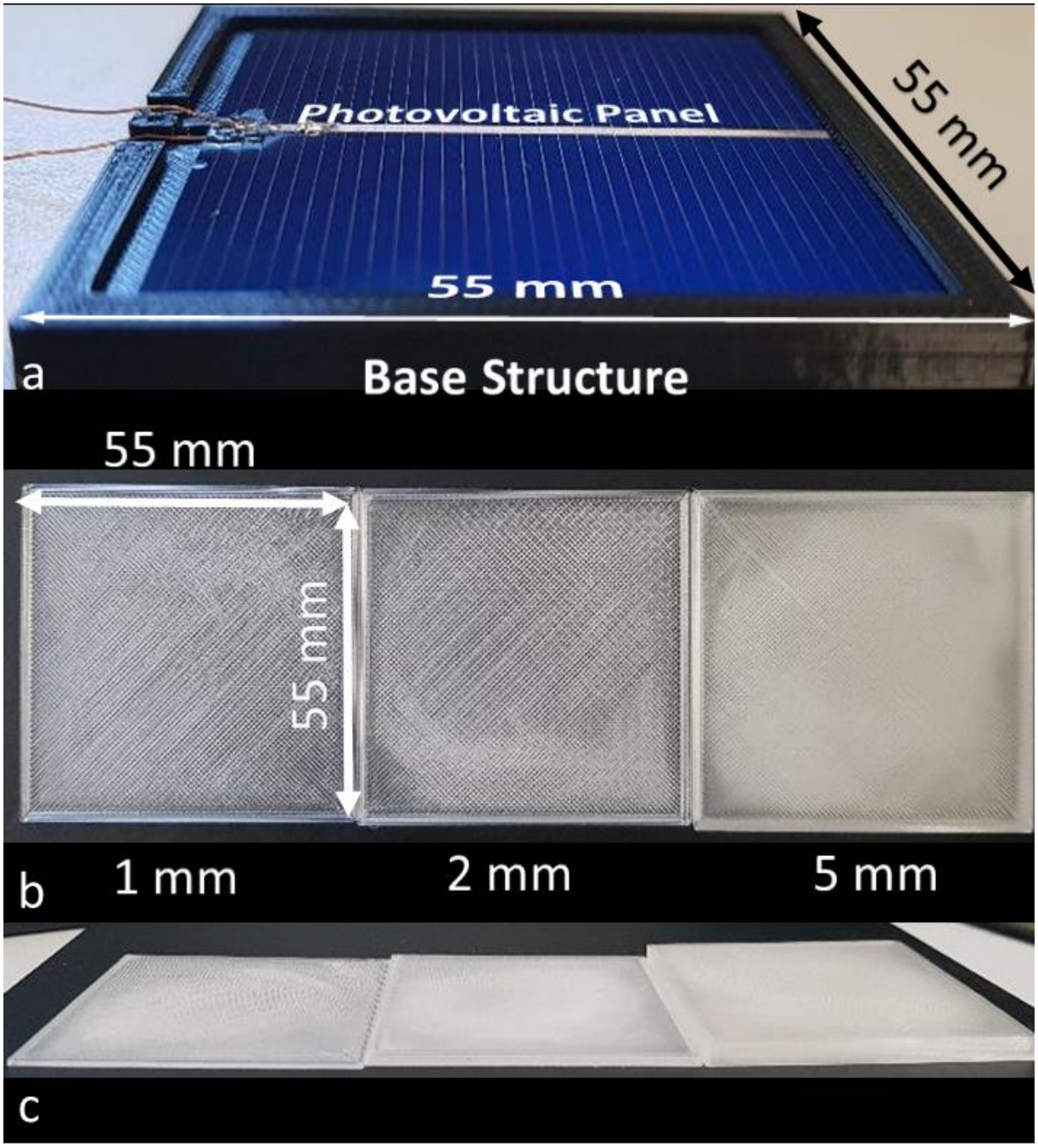

Figure 5.23 a) Photovoltaic panel placed on top of the base 3D printed structure. b) Top view of the 1mm, 2mm and 5mm 3D printed transparent covers. c) side view of the 3D printed covers [259] **Copyright © 2020, IEEE**

5.6.4 Results

As expected, the thick cloth absorbed most of the light, and virtually no output was detected by the SMU. The exact opposite could be observed when there was no cover, and all other results are compared with this as the reference point. From the experimental results, a clear pattern emerges as observed from Figure

5.24. The thickness of the covers plays a significant role in the effectiveness of the photovoltaic panel.

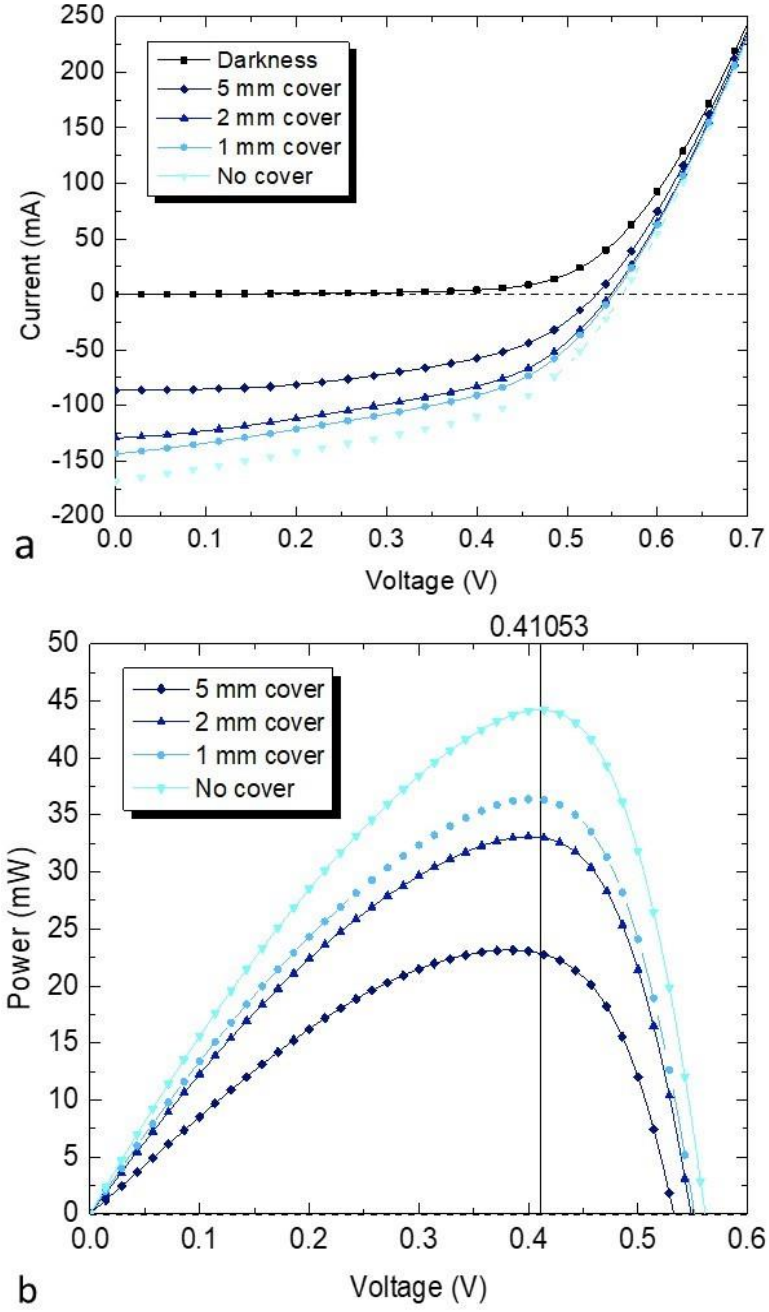

Figure 5.24 a) Graph representing the current with respect to voltage recorded from the solar panel covered completely, 5mm, 2mm, 1mm and no cover. b) Power with respect to voltage for 5mm, 2mm ,1 mm and cover. [259] **Copyright © 2020, IEEE**

In all settings, the output voltage reaches a special point as shown in Figure 5.24b: the maximum power voltage (VMPP). The output power reaches its peak (PMPP) when the output voltage is at VMPP. In all cases, at VMPP=0.41V, the device has the highest efficiency. From that point, we can compare different settings. When

the device was uncovered, it generated a maximum power of PMPP=43.8mW. Once a cover is introduced, the energy generated dropped. For the 1mm PLA cover, the energy generation dropped significantly with the PMPP measured at 36.4mW. The efficiency of the device dropped even further down to PMPP=33.1mW with the use of the 2mm cover. The 5mm thickness cover was found to drop the energy generation down to 23.1mW, the lowest value from all PLA covers.

As expected, all 3D printed covers have reduced the effectiveness of the photovoltaic panel in terms of power generation. The 1mm cover reduced the efficiency by 16.9%, the 2mm by 24.4%, and the 5mm by 47.3%. As table 5.4 shows, the covers have a clear reduction in the efficiency. This is expected as with increasing thickness of the material more photons are absorbed, resulting in a constant reduction of the energy generated. The 1 mm cover has the least effect on the power generation. Even that the 16.9% reduction on the ability of photovoltaic panel to generate power is considerable, we were able to power ten ICs consistently under those conditions. This arrangement also provided a significant protection of the device from mechanical stress, dust and other hazards.

Table 5.4 Photovoltaic Panel Performance. Adapted from: [259] **Copyright © 2020, IEEE**

COVER TYPE	**PERFORMANCE**	
	Power Output	Reduction
NO COVER	43.8mW	-
1MM	36.4mW	16.9%
2MM	33.1mW	24.4%
5MM	23.1mW	47.3%

This work presents a novel study of 3D printed transparent materials as protective cover for photovoltaic panels and their effect on the energy harvesting capabilities of such devices. The study presents the use and advantages of 3D printed protective covers for fragile photovoltaic cells. We observed that the 1mm thickness cover provides significant durability to the energy harvesting device with a small reduction in the performance of 16.9%. The device with this cover generates 36.4 mW. With this amount of power generated it is possible to power around 10 ultra-lower power ICs. This will alleviate some of the high demand energy requirements of robotics/prosthetics. The excess generated from the

device can be further stored and use in a later time. Also, this device can be used as a sensor for ambient light and/or time of the day. An extension to this work can be found in a collaborative effort using photovoltaic panels in an flexible Eskin approach[265].

5.7 Summary

This Chapter presented various novel works related to smart structures from tactile sensors to embedded electronics and energy harvesting devices. Major issues with traditional approaches are related to durability, flexibility, wear and tear, and wiring and it is possible to be resolved with the approach presented in this thesis. AM techniques show an ulternative method of producing and embedding sensors and electronics in tightly packed space such as a fingertip with some drawback in sensitivity. The parallel fabrication of the transducer and the sensing elements provide substantial durability to the tactile devices. Investigation of many materials was conducted resulting in a plethora of sensors. Alongside tactile sensing, energy harvesting devices were used to contribute to the autonomy of robotic systems.

The following Chapter presents modifications of commercial 3D printers used in this work to develop the various devices presented in this thesis. This includes both commercial systems and a newly developed closed-loop extruder mechanism for paste-like complex materials such as Ecoflex.

Chapter 6: Development of new extruder system

6.1 Introduction

3D printers have been heavily modified to expand their capabilities using a variety of methods depending on the desired purpose. Extruder mechanisms have been developed for deposition of pastes to develop interesting solutions for biomedical and electronic applications and were presented in section 2.5. These modifications are termed as Direct Ink Writing (DIW) extruder mechanisms. The recently developed DIW systems have focused heavily on optimizing the printing of materials with similar viscosities, leading to a narrow range of materials that can be used with the systems. DIW extruders, currently use direct drive systems which lead to uncontrollable deposition after start and stop commands, oozing, occasional inability to retract the material, and limitations on the size of the syringes that are compatible with the systems. Importantly, most of these systems can only print one material at a time and do not allow mixing multipart materials (e.g., nanocomposites) on the go, and thus cannot be used for advanced structures based on complex materials.

In section 5.3.2 we presented a 3D printing sensorised phalanx using such a system. Figure 7.6 in the Appendix presents the DIW extruder mechanism used for the deposition of the graphite ink. The extruder mechanism (Discov3ry Paste Extruder) is a commercially available DIW system that can be plugged in an available stepper motor driver on the circuit board of the 3D printer (Duet 2). The system used showed all the problems discussed above, and it was clear that such a system requires improvements as reliability was an issue.

To address and advance the current technology of such systems, this section focuses on a custom-made 3D printed DIW extruder (Figure 6.1), which utilizes a double extrusion mechanism and a pressure sensor for feedback. The DIW extruder

uses two stepper motors and off-the-shelf control electronics, resulting in an inexpensive system that is affordable even for hobbyists. The system is able to mix multipart materials in different ratios and print them to develop innovative smart structures. Materials such as Polydimethylsiloxane (PDMS) or Ecoflex can be printed with no need for manual mixing thus providing better control of deposition. The system shows no leaking issues compared to other systems while also being compact, lightweight and portable.

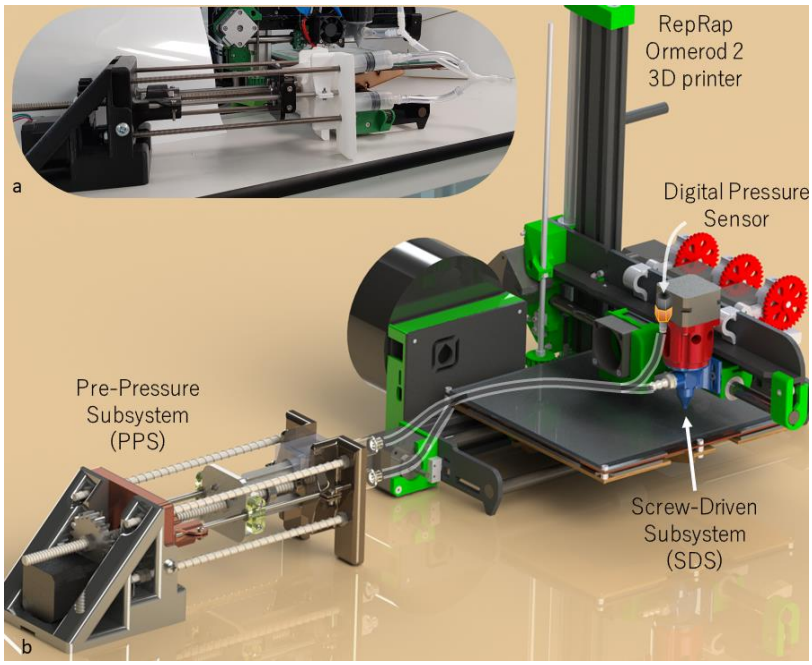

Figure 6.1 a) Fully assembled customized 3D printer with in-house DIW system, b) CAD representation of the custom 3D printer.

6.2 Design & fabrication of paste extruders

The DIW system can be divided into two subsystems that are complementary to each other. The first is a Pre-Pressure-Subsystem (PPS) (Figure 6.2) and the second is a Screw-Driven-Subsystem (SDS) (Figure 6.3). All the parts were designed in a CAD program (SolidWorks) and most of these were fabricated using an FDM 3D printer (S5, Ultimaker).

6.2.1 Pre-Pressure-Subsystem

The PPS system, shown in figure 6.2, uses a stepper motor to convert rotating motion to linear. Specifically, the PPS is designed to mount two syringes, one placed on the top and a second can be inserted from the bottom of the PPS (Figure

6.2a, 6.2b). The syringes are attached with female Luer to Barb hose adapters and are connected together with flexible tubes (8mm external diameter Flexible PVC, RS Components) and a Y-connector. The common output from the connector is connected to a tube and its ending splits again with another Y-connector. One end is connected to a pressure sensor (PX3AN2BS100PAAAX, Honeywell) and the second is connected to the inlet of the SDS system.

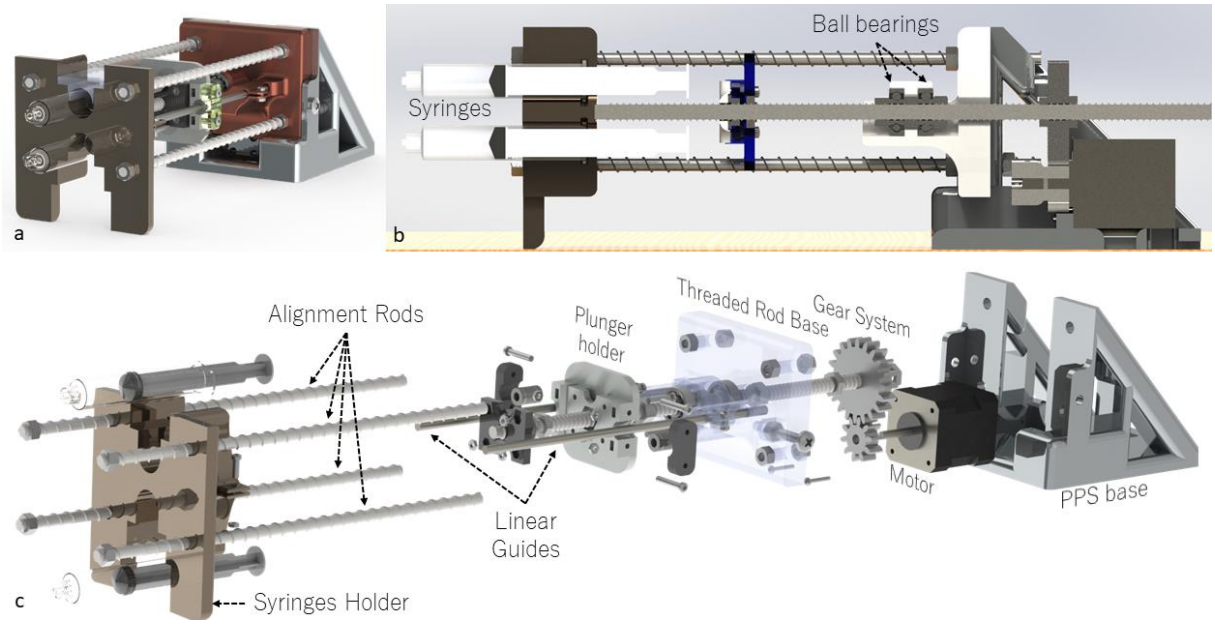

Figure 6.2 a) CAD design of the assembled PPS system. b) Cross Section view of the PPS system. c) Exploded view of the PPS system.

The syringe barrels are placed on a large piece of PLA support structure which incorporates the syringes' holders at the front of the PPS system (Figure 6.2c). The barrel parts of the syringes are secured and cannot move or rotate. The PPS core is an 8mm threaded rod (leadscrew mechanism), as shown in figure 6.2. The threaded rod is attached to a 2:1 ratio 3D printed drive gear system. The driving gear is connected to a Nema 17 stepper motor, that drives the system. A leadscrew is located in the middle of the threaded rod and is attached to two pieces of PLA support structure that enclose the leadscrew. The largest of the two pieces is designed to attach the two syringe plungers whereas the sides of the part are attached to two linear bearings which restrict the entire structure from rotating but allow the system to move forwards and backwards along the threaded rod's length. The threaded rod is attached to the threaded rod base piece that has a narrow gap for the rod to barely go through. Two roll bearings are placed at the opposite sides of the narrow gap but are not able to go through. Two nuts then

follow and are firmly attached next to the bearings. This arrangement allows the threaded rod to rotate freely but restricts movement backwards or forwards from its position (Figure 6.2b). The three large PLA pieces, namely the syringe base, threaded rod base and motor base, are attached to each other using four smaller threaded rods and nuts to allow for adjustments and better alignment of all the parts of the PPS. This means that once the motor rotates, the plunger holder (Figure 6.2c) can travel back and forward alongside the length of the threaded rod and in turn, move the plungers of the syringes. This pressurizes the material in the syringes and pushes or retracts the material.

6.2.2 Screw-Driven-Subsystem design

The material in the syringe travels from the PPS through the tube and ends in the inlet of the SDS. The SDS pushes the multi-material out of the outlet onto the bed of the printer. The SDS is a screw-based mechanical design (Figure 6.3a). Figure 6.3b depicts the fully assembled SDS design in CAD. The system's crucial component is a helical/screw structure, as seen in the cross-sectional view in figure 6.3c. The shaft of the screw passes through an oil ring that prevents printing material from leaking upwards and out of the system and allows the part to rotate with minimum friction. The shaft of the screw is then attached to the motor connector piece which itself is attached to the motor shaft. This arrangement transfers the rotation of the motor shaft to the helical/screw part in a 1:1 ratio. The oil ring is epoxied on the gear housing part of the SDS. The housing part is attached to the rotor and the nozzle part via M3 bolts and nuts. The nozzle piece of the system has two gaps on each side for M3 bolts which are attached to the 3D printer's x-carriage. The gaps allow the system to slide up and down to adjust the nozzle height on the printer.

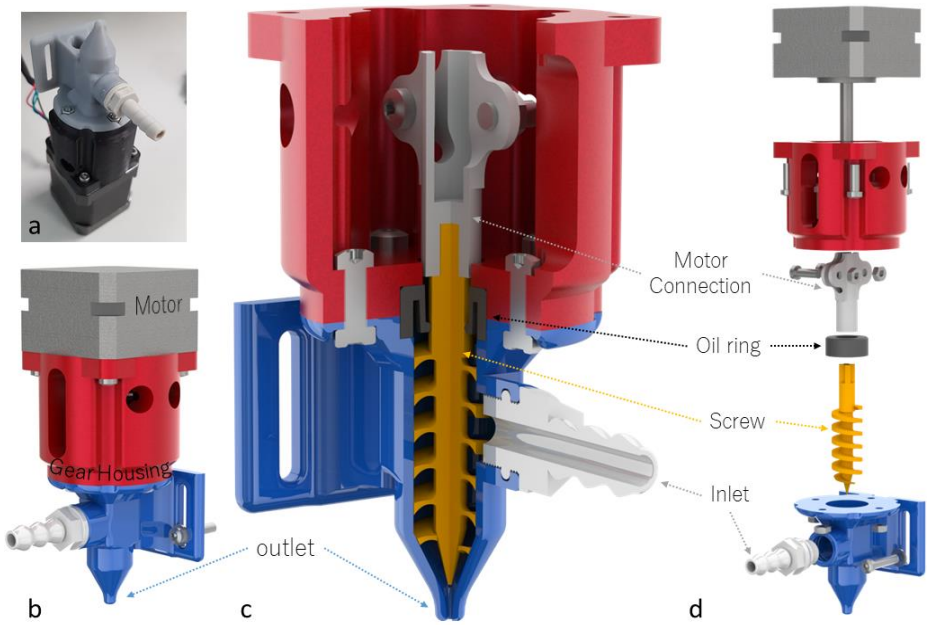

Figure 6.3 a) Fully assembled SDS. b) Assembly CAD design. c) Cross-sectional view of the subsystem. d) Exploded view of the subsystem.

The chamber that houses the screw is cylindrically shaped and is 12 mm in diameter with a total length of 40 mm. In the last 12mm, the chamber's diameter decreases smoothly. That reduces the need for high pressure extrusion due to Poiseuille's law as the length of the material that needs to travel from the source of the pressure (SDS helical screw) to the outlet is less than 3 mm. The screw's diameter has a 0.2 mm offset from the chamber's walls. The smaller the gap between the chamber's wall and the screw, the harder it will be for material to slip through the gap. This small gap also prevents backflow and helps to build pressure for the extrusion of the material. The screw has a pitch of 5mm and six complete revolutions. Two nozzles were fabricated for the purpose of testing the system's performance under different outlet diameters. The first nozzle has a diameter of 1mm and was produced using a FDM 3D printer and the second is a 0.5mm nozzle produced using a Stereolithography (SLA) 3D printer.

The proposed SDS system offers substantial advantages over the Bowden-tube systems, which is typically used by common 3D printers. The Bowden tube-based systems have drawbacks such as difficulty in controlling the amount of extruded material. Further, the need for pressure to build up in these systems and the large distance between the syringe and the nozzle cannot produce accurate translation of the motor's rotation to material extrusion. These problems are addressed by

the SDS mechanism, which is also advantageous over other mechanisms for application of pressure such as pneumatic systems. Such systems also have difficulties related to integration with existing electronics in the 3D printers, require pressurized cylinders/compressors, and occasionally do not reproduce the same flow rates. Further, pneumatic systems are often expensive and immobile. The system presented here demonstrates a portable alternative with pressure feedback for pressure control and monitoring.

6.3 Electronics and integration of extruder on 3D printer

The PPS and SDS are controlled from two different electronics boards. The PPS is controlled by a custom-made electronics board based on an Atmel microcontroller, while the SDS is controlled via the printer's electronics. The extruder mechanism was attached to an open-source 3D printer (Ormerod 2, RepRap) which was modified for the purpose of integration. The SDS and the 3D printer are controlled by the Duet 3 Main Board 6HC (Duet3D). The stepper motor of the SDS is connected to the second extruder stepper driver. The Duet similarly controls the SDS stepper as it controls other FDM feeder motors. In the firmware, a second extruder is enabled with cold extrusion, to bypass the detection of a heating element at the nozzle, and the steps per mm is set to 80 steps per mm. The explanation of how this number is derived can be seen in Appendix B.

For the PPS, a custom PCB was designed, and an Atmel microcontroller was programmed to control the system. Figures 7.7 and 7.8 in the Appendix present the schematic and PCB layout, respectively. The stepper motor of the PPS is connected to the PCB and is driven by a DRV8825 stepper motor driver (JYOPTO). The DRV8825's digital input pins are connected to the microcontroller and the system was set up in half-stepping mode. The pressure sensor, which is located near the inlet of the SDS, provides the pressure feedback for the PPS and it is connected to the Atmel microcontroller. The Duet board and the Atmel were connected via one Input-Output (I/O) pin, where the Duet controls the pin's digital output, and the Atmel receives the information. The Duet board can set the pin to 'high' to indicate that the 2nd extruder is currently active and 'low' to indicate that it is inactive. The PPS also utilizes an end-stop switch which, when pressed, allows the system to recognize that the material in the syringe is depleted. To this

end, an LED is used as a visual indicator. A custom-made GUI made in Visual Studios was programmed in C# to visualize the pressure, control the PPS, and record the data and state of the system.

6.4 Performance of 3D custom-made DIW extruder

Two different material formulations, targeting different applications, were printed using two different nozzle diameters (0.5mm and 1mm). The first material tested was a food condiment (mayonnaise, Hellman's Real) and the second is a two-part Silicone rubber (Polycraft GP-3481F RTV, Polygraft). The rheological properties of these materials are significantly different to each other, and hence they provide a good challenge to the system. The food condiment's viscosity was about 65,000 cp for low revolution per minute (rpm) of the spindle and decreases with increasing rpm and finally settles at 5000 cp at 100 rpm. The base material of Silicone rubber showed an average viscosity of 39,000 cp before adding the catalyst. To evaluate the system, we also varied the printing parameters such as pressure, printing speed and material flow.

The developed system was characterized for the line width deposited using each set of printing parameters that we altered. Two test structures were used for the evaluation of the developed system. The first test structure design was a model containing 5 straight lines with length of 10 cm, width of 1 mm, and height of 0.5mm. Both nozzles (1 mm and 0.5mm) were used for this design. The second test structure is a CAD design containing 5 lines with 0.5mm width, 10 cm length, and 0.25mm height and it was tested only with the 0.5 mm diameter nozzle. It is generally suggested to print using a layer height that is half the nozzle's diameter and this is the reason for the difference between the two test designs. A few printing parameters were constant in all the characterization processes. Those are: all walls were removed from all settings (bottom/top, sides), 100% infill, heated bed was off, and printing was carried out at ambient temperatures.

6.4.1 Pressure variation

Firstly, the materials were tested under pressure without printing to extract the suitable pressure range. Each material was mounted on the system individually,

pressure was slowly increasing to observe when and if the material would start oozing from the nozzle. The food condiment was not oozing from the nozzle for pressures up to 1 PSI. In contrast, the silicone-based material started oozing at pressures of 0.5 PSI. Following this, the constant pressure of 0.5, 1 and 1.5PSI were used for the models mentioned above. The rest of the printer parameters were unaltered, and they were: printing speed was set to 5mm/s and material flow was set to 100%. In total, 18 prints were obtained to extract the information for all pressures and system arrangements (3 pressure settings, 2 materials, 3 printing setups). The printing setups were, the model with 1mm width design lines with the 1mm nozzle, the 1 mm width design with the 0.5 mm nozzle and the 0.5mm design with the 0.5 mm nozzle. Each print was photographed, and each line was analysed for its average width and all 5 lines were averaged out.

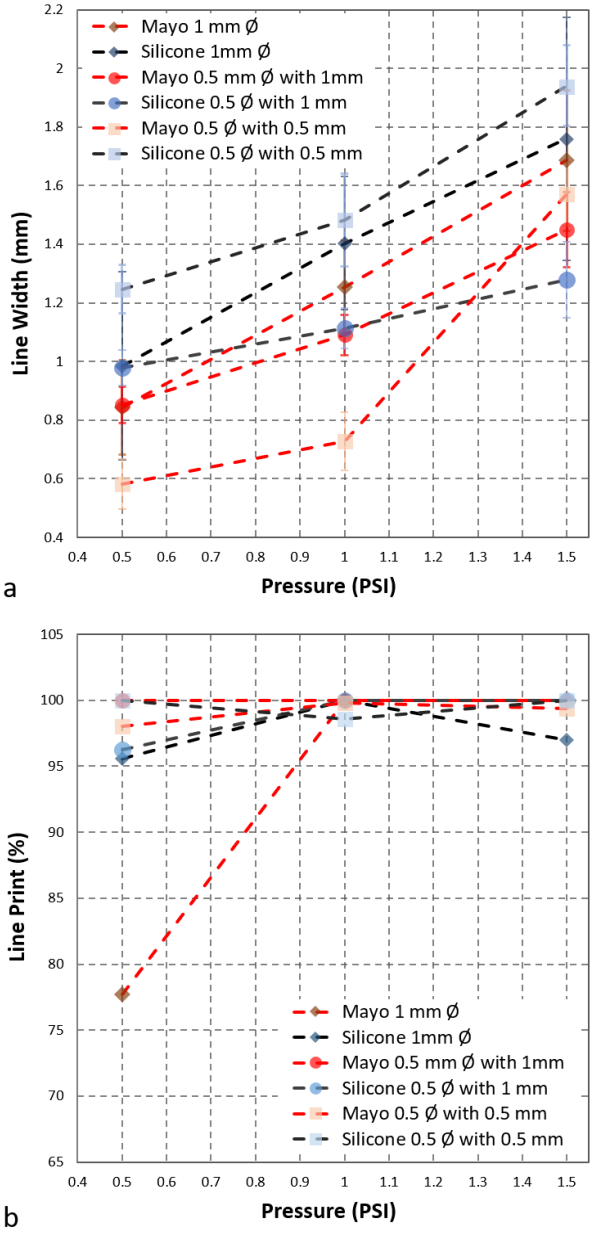

Figure 6.4 Results of printing at different pressures

a) Average line width of 5 printed lines with respect to pressure, b) Percentage ratio of printed lines length to designed length with respect to pressure.

Figure 6.4a shows the average printed line width with respect to pressure for each printing setting. The results show that the line width of both materials (silicone and food condiment) increases linearly with increasing pressure. The average rate of change and standard deviation for the condiment were 0.8 mm/PSI and 0.123 mm respectively and were 0.6mm/PSI and 0.18mm for silicon material. Figure 6.4b shows the percentage ratio between actual printing length over designed line length. In some cases, the prints did suffer from insufficient flow of the material, resulting in prints having droplet like formation instead of an actual line. The percentage print varied with pressure but also with the material. The higher the

pressure, the more is the likelihood of the print lines being continuous and uniform. Figure 7.9 in the Appendix presents all these printed structures.

6.4.2 Printing Speed

The second parameter used to characterize the system was printing speed. This was done to see how fast the printer can print reliably and the effect the faster movement of printer has to the line width. Each material was tested separately with the PPS providing a constant pressure of 1 PSI. The printing speeds tested were: 2, 5, 10 and 20mm/s and a total of 24 prints were obtained. Figure 6.5a presented the average linewidth for all 5 printed lines with respect to printed speed. Figure 6.5b presents the percentage ratio between printed line length over designed length with respect to printed speed. These results show that the condiment material is less affected by printed speeds. On average, all printed lines were not discontinuous, and the deviation is relatively low (average deviation for all print setting of the mayo is 0.088mm). Materials with rheological properties such as the condiment are affected by the SDS system as the rotation of the screw can provide enough pressure to the material for extrusion. In this scenario, the PPS acts as a tank for the SDS to control the deposition. The screw acts as an isolated piston and it deposits the material uniformly, as long there is enough material and pressure in the inlet. Therefore, speed does not have a significant effect on the prints. The rotation of the screw matches the printer's movement and therefore the amount of material deposited is the same.

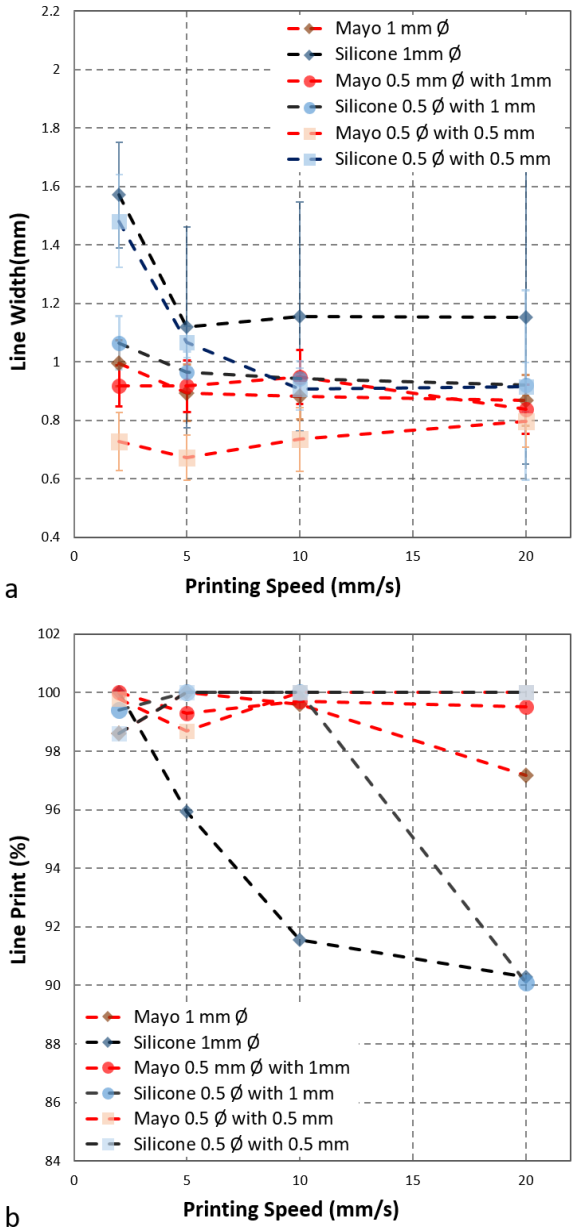

Figure 6.5 a) Average line width with respect to speed b) percentage ratio of printed lines length to designed length with respect to printing speed.

In contrast to the above, the printing of silicone is affected by the speed. As the printer moves faster, the fast rotation of the screw cannot fully compensate for material that the PPS is contributing. Therefore, for the same print, lesser material is extruded from the nozzle at higher speeds. On average, the line width decreased at a rate of 0.016 mm per mm/s, while the deviation from low speeds to high speeds increases rapidly. This further worsened when the print was evaluated for the percentage length printed over designed length. At low speeds, silicone has little droplet-like formation on the printed bed, but the effect is regular once the speed increases.

6.4.3 Increasing Flow

The last parameter tested was the percentage flow of the material. This setting changes the screw rotation percentage per line. This testing presents the effect of the ratio of revolutions of the SDS system per line. Five different flow rates were tested, namely, 10%, 20%, 50%, 100% and 150% resulting in 30 different prints. Figure 6.6 presents the data acquired from these tests. Figure 6.6a shows the line width with respect to percentage flow. The percentage ratio of actual printed length over the designed length with respect to flow percentage is given in figure 6.6b.

This set of experimentation shows that SDS has greater influence on the mayo, while PPS can influence the flow of silicone. In fact, the line width of the silicone does not change significantly with increased flow. In contrast, line width of mayo changes with the increase of flow at a rate of 0.0047 mm per flow percentage. The relation between the flow and the line width is linear and the deviation for mayo is 0.11 mm. As the screw rotates more times per line, more material is deposited on the printer's bed. This is magnified even further when the percentage printed lines are compared to the expected. In general, the flow of the materials was too low to print continuous lines and droplets were observed in most of the print settings, especially for the prints with layer height of 0.5 mm. Once the material flow was high enough all prints were continuous.

In contrast to condiment material, silicone could flow in the SDS chamber, resulting in material flow. The SDS does not provide a significant pressure drop in the chamber for silicone, and can flow from an inlet to an outlet, at this pressure. The pressure difference between inlet and outlet for the silicone is mainly provided by the PPS (1PSI). Even though the screw seems to have no effect on the line width, it can still affect the deposition of the material. As can be seen in figure 6.6b, the faster the screw rotates, the less likely a droplet can form. That is caused by the screw's ability to push the material out towards the nozzle. At 10% flow silicone is printed in more droplet-like forms. Once the flow setting was increased the droplet formation was minimized.

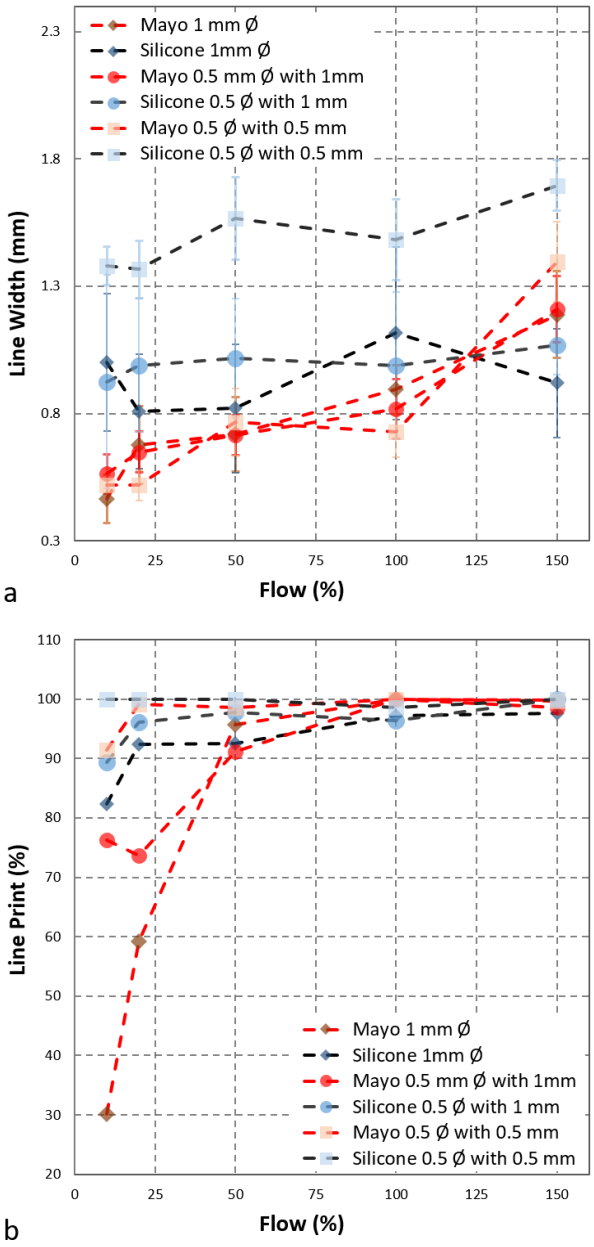

Figure 6.6 a) Average line width with respect to percentage flow b) Percentage ratio of printed lines length to designed length with respect to percentage flow.

6.4.4 Nozzle diameter

The effect of the nozzle diameter has on the printing quality could be derived from the above experiments. For example, by comparing different nozzles (1mm and 0.5 mm diameter) with the same CAD model (1mm width lines at 0.5 mm layer height), it is easy to see the effect of nozzles have on the printed lines. In fact, we observed that the nozzle diameter has a significant effect on the quality of the print. From Poiseuille's law, the smaller diameter outlet used, should reduce the flow of the material (under same pressure) resulting in deposition of lesser

material on the bed. Both nozzles at low pressure show similar results but once the pressure increases, the width of the lines start to diverge with the wider nozzle diameter printing thicker lines compared to the narrower nozzle. The 1mm nozzle showed an increase in line width of 0.841 and 0.775 mm/PSI for mayo and silicone, respectively. For the 0.5 mm diameter nozzle, the rates were 0.596 and 0.3mm/PSI for mayo and silicone, respectively. Also, the narrower nozzle has lesser deviation in each pressure setting, thus increasing the uniformity in deposition.

The nozzles follow a similar trend with respect to speed. The nozzle diameter shows little to no effect on the line width when the food condiment is considered. For mayo, the SDS system significantly influences the material deposition, therefore, there is no significant change based on the nozzle diameter. Silicone has a small difference in the line width, with the narrowest nozzle depositing thinner lines. Likewise, when flow is considered, the nozzle diameter seems to play no role for the mayo as the difference in the print for both nozzles is insignificant. The nozzle diameter does not affect the line width but can increase the reliability of the printing as it decreases the amount and length of discontinuous lines. The same is true for the silicone. The narrowest nozzle does not affect the printing lines width but decreases the gaps between the prints.

6.5 Autonomous manufacturing

To illustrate the capability of the developed system, a variety of test structures were fabricated as described below.

6.5.1 Two-part elastomer mixing and printing

A thin smiley face-like structure was printed using the developed 3D printer. For this, we used Ecoflex - an elastomer with two parts that are required to be mixed for proper functioning. It is commonly mixed in 1:1 ratio and widely used as substrate in flexible electronics or to develop soft robotic structures. The CAD design resembles a face with two cheekbones, to evaluate the capability for z-axis printing of Ecoflex. The thickness of the smiley face was 0.6mm and the bone cheeks reached a height of 2.8mm with the face covering a circular area with

diameter of 80mm. The design was printed using 0.2mm layer height at 100% infill with a printing speed of 5mm/s.

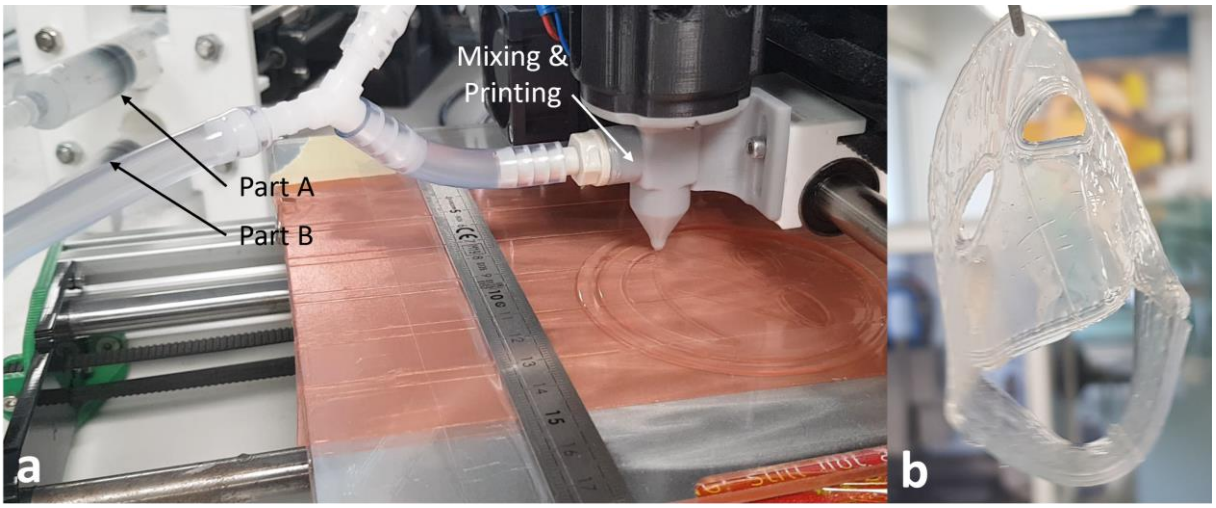

Figure 6.7 Printed smiley-face without premixing. a) printing to realize the structure. b) final result of automatic 3D printing of two-part elastomer.

To fabricate the face design, the PPS was mounted with two identical syringes, each containing one part of the two-part elastomer at the same volumetric marker. This resulted in a 1:1 of part A and part B, mixed on the go inside the SDS chamber and printed on the surface of the 3D printer bed. For faster curing, the bed of the printer was heated at 40^{o}C. This also ensured that the subsequent layers printed on top have a solid structure for better resolution. The total time of the print is approximately 1 hour. Once the print was finished, the fabricated design was left for about 30 minutes at 40^{o}C on the print bed. Figure 6.7a shows the printing of two-part elastomer and figure 6.7b shows the completed 3D printed face-like structure.

6.5.2 Color Mixing

To further validate the ratio printing and mixing procedure, a CAD file for a disc-like structure was generated. Two different prints were carried out to demonstrate the mixing capabilities of the system. The PPS was mounted with two syringes one containing a blue color paint and the second containing a white color paint. For the first print, both syringes have an inner diameter of 20 mm, therefore the ratio between the blue and white was 1:1. Figure 6.8a shows the result of the printing process. The second print is the same disc design, but with different diameter syringes. The ratio for this print between the blue and white colors is

10:7. Figure 6.8b shows the result of this print, which clearly shows a different mixing ratio as the color of the printed structure has strong presence of blue color.

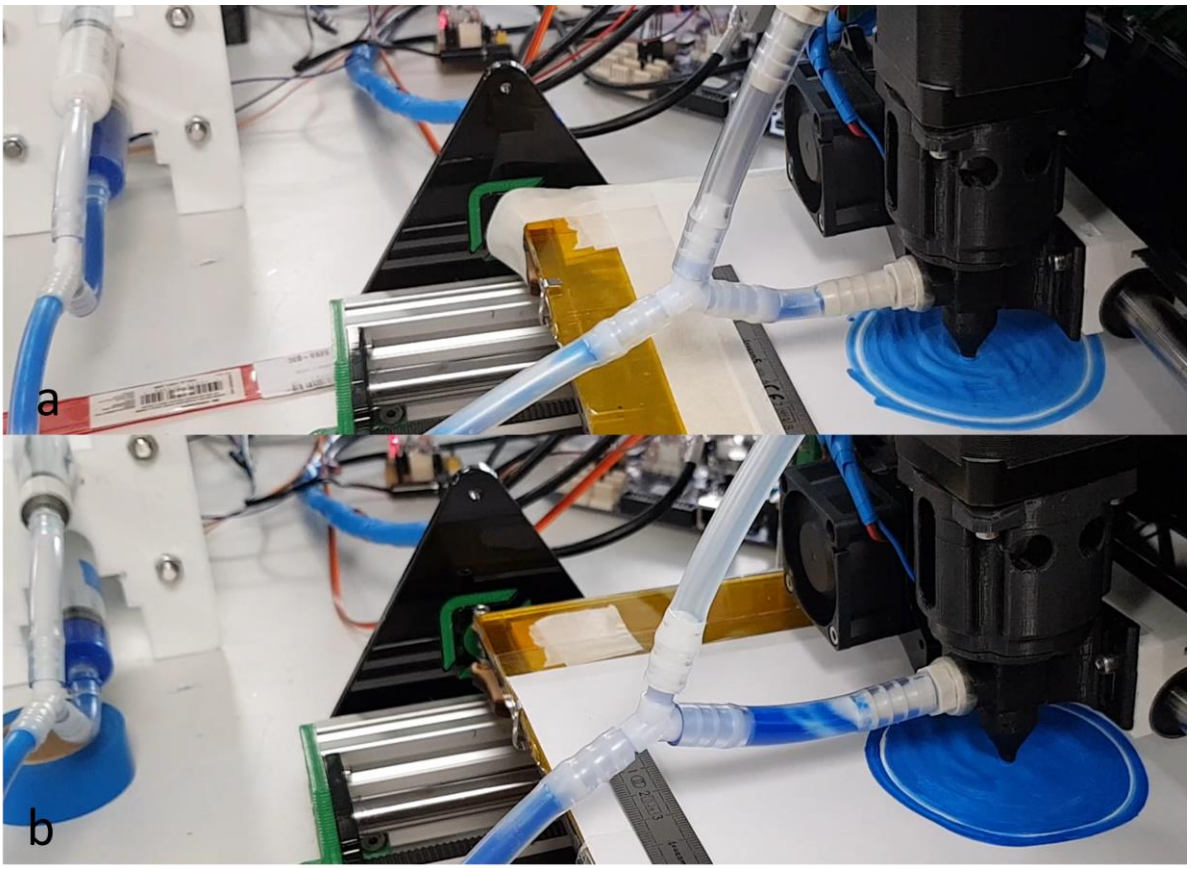

Figure 6.8 Print of disk-like design on paper while two materials are mixed on the go, a) 3D printing of 1:1 ratio of dark blue and white colours b) 3D printing of 10:7 ratio of dark blue and white colours.

6.5.3 Food Based material printing

A major advantage of 3D printing is its versatility and possibility to alter the models without the need for fabricating different moulds every time the design changes. This is further advanced with printing of different types of materials. For example, the developed system was evaluated for its capability to print food-based materials such as mayonnaise and melted chocolate and the printed structures are shown in figure 6.9.

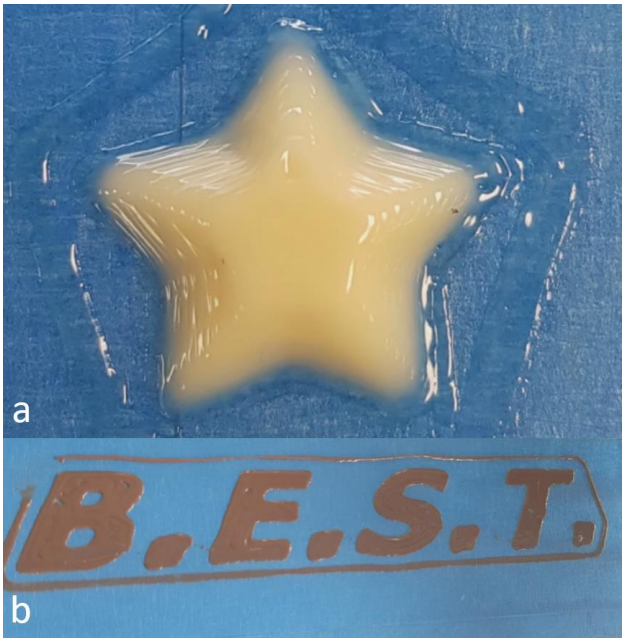

Figure 6.9 Print of food related materials a) Star shape food additive b) 3D printing of 'BEST' with melted chocolate.

6.5.4 Fully 3D printed embedded Tactile sensors

In robotic applications, a major challenge is the fabrication of tactile sensors that are robust, soft, and low-cost. The system provides the ability to produce such tactile sensors in an automated process. To demonstrate this, we obtained a 3D printed tactile fingertip using the DIW system in combination with the FDM nozzle on the printer. The device has three embedded capacitive pressure sensors located at the tip, left, and right sides of the fingertip. All materials, including the encapsulation, conductive layer, and dielectric (silicone), were 3D printed. The bottom part of the finger is made from PLA. The conductive plates of the sensors are fabricated using conductive PLA (Proto-pasta) filament using the FDM nozzle. Once the base and bottom electrodes were printed, the encapsulation layer made from TPU was printed using the FDM nozzle. The device has three cavities which were filled with dielectric material using custom-made extruder (Figure 6.10a). After this, the material was left to cure for 3 hours, while the heated bed was set to 40^{o}C. After this, a masking tape was placed on the surface of the dielectric layer, as printing directly on top of the dielectric was found to be challenging. Then, the printer continued printing the top electrodes and once those were printed, the material was changed to TPU to encapsulate the entire structure resulting in a soft 3D printed capacitive tactile finger with three

embedded force sensors. Figure 6.10b shows the finger pressed and the response of the sensor.

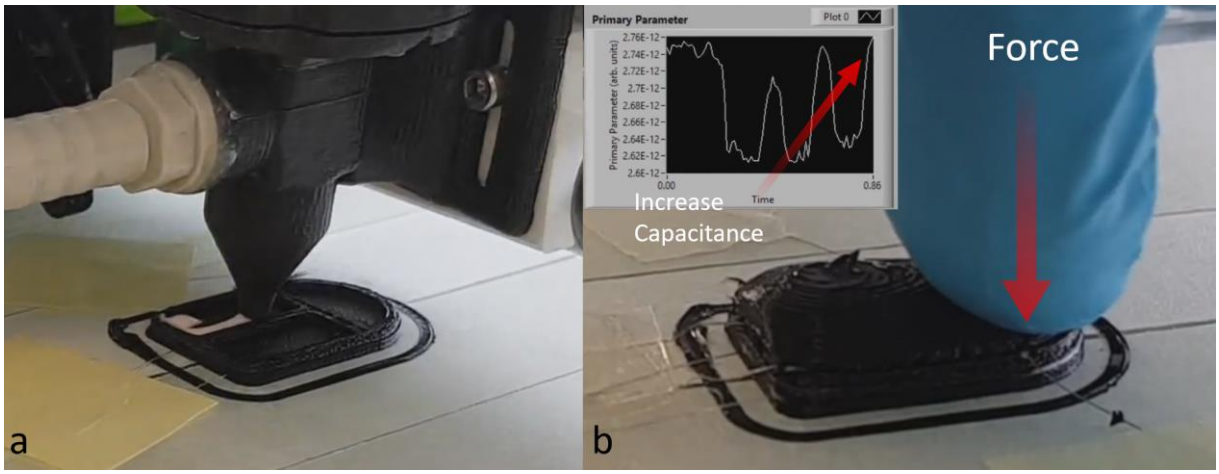

Figure 6.10 3D printed phalanx with embedded capacitive touch sensor. a) printing of the dielectric layer of the sensorised phalanx. b) testing of the sensorised phalanx for its response at different applied pressures.

6.5.5 Characterization of fully 3D printed tactile sensors

To further validate the system, five fully 3D printed sensors where fabricated similar to the one described above with only one difference. The fingers had only one capacitive sensor (the separation was removed therefore forming only one sensing structure). The five fingers were tested for dynamic and static response.

Figure 6.11 presents the dynamic response of the five sensors. For each sensor a force of 2N was applied for 7 consecutive cycles, then 5N and lastly for 9N.

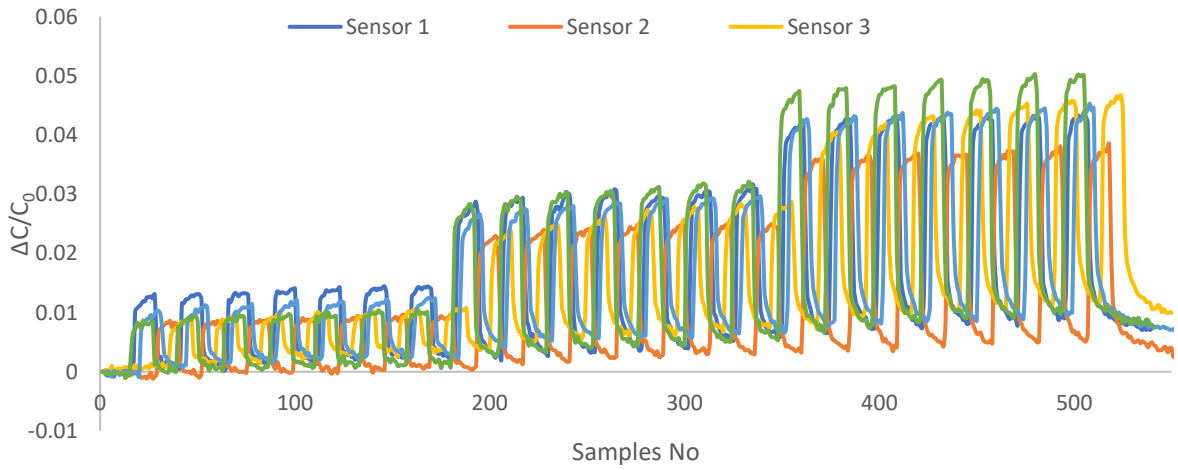

Figure 6.11 Cycling response for five fully 3D printed tactile sensors

Figure 6.12 presents the static response of the five sensors. All sensors show similar response in the tested range of 0N up to 11N. The sensitivity of each device is presented in table 6.1. The average sensitivity of the devices is 0.00406 N^{-1} with an average deviation of 0.000362.

Table 6.1 Sensitivity of the five devices in the entire range of testing

Device	Sensitivity (N^{-1})
Sensor 1	0.0036
Sensor 2	0.0037
Sensor 3	0.004
Sensor 4	0.00414
Sensor 5	0.0049

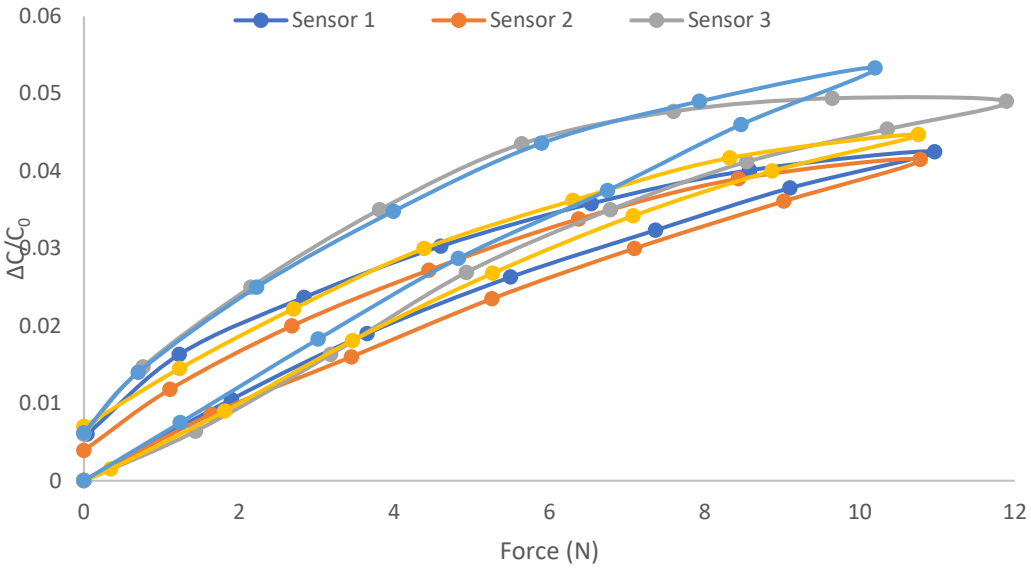

Figure 6.12 Static response of the sensors for force between 0N-11N

This presents the superiority of the approach of 3D printing tactile sensors using the above extruder mechanism, compared to previous approaches of drop casting the dielectric or/and electrode. The uniformity in the response shows not only the possibility of automation in smart structures but also the reproducibility of the results.

6.6 Summary

The current state-of-the-art FDM 3D printers are lacking the tools needed to fabricate complex/intelligent and smart structures while being cost-effective. Other 3D printers with similar capabilities are expensive and bulky in comparison. To overcome the limitations of FDM printing, a new 3D printing extruder

mechanism is presented in this chapter. The developed printer can print filaments and paste-like materials in the same print, while utilizing a pressure sensor for feedback. The system utilizes the mounted syringes with different barrel diameters to show mixing of multipart and multimaterials (in desired ratios) on the go and print them to enable complex 3D smart structures. The results show the extruder mechanism can handle diverse materials with different rheological properties. Furthermore, the system is free from previous common problems to direct drive, Bowden tube, and pneumatic DIW systems such as uncontrollable deposition, leaking, and delay between initiating printing and material deposition on the bed. The developed system does not rely on bulky equipment such as compressors, and thus offers better portability due to its reduced size and weight. The presented extruder mechanism is also capable of manufacturing complex structures in an automated manner and can be used in many fields from food decoration to complex electronics and robotics.

Chapter 7: Conclusion and Future work

7.1 Conclusion

The rapid progress in the development of smart structures in recent years pave the way for the future society. Additive Manufacturing, in particularly, has infiltrated most industries due to its versatility. The field of robotics, especially, benefit from the advancement in 3D printing as it allows complex designs to be manufactured seamlessly. Multimaterial printing can provide more functionality to the printed structure, enhancing them with sensors, embedded electronics, interconnects and energy storage capabilities. These active elements can drive the next industrial revolution of smart devices using AM as the core element. As an example, a robotic 3D printed hand and wrist was developed and equipped with power energy harvesting devices, tactile sensors and embedded electronics.

In this regard, various sensors, with different designs and materials were explored. A variety of different fabrication techniques were examined. State-of-the-art 3D printing mechanisms were used, and weaknesses and shortcomings were identified, while presenting alternative arrangements.

The following are the significant outcomes of the research.

1. The first reported 3D printed hand with intrinsic soft capacitive sensors with the accompanied electronics embedded in the phalanx of the fingertip. The fingertip's design is presented in sections 3.3.1.2 and in section 5.3.2 the fabrication and performance can be seen. The tightly integrated sensing within the 3D printed structures could pave the way for a new generation of truly smart material systems. The fabrication process presented introduces a cost-effective alternative method for tactile sensing systems that otherwise require complex, expensive, and specialized equipment. In this regard, compared to the state-of-the-art robotic or

prosthetic hands, the presented approach could lead to robust and affordable hands with more functionalities. Furthermore, the multimaterial 3D printing methodology offers efficient use of 3D space through embedded components.

2. This thesis emphasises the advantages of fabrication of the packaging and the sensing elements in one single step resulting in a durable arrangement. In this thesis, sections 3.3.2 and 5.4, a novel sensorised insole with most of the surface area occupied by transducing elements, was presented. This has the potential to be used in anthropomorphic robotic systems and wearables where extreme load conditions are expected during walking or standing, while providing sensory feedback. The sensors were tested for loads up to 1000 N, which is the equivalent to a load it would experience when an above average male adult was standing on one leg and his toe. This approach can be used not only for robotic systems but also in wearables to monitor the performance of athletes and in health/rehabilitation applications.

3. A novel 3D printer, able to print filaments, multipart and multimaterials without the need of premixing complex materials at different ratios. This system was developed to overcome issues with state-of-the-art multimaterial 3D printers and was described in detail in section 6.

3D printing technologies presents a new methodology for the development of new smart structures that could not be produced by other means. That includes practical solutions to everlasting problems with tactile sensing. This approach has the potential to overcome problems with wear and tear, wiring and electrode bonding in traditional Eskin approaches, while simultaneously being attractive due to ease of customization, simplicity of manufacturing, low-cost, durability, and resource efficiency.

7.2 Future work

The focus of this work is based in the development of smart and intelligent structures for robotic applications. 3D printing is a relatively recent manufacturing technology and is constantly evolving and attracting many industries and

researchers. The progress in 3D printing techniques drives the field to more and more unique uses from decorative structures to fully 3D printed houses, from scaffolds to tactile sensors and more. However, various challenges still lay ahead.

From sensors point of view:

1. Improvements with the adhesion between different materials and processes are needed. It has presented a significant challenge to overcome as masking is non-ideal. Masking can affect the performance of the sensor and can introduce variation in the response from sensor to sensor.

2. The sensitivity of the devices shown in this thesis can be further improved with the use of composite materials. The packaging can reduce the sensitivity of the devices and improving the sensitivity would be beneficial for fine texture detection.

3. Increasing the number and types of tactile sensors to develop stack sensing arrays (such as capacitive and piezoresistive) that could provide multiple tactile information. Also, the design of the sensors can be done using sophisticated algorithms such as generative design to further improve the overall system.

From 3D printing tools point of view:

1. 3D printing processes resolution can still be considered low. The diameter nozzles of FDM printers, currently, do not offer a resolution that is needed to match the human skin structural complexity. This could resolve some of the issues mentioned above.

2. Enhancing the 3D printing extruder developed and presented in chapter 6 with a heater and thermistor for even more complex materials that need specific temperatures. UV light attached to the nozzle could provide an automated method to cure photocuring materials.

From 3D printed smart structures and towards anthropomorphic robotics point of view:

1. The robotic hand and wrist structures printed with a single material (PLA) can be enhanced with the use of multimaterial printing. 3D printed capacitors or batteries can be printed simultaneously in the structures of the hand. This will lead to parts having the ability to store energy and elevating the need for traditional batteries for better autonomy and weight reduction.

2. Utilize the current knowledge and scale up towards anthropomorphic and biomimetic robotic systems with intrinsic sensors and embedded electronics. This can pave the way for autonomous systems from robotaxis to robotic nurses and smart cities.

APPENDIX

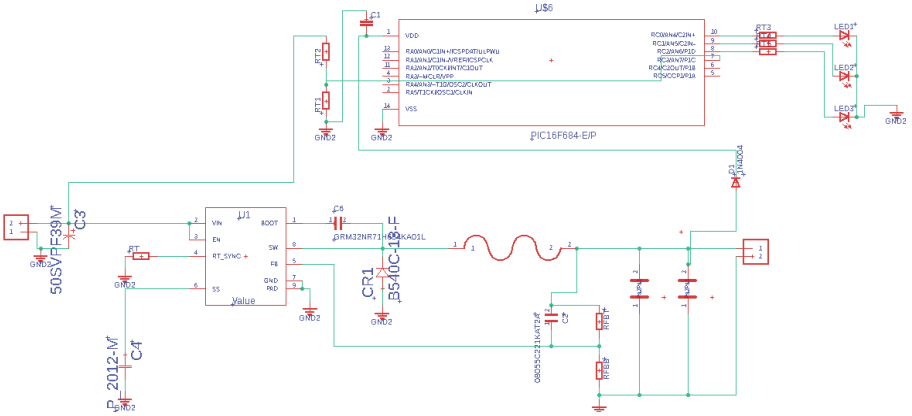

Figure 7.1 Power management schematic

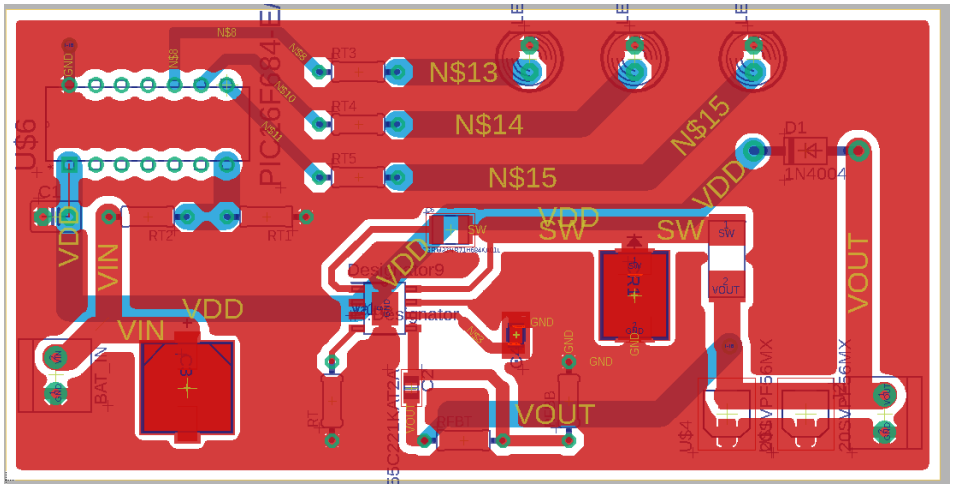

Figure 7.2 PCB Layout of power management circuit

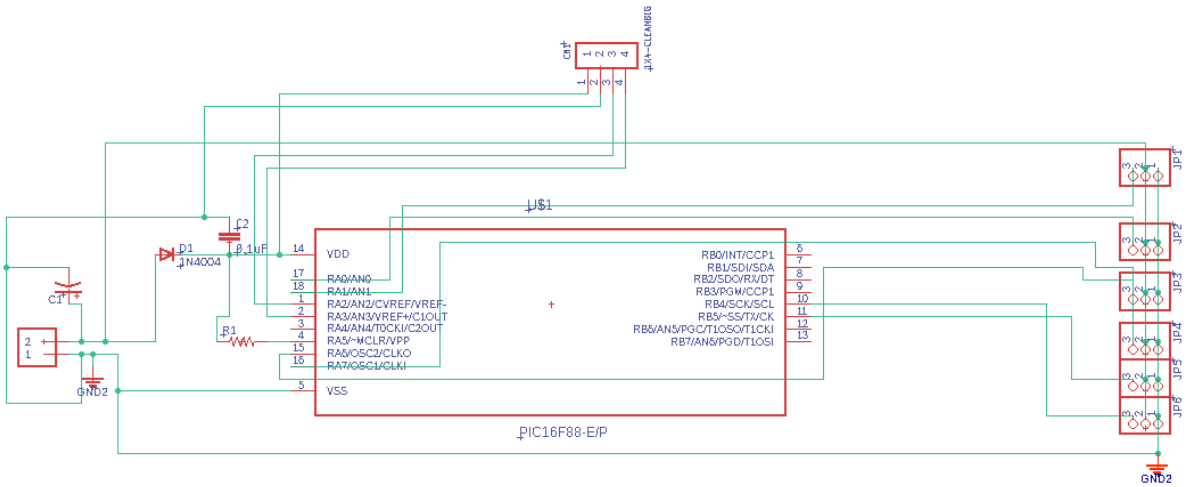

Figure 7.3 Control circuit schematics

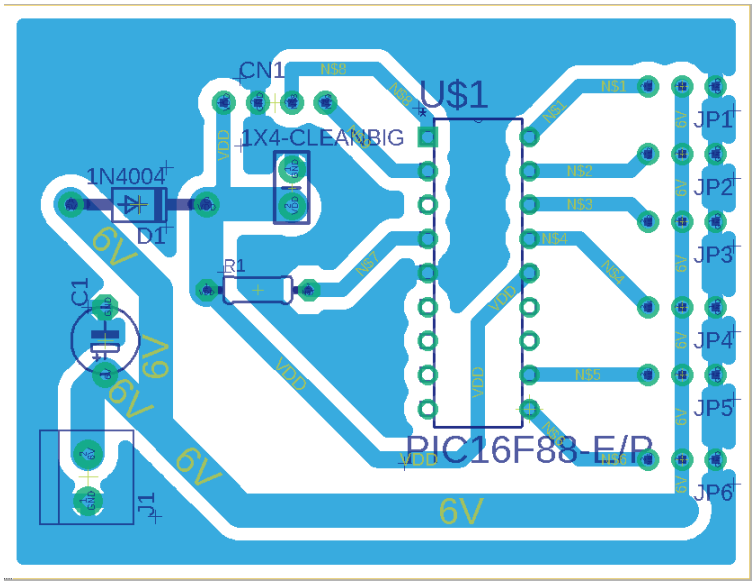

Figure 7.4 PCB layout of the control circuit

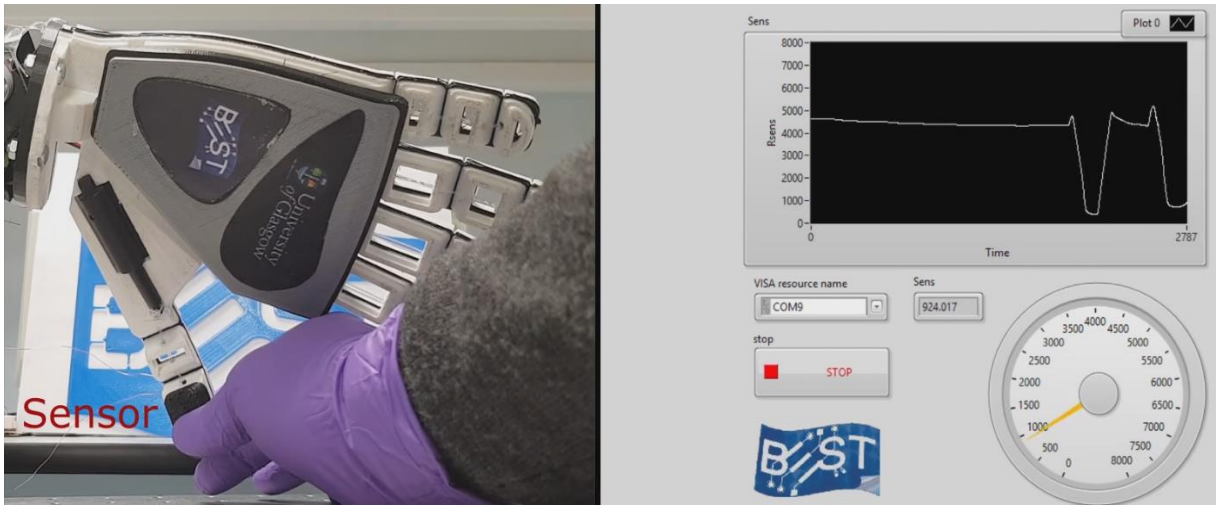

Figure 7.5 Robotic hand with SensAct device embedded on the fingertip been pressed and LabVIEW GUI presenting the resistance of the device. [258]

A. Preparation of two-part rubber

The two-part rubber was mixed in a 1:1 volume ratio for 3 min and kept under vacuum for 1 min to remove air trapped in the mixture. After that, it was poured on top of the device. The device was placed on the build plate of the 3D printer, which was set at 60 °C, and a hot air gun (set at 100 °C) was directed on top of the device for 1 h with minimal flow to accelerate the curing process of the EcoFlex.

Figure 7.6 Customized FDM desktop 3D printer for paste extrusion

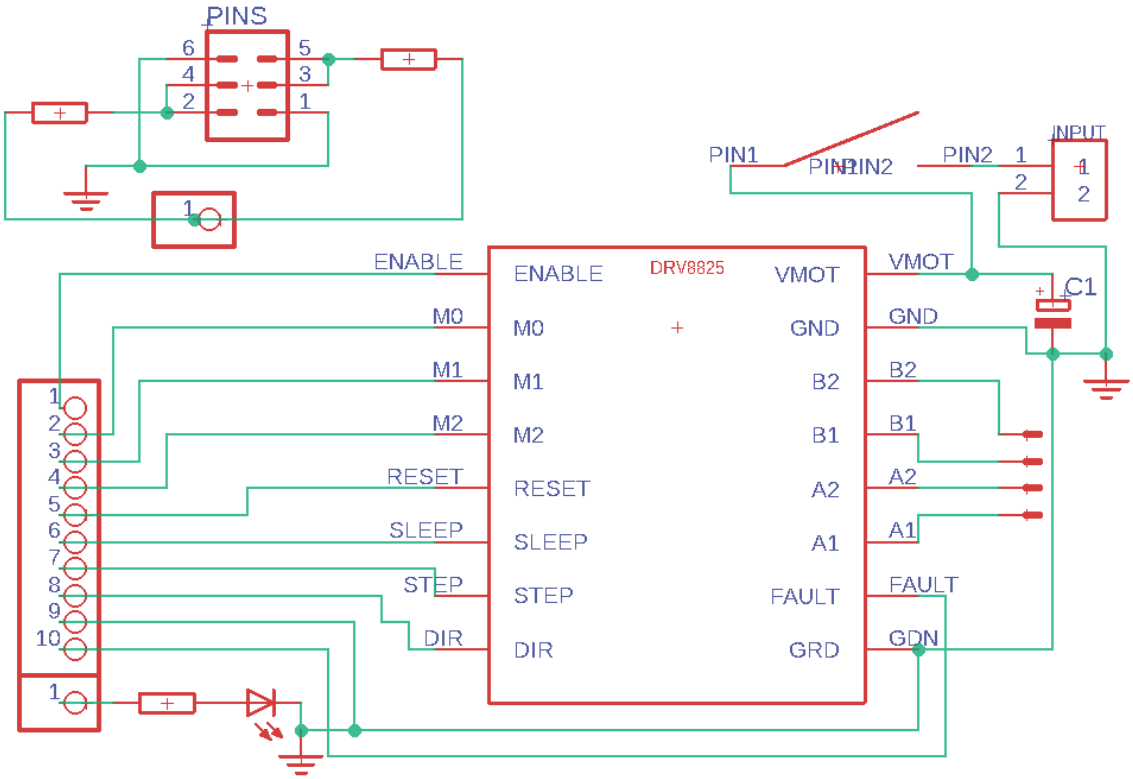

Figure 7.7 PPS electronic schematic

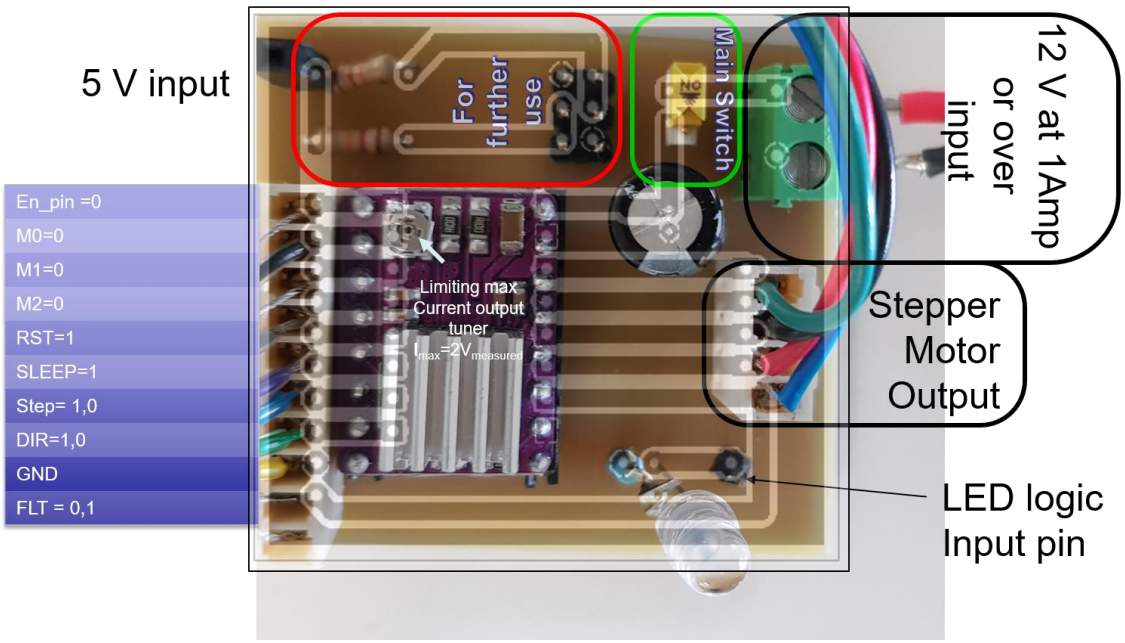

Figure 7.8 PCB of the PPS system.

B. Steps per millimetre calculation

The SDS can be viewed as a leadscrew driven mechanical system and the stepper motor step angle is 1.8 (200 per revolution). The driver has 1/16 micro stepping, that was set from the firmware, and the leadscrew pitch is 5 mm, by design, and the ratio between the chamber diameter and nozzle diameter is 10:1. The steps per mm is 64 steps per mm.

$$\frac{200\ steps\ per\ revolution * 16\ microstepping}{5\ mm\ pitch * 10\ diameter\ ratio} = 64\ steps\ per\ mm \quad (1)$$

That number would be true if the materials did behave as solids, but liquids do have a resistive behavior and some of the material was resisting in moving towards the nozzle therefore we increased the steps per mm to 80 as this showed to be more accurate through our experimentation.

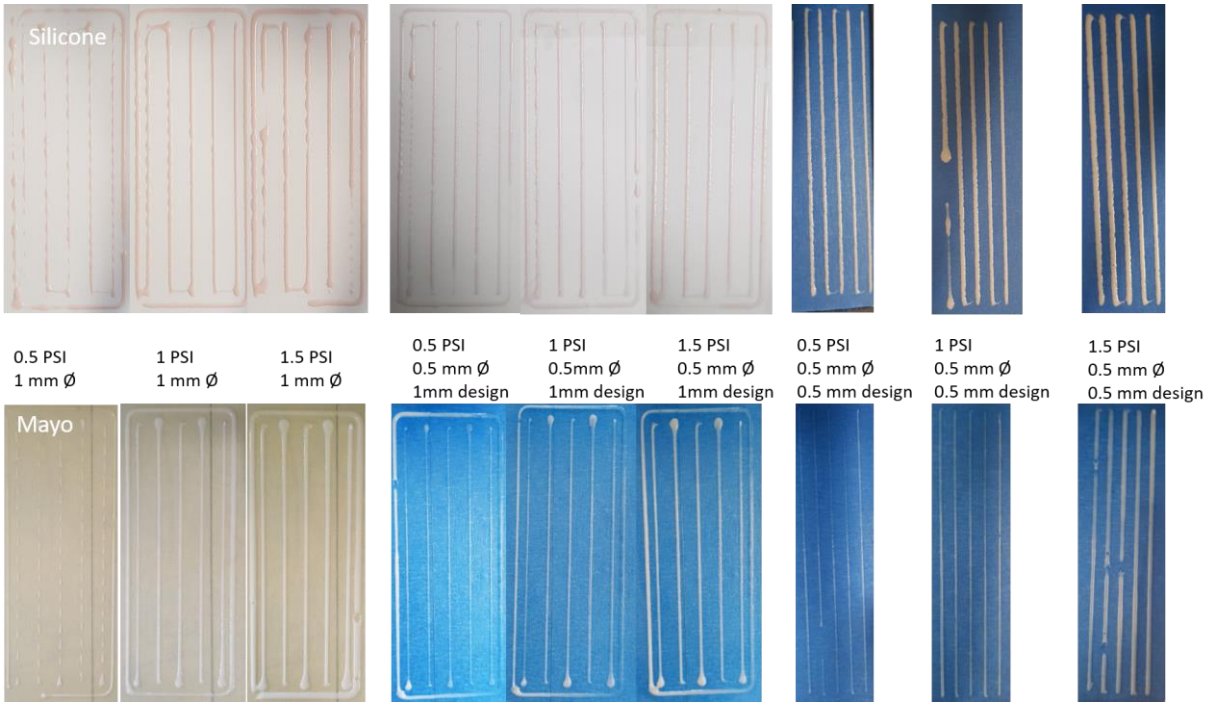

Figure 7.9 3D printed lines for Silicone based rubber and food condiment at different pressures and nozzle diameters.

REFERENCES

[1] M. I. Tiwana, S. J. Redmond, and N. H. Lovell, "A review of tactile sensing technologies with applications in biomedical engineering," *Sensors Actuators A Phys.*, vol. 179, pp. 17–31, Jun. 2012, doi: 10.1016/J.SNA.2012.02.051.

[2] L. Massari *et al.*, "A Machine-Learning-Based Approach to Solve Both Contact Location and Force in Soft Material Tactile Sensors," *Soft Robot.*, vol. 7, no. 4, pp. 409–420, Dec. 2019, doi: 10.1089/soro.2018.0172.

[3] X. Jiang, R. Chen, and H. Zhu, "Recent progress in wearable tactile sensors combined with algorithms based on machine learning and signal processing," *APL Mater.*, vol. 9, no. 3, p. 30906, Mar. 2021, doi: 10.1063/5.0043842.

[4] L. Guozhen, L. Shiqiang, W. Liangqi, and Z. Rong, "Skin-inspired quadruple tactile sensors integrated on a robot hand enable object recognition," *Sci. Robot.*, vol. 5, no. 49, p. eabc8134, Dec. 2020, doi: 10.1126/scirobotics.abc8134.

[5] A. J. Spiers, M. V Liarokapis, B. Calli, and A. M. Dollar, "Single-Grasp Object Classification and Feature Extraction with Simple Robot Hands and Tactile Sensors," *IEEE Trans. Haptics*, vol. 9, no. 2, pp. 207–220, 2016, doi: 10.1109/TOH.2016.2521378.

[6] W. Navaraj and R. Dahiya, "Fingerprint-Enhanced Capacitive-Piezoelectric Flexible Sensing Skin to Discriminate Static and Dynamic Tactile Stimuli," *Adv. Intell. Syst.*, vol. 1, no. 7, p. 1900051, Nov. 2019, doi: https://doi.org/10.1002/aisy.201900051.

[7] J. A. McGrath, R. A. J. Eady, and F. M. Pope, “Anatomy and organization of human skin,” *Rook’s Textb. dermatology*, vol. 1, pp. 2–3, 2004.

[8] A. Kalra, A. Lowe, and A. M. Al-Jumaily, “Mechanical behaviour of skin: a review,” *J. Mater. Sci. Eng*, vol. 5, no. 4, p. 1000254, 2016.

[9] B. Schittek, M. Paulmann, I. Senyurek, and H. Steffen, “The role of antimicrobial peptides in human skin and in skin infectious diseases,” *Infect. Disord. Targets (Formerly Curr. Drug Targets-Infectious Disord.*, vol. 8, no. 3, pp. 135–143, 2008.

[10] R. S. Dahiya and M. Valle, *Robotic tactile sensing: technologies and system*. Springer, 2013.

[11] F. Iheanacho and A. R. Vellipuram, “Physiology, Mechanoreceptors,” 2019.

[12] A. S. French and P. H. Torkkeli, “Mechanoreceptors,” in *Encyclopedia of Neuroscience*, Elsevier, 2009, pp. 689–695.

[13] N. N. L. *et al.*, “Meissner corpuscles and their spatially intermingled afferents underlie gentle touch perception,” *Science (80-.).*, vol. 368, no. 6497, p. eabb2751, Jun. 2020, doi: 10.1126/science.abb2751.

[14] Z. Halata and K. I. Baumann, “Anatomy of receptors,” in *Human haptic perception: Basics and applications*, Springer, 2008, pp. 85–92.

[15] J. Abraham and S. Mathew, “Merkel Cells: A Collective Review of Current Concepts,” *Int. J. Appl. basic Med. Res.*, vol. 9, no. 1, pp. 9–13, 2019, doi: 10.4103/ijabmr.IJABMR_34_18.

[16] Y. Kumaresan, G. Min, A. S. Dahiya, A. Ejaz, D. Shakthivel, and R. Dahiya, “Kirigami and Mogul-Patterned Ultra-Stretchable High-Performance ZnO Nanowires-Based Photodetector,” *Adv. Mater. Technol.*, vol. 7, no. 1, p. 2100804, Jan. 2022, doi: https://doi.org/10.1002/admt.202100804.

[17] P. Karipoth, A. Christou, A. Pullanchiyodan, and R. Dahiya, “Bioinspired Inchworm- and Earthworm-like Soft Robots with Intrinsic Strain Sensing,” *Adv. Intell. Syst.*, vol. n/a, no. n/a, p. 2100092, Sep. 2021, doi: https://doi.org/10.1002/aisy.202100092.

[18] L. Manjakkal, L. Yin, A. Nathan, J. Wang, and R. Dahiya, “Energy Autonomous Sweat-Based Wearable Systems,” *Adv. Mater.*, vol. 33, no. 35, p. 2100899, Sep. 2021, doi: https://doi.org/10.1002/adma.202100899.

[19] Y. Kumaresan, O. Ozioko, and R. Dahiya, “Multifunctional Electronic Skin With a Stack of Temperature and Pressure Sensor Arrays,” *IEEE Sens. J.*, vol. 21, no. 23, pp. 26243–26251, 2021, doi: 10.1109/JSEN.2021.3055458.

[20] R. S. Beeresha, A. M. Khan, and H. V Manjunath-Reddy, “Design and optimization of interdigital capacitor,” *Int. J. Res. Eng. Technol.*, vol. 5, no. 21, pp. 73–78, 2016.

[21] K. Weiss and H. Worn, “The working principle of resistive tactile sensor cells,” in *IEEE International Conference Mechatronics and Automation, 2005*, 2005, vol. 1, pp. 471-476 Vol. 1, doi: 10.1109/ICMA.2005.1626593.

[22] A. S. Fiorillo, C. D. Critello, and S. A. Pullano, “Theory, technology and applications of piezoresistive sensors: A review,” *Sensors Actuators A Phys.*, vol. 281, pp. 156–175, 2018.

[23] G. Yoshikawa *et al.*, “Two Dimensional Array of Piezoresistive Nanomechanical Membrane-Type Surface Stress Sensor (MSS) with Improved Sensitivity,” *Sensors* , vol. 12, no. 11. 2012, doi: 10.3390/s121115873.

[24] P. Alpuim, V. Correia, E. S. Marins, J. G. Rocha, I. G. Trindade, and S. Lanceros-Mendez, “Piezoresistive silicon thin film sensor array for biomedical applications,” *Thin Solid Films*, vol. 519, no. 14, pp. 4574–4577, 2011, doi: https://doi.org/10.1016/j.tsf.2011.01.300.

[25] G. Gautschi, “Piezoelectric sensors,” in *Piezoelectric Sensorics*, Springer, 2002, pp. 73–91.

[26] L. Zou, C. Ge, Z. J. Wang, E. Cretu, and X. Li, “Novel Tactile Sensor Technology and Smart Tactile Sensing Systems: A Review,” *Sensors* , vol. 17, no. 11. 2017, doi: 10.3390/s17112653.

[27] N. F. Lepora, “Soft Biomimetic Optical Tactile Sensing with the TacTip: A Review,” *arXiv Prepr. arXiv2105.14455*, 2021.

[28] C. Sferrazza and R. D'Andrea, "Design, Motivation and Evaluation of a Full-Resolution Optical Tactile Sensor," *Sensors* , vol. 19, no. 4. 2019, doi: 10.3390/s19040928.

[29] C. D. Dimitrakopoulos and D. J. Mascaro, "Organic thin-film transistors: A review of recent advances," *IBM J. Res. Dev.*, vol. 45, no. 1, pp. 11–27, 2001, doi: 10.1147/rd.451.0011.

[30] C. D. Dimitrakopoulos, B. K. Furman, T. Graham, S. Hegde, and S. Purushothaman, "Field-effect transistors comprising molecular beam deposited α,ω-di-hexyl-hexathienylene and polymeric insulator," *Synth. Met.*, vol. 92, no. 1, pp. 47–52, 1998, doi: https://doi.org/10.1016/S0379-6779(98)80021-0.

[31] J. Ouyang, "Application of intrinsically conducting polymers in flexible electronics," *SmartMat*, vol. 2, no. 3, pp. 263–285, Sep. 2021, doi: https://doi.org/10.1002/smm2.1059.

[32] M. H. Lee, "Tactile Sensing: New Directions, New Challenges," *Int. J. Rob. Res.*, vol. 19, no. 7, pp. 636–643, Jul. 2000, doi: 10.1177/027836490001900702.

[33] H. A. Ernst, "MH-1, a computer-operated mechanical hand," 1962.

[34] T. G. Strickler III, "Design of an optical touch sensing system for a remote manipulator." Massachusetts Institute of Technology, 1966.

[35] A. K. Bejczy, "Effect of hand-based sensors on manipulator control performance," *Mech. Mach. Theory*, vol. 12, no. 5, pp. 547–567, 1977, doi: https://doi.org/10.1016/0094-114X(77)90048-9.

[36] H. R. Nicholls and M. H. Lee, "A Survey of Robot Tactile Sensing Technology," *Int. J. Rob. Res.*, vol. 8, no. 3, pp. 3–30, Jun. 1989, doi: 10.1177/027836498900800301.

[37] W. E. Snyder and J. S. Clair, "Conductive elastomers as sensor for industrial parts handling equipment," *IEEE Trans. Instrum. Meas.*, vol. 27, no. 1, pp. 94–99, 1978.

[38] M. Briot, “The utilization of an artificial skin sensor for the identification of solid objects,” in *9th Int. Symp. on Industrial Robots*, 1979, pp. 13–15.

[39] M. H. E. Larcombe, “Why carbon fibres can give robots a strong sense of grip,” *Sens. Rev.*, 1981.

[40] Y.-F. Fu *et al.*, “Super soft but strong E-Skin based on carbon fiber/carbon black/silicone composite: Truly mimicking tactile sensing and mechanical behavior of human skin,” *Compos. Sci. Technol.*, vol. 186, p. 107910, 2020.

[41] C. Guo, Y. Kondo, C. Takai, and M. Fuji, “Piezoresistivities of vapor-grown carbon fiber/silicone foams for tactile sensor applications,” *Polym. Int.*, vol. 66, no. 3, pp. 418–427, 2017.

[42] P. Huang, Z. Xia, and S. Cui, “3D printing of carbon fiber-filled conductive silicon rubber,” *Mater. Des.*, vol. 142, pp. 11–21, 2018.

[43] R. Vallett, R. Young, C. Knittel, Y. Kim, and G. Dion, “Development of a carbon fiber knitted capacitive touch sensor,” *MRS Adv.*, vol. 1, no. 38, pp. 2641–2651, 2016.

[44] X. Liao *et al.*, “Hetero-contact microstructure to program discerning tactile interactions for virtual reality,” *Nano Energy*, vol. 60, pp. 127–136, 2019.

[45] S. M. Doshi and E. T. Thostenson, “Thin and flexible carbon nanotube-based pressure sensors with ultrawide sensing range,” *ACS sensors*, vol. 3, no. 7, pp. 1276–1282, 2018.

[46] B. E. Robertson and A. J. Walkden, “Tactile Sensor System for Robotics,” *Meas. Control*, vol. 18, no. 7, pp. 262–265, Sep. 1985, doi: 10.1177/002029408501800703.

[47] P. Dario, D. De Rossi, C. Domenici, and R. Francesconi, “Ferroelectric polymer tactile sensors with anthropomorphic features,” in *Proceedings. 1984 IEEE International Conference on Robotics and Automation*, 1984, vol. 1, pp. 332–340, doi: 10.1109/ROBOT.1984.1087209.

[48] R. A. Boie, “Capacitive impedance readout tactile image sensor,” in *Proceedings. 1984 IEEE International Conference on Robotics and*

Automation, 1984, vol. 1, pp. 370–378, doi: 10.1109/ROBOT.1984.1087186.

[49] Z. Chu, P. M. Sarro, and S. Middelhoek, “Silicon three-axial tactile sensor,” *Sensors Actuators A Phys.*, vol. 54, no. 1, pp. 505–510, 1996, doi: https://doi.org/10.1016/S0924-4247(95)01190-0.

[50] S. Omata and Y. Terunuma, “New tactile sensor like the human hand and its applications,” *Sensors Actuators A Phys.*, vol. 35, no. 1, pp. 9–15, 1992, doi: https://doi.org/10.1016/0924-4247(92)87002-X.

[51] R. E. Ellis, S. R. Ganeshan, and S. J. Lederman, “A tactile sensor based on thin-plate deformation,” *Robotica*, vol. 12, no. 4, pp. 343–351, 1994.

[52] J. S. Son, E. A. Monteverde, and R. D. Howe, “A tactile sensor for localizing transient events in manipulation,” in *Proceedings of the 1994 IEEE International Conference on Robotics and Automation*, 1994, pp. 471–476.

[53] E. S. Kolesar and C. S. Dyson, “Object imaging with a piezoelectric robotic tactile sensor,” *J. microelectromechanical Syst.*, vol. 4, no. 2, pp. 87–96, 1995.

[54] D. J. Beebe, D. D. Denton, R. G. Radwin, and J. G. Webster, “A silicon-based tactile sensor for finger-mounted applications,” *IEEE Trans. Biomed. Eng.*, vol. 45, no. 2, pp. 151–159, 1998.

[55] O. A. Lindahl and S. Omata, “Impression technique for the assessment of oedema: comparison with a new tactile sensor that measures physical properties of tissue,” *Med. Biol. Eng. Comput.*, vol. 33, no. 1, pp. 27–32, 1995, doi: 10.1007/BF02522941.

[56] T. Ohtsuka, A. Furuse, T. Kohno, J. Nakajima, K. Yagyu, and S. Omata, “New tactile sensor techniques for localization of pulmonary nodules.,” *Int. Surg.*, vol. 82, no. 1, pp. 12–14, 1997.

[57] T. Ohtsuka, A. Furuse, T. Kohno, J. Nakajima, K. Yagyu, and S. Omata, “Application of a new tactile sensor to thoracoscopic surgery: experimental and clinical study,” *Ann. Thorac. Surg.*, vol. 60, no. 3, pp. 610–614, 1995.

[58] M. R. Wolffenbuttel and P. P. L. Regtien, “Polysilicon bridges for the

realization of tactile sensors," *Sensors Actuators A Phys.*, vol. 26, no. 1, pp. 257–264, 1991, doi: https://doi.org/10.1016/0924-4247(91)87002-K.

[59] D. J. Beebe, A. S. Hsieh, D. D. Denton, and R. G. Radwin, "A silicon force sensor for robotics and medicine," *Sensors Actuators A Phys.*, vol. 50, no. 1, pp. 55–65, 1995, doi: https://doi.org/10.1016/0924-4247(96)80085-9.

[60] Y. Yamada and M. R. Cutkosky, "Tactile sensor with 3-axis force and vibration sensing functions and its application to detect rotational slip," in *Proceedings of the 1994 IEEE International Conference on Robotics and Automation*, 1994, pp. 3550–3557.

[61] B. L. Gray and R. S. Fearing, "A surface micromachined microtactile sensor array," in *Proceedings of IEEE International Conference on Robotics and Automation*, 1996, vol. 1, pp. 1–6 vol.1, doi: 10.1109/ROBOT.1996.503564.

[62] B. Tise, "A compact high resolution piezoresistive digital tactile sensor," in *Proceedings. 1988 IEEE International Conference on Robotics and Automation*, 1988, pp. 760–764 vol.2, doi: 10.1109/ROBOT.1988.12150.

[63] Z.-P. Luo, L. J. Berglund, and K.-N. An, "Validation of F-Scan pressure sensor system: a technical note," *J. Rehabil. Res. Dev.*, vol. 35, p. 186, 1998.

[64] Interlink Electronics Inc, "FSR sensor," 1997.

[65] F. Vecchi, C. Freschi, S. Micera, A. M. Sabatini, P. Dario, and R. Sacchetti, "Experimental evaluation of two commercial force sensors for applications in biomechanics and motor control," 2000.

[66] N. Li, D. Yang, L. Jiang, H. Liu, and H. Cai, "Combined use of FSR sensor array and SVM classifier for finger motion recognition based on pressure distribution map," *J. Bionic Eng.*, vol. 9, no. 1, pp. 39–47, 2012.

[67] A. S. Sadun, J. Jalani, and J. A. Sukor, "Force Sensing Resistor (FSR): a brief overview and the low-cost sensor for active compliance control," in *First International Workshop on Pattern Recognition*, 2016, vol. 10011, p. 1001112.

[68] S. C. Ahn, S. J. Hwang, S. J. Kang, and Y. H. Kim, "Development and

evaluation of a new gait phase detection system using FSR sensors and a gyrosensor," *J. Korean Soc. Precis. Eng.*, vol. 21, no. 10, pp. 196–203, 2004.

[69] P. S. Malvade, A. K. Joshi, and S. P. Madhe, "IoT based monitoring of foot pressure using FSR sensor," in *2017 International Conference on Communication and Signal Processing (ICCSP)*, 2017, pp. 635–639.

[70] S. Ahn, Y. Jeong, D. Kim, and H. Kim, "Development of the non-wearable system with FSR sensors for correction of sitting position," in *2015 Second International Conference on Computing Technology and Information Management (ICCTIM)*, 2015, pp. 140–143.

[71] N. K. Rana, "Application of force sensing resistor (FSR) in design of pressure scanning system for plantar pressure measurement," in *2009 Second International Conference on Computer and Electrical Engineering*, 2009, vol. 2, pp. 678–685.

[72] A. Ke *et al.*, "Fingertip tactile sensor with single sensing element based on FSR and PVDF," *IEEE Sens. J.*, vol. 19, no. 23, pp. 11100–11112, 2019.

[73] M. R. U. Islam and S. Bai, "Intention detection for dexterous human arm motion with FSR sensor bands," in *Proceedings of the Companion of the 2017 ACM/IEEE International Conference on Human-Robot Interaction*, 2017, pp. 139–140.

[74] S. Pirozzi, "Tactile Sensors for Robotic Applications," *Sensors*, vol. 20, no. 24. Multidisciplinary Digital Publishing Institute, p. 7009, 2020.

[75] W. Chen, H. Khamis, I. Birznieks, N. F. Lepora, and S. J. Redmond, "Tactile sensors for friction estimation and incipient slip detection—Toward dexterous robotic manipulation: A review," *IEEE Sens. J.*, vol. 18, no. 22, pp. 9049–9064, 2018.

[76] T. P. Tomo *et al.*, "Covering a Robot Fingertip With uSkin: A Soft Electronic Skin With Distributed 3-Axis Force Sensitive Elements for Robot Hands," *IEEE Robot. Autom. Lett.*, vol. 3, no. 1, pp. 124–131, 2018, doi: 10.1109/LRA.2017.2734965.

[77] T. Yamaguchi, T. Kashiwagi, T. Arie, S. Akita, and K. Takei, “Human-Like Electronic Skin-Integrated Soft Robotic Hand,” *Adv. Intell. Syst.*, vol. 1, no. 2, p. 1900018, Jun. 2019, doi: https://doi.org/10.1002/aisy.201900018.

[78] A. Levi, M. Piovanelli, S. Furlan, B. Mazzolai, and L. Beccai, “Soft, Transparent, Electronic Skin for Distributed and Multiple Pressure Sensing,” *Sensors* , vol. 13, no. 5. 2013, doi: 10.3390/s130506578.

[79] P. Cosseddu *et al.*, “Inkjet printed Organic Thin Film Transistors based tactile transducers for artificial robotic skin,” in *2012 4th IEEE RAS & EMBS International Conference on Biomedical Robotics and Biomechatronics (BioRob)*, 2012, pp. 1907–1912, doi: 10.1109/BioRob.2012.6290775.

[80] H. Lee, J. Chung, S. Chang, and E. Yoon, “Normal and Shear Force Measurement Using a Flexible Polymer Tactile Sensor With Embedded Multiple Capacitors,” *J. Microelectromechanical Syst.*, vol. 17, no. 4, pp. 934–942, 2008, doi: 10.1109/JMEMS.2008.921727.

[81] A. Schmitz, P. Maiolino, M. Maggiali, L. Natale, G. Cannata, and G. Metta, “Methods and Technologies for the Implementation of Large-Scale Robot Tactile Sensors,” *IEEE Trans. Robot.*, vol. 27, no. 3, pp. 389–400, 2011, doi: 10.1109/TRO.2011.2132930.

[82] T. Mouri, H. Kawasaki, K. Yoshikawa, J. Takai, and S. Ito, “Anthropomorphic robot hand: Gifu hand III,” 제어로봇시스템학회 국제학술대회 논문집, pp. 1288–1293, 2002.

[83] G. Cannata, M. Maggiali, and J. G. Rocha, “Design of a tactile sensor for robot hands,” *Sensors Focus Tactile Force Stress Sensors*, pp. 271–288, 2008.

[84] L. Natale and E. Torres-Jara, “A sensitive approach to grasping,” in *Proceedings of the sixth international workshop on epigenetic robotics*, 2006, vol. 72, pp. 247–256.

[85] S. Li *et al.*, “Vision-based teleoperation of shadow dexterous hand using end-to-end deep neural network,” in *2019 International Conference on Robotics and Automation (ICRA)*, 2019, pp. 416–422.

[86] F. Rothling, R. Haschke, J. J. Steil, and H. Ritter, “Platform portable anthropomorphic grasping with the bielefeld 20-dof shadow and 9-dof tum hand,” in *2007 IEEE/RSJ International Conference on Intelligent Robots and Systems*, 2007, pp. 2951–2956.

[87] A. G. Eguiluz, I. Rañó, S. A. Coleman, and T. M. McGinnity, “Reliable object handover through tactile force sensing and effort control in the shadow robot hand,” in *2017 IEEE International Conference on Robotics and Automation (ICRA)*, 2017, pp. 372–377.

[88] T. B. Martin, R. O. Ambrose, M. A. Diftler, R. Platt, and M. J. Butzer, “Tactile gloves for autonomous grasping with the NASA/DARPA Robonaut,” in *IEEE International Conference on Robotics and Automation, 2004. Proceedings. ICRA’04. 2004*, 2004, vol. 2, pp. 1713–1718.

[89] P. Serra Bergeron and S. Mosquera Costas, “Integration of sensors in a BarrettHand with ROS.” Universitat Politècnica de Catalunya, 2014.

[90] A. Polishchuk, W. T. Navaraj, H. Heidari, and R. Dahiya, “Multisensory Smart Glove for Tactile Feedback in Prosthetic Hand,” *Procedia Eng.*, vol. 168, pp. 1605–1608, 2016, doi: https://doi.org/10.1016/j.proeng.2016.11.471.

[91] C. Melchiorri, G. Palli, G. Berselli, and G. Vassura, “Development of the ub hand iv: Overview of design solutions and enabling technologies,” *IEEE Robot. Autom. Mag.*, vol. 20, no. 3, pp. 72–81, 2013.

[92] J.-H. Bae, S.-W. Park, J.-H. Park, M.-H. Baeg, D. Kim, and S.-R. Oh, “Development of a low cost anthropomorphic robot hand with high capability,” in *2012 IEEE/RSJ International Conference on Intelligent Robots and Systems*, 2012, pp. 4776–4782.

[93] Shadow Robot Company, “Shadow Robot Company Hand with BioTac sensors,” 2021. https://www.shadowrobot.com/telerobots/ (accessed Dec. 11, 2021).

[94] C. Mayousse, C. Celle, E. Moreau, J.-F. Mainguet, A. Carella, and J.-P. Simonato, “Improvements in purification of silver nanowires by decantation and fabrication of flexible transparent electrodes. Application to capacitive

touch sensors," *Nanotechnology*, vol. 24, no. 21, p. 215501, 2013.

[95] X. Wang, T. Li, J. Adams, and J. Yang, "Transparent, stretchable, carbon-nanotube-inlaid conductors enabled by standard replication technology for capacitive pressure, strain and touch sensors," *J. Mater. Chem. A*, vol. 1, no. 11, pp. 3580–3586, 2013.

[96] S. Boukhenous and M. Attari, "A low cost sensing system for foot stress recovering on a Freeman platform," in *2011 18th IEEE International Conference on Electronics, Circuits, and Systems*, 2011, pp. 276–280.

[97] S. Caviglia, M. Valle, and C. Bartolozzi, "Asynchronous, event-driven readout of POSFET devices for tactile sensing," in *2014 IEEE International Symposium on Circuits and Systems (ISCAS)*, 2014, pp. 2648–2651.

[98] P. S. Girão, P. M. P. Ramos, O. Postolache, and J. M. D. Pereira, "Tactile sensors for robotic applications," *Measurement*, vol. 46, no. 3, pp. 1257–1271, 2013.

[99] S. Takamatsu, T. Yamashita, T. Imai, and T. Itoh, "Fabric touch sensors using projected self-capacitive touch technique," *Sens. Mater*, vol. 25, pp. 627–634, 2013.

[100] A. S. Anisimov *et al.*, "16.3: Printed Touch Sensors Using Carbon NanoBud® Material," in *Sid Symposium Digest of Technical Papers*, 2014, vol. 45, no. 1, pp. 200–203.

[101] J. Seo *et al.*, "Touch sensors based on planar liquid crystal-gated-organic field-effect transistors," *AIP Adv.*, vol. 4, no. 9, p. 97109, 2014.

[102] E.-S. Choi, M.-H. Jeong, K. W. Choi, C. Lim, and S.-B. Lee, "Flexible and transparent touch sensor using single-wall carbon nanotube thin-films," in *2010 3rd International Nanoelectronics Conference (INEC)*, 2010, pp. 718–719.

[103] A. Y. Benbasat, S. J. Morris, and J. A. Paradiso, "A wireless modular sensor architecture and its application in on-shoe gait analysis," in *SENSORS, 2003 IEEE*, 2003, vol. 2, pp. 1086–1091.

[104] R. S. Dahiya, P. Mittendorfer, M. Valle, G. Cheng, and V. J. Lumelsky, “Directions Toward Effective Utilization of Tactile Skin: A Review,” *IEEE Sens. J.*, vol. 13, no. 11, pp. 4121–4138, 2013, doi: 10.1109/JSEN.2013.2279056.

[105] Y. Yang *et al.*, “Human skin based triboelectric nanogenerators for harvesting biomechanical energy and as self-powered active tactile sensor system,” *ACS Nano*, vol. 7, no. 10, pp. 9213–9222, 2013.

[106] S. M. M. De Rossi *et al.*, “Development of an in-shoe pressure-sensitive device for gait analysis,” in *2011 Annual International Conference of the IEEE Engineering in Medicine and Biology Society*, 2011, pp. 5637–5640.

[107] S. Khan, L. Lorenzelli, and R. S. Dahiya, “Technologies for printing sensors and electronics over large flexible substrates: a review,” *IEEE Sens. J.*, vol. 15, no. 6, pp. 3164–3185, 2014.

[108] W. S. Wong and A. Salleo, *Flexible electronics: materials and applications*, vol. 11. Springer Science & Business Media, 2009.

[109] K. Takei *et al.*, “Nanowire active-matrix circuitry for low-voltage macroscale artificial skin,” *Nat. Mater.*, vol. 9, no. 10, pp. 821–826, 2010.

[110] C. G. Núñez, F. Liu, W. T. Navaraj, A. Christou, D. Shakthivel, and R. Dahiya, “Heterogeneous integration of contact-printed semiconductor nanowires for high-performance devices on large areas,” *Microsystems Nanoeng.*, vol. 4, no. 1, pp. 1–15, 2018.

[111] A. Christou, F. Liu, and R. Dahiya, “Development of a highly controlled system for large-area, directional printing of quasi-1D nanomaterials,” *Microsystems Nanoeng.*, vol. 7, no. 1, pp. 1–12, 2021.

[112] A. Zumeit, A. S. Dahiya, A. Christou, D. Shakthivel, and R. Dahiya, “Direct roll transfer printed silicon nanoribbon arrays based high-performance flexible electronics,” *npj Flex. Electron.*, vol. 5, no. 1, pp. 1–10, 2021.

[113] T. Makimoto, K. Kumakura, Y. Kobayashi, T. Akasaka, and H. Yamamoto, “A vertical InGaN/GaN light-emitting diode fabricated on a flexible substrate

by a mechanical transfer method using BN," *Appl. Phys. Express*, vol. 5, no. 7, p. 72102, 2012.

[114] J. Jang, Y. S. Jun, H. Seo, M. Kim, and J.-U. Park, "Motion detection using tactile sensors based on pressure-sensitive transistor arrays," *Sensors*, vol. 20, no. 13, p. 3624, 2020.

[115] W. Taube Navaraj *et al.*, "Nanowire FET based neural element for robotic tactile sensing skin," *Front. Neurosci.*, vol. 11, p. 501, 2017.

[116] S. Chen, K. Jiang, Z. Lou, D. Chen, and G. Shen, "Recent developments in graphene-based tactile sensors and e-skins," *Adv. Mater. Technol.*, vol. 3, no. 2, p. 1700248, 2018.

[117] R. S. Dahiya, M. Valle, G. Metta, L. Lorenzelli, and C. Collini, "Tactile sensing arrays for humanoid robots," in *2007 Ph. D Research in Microelectronics and Electronics Conference*, 2007, pp. 201–204.

[118] T. Yang, D. Xie, Z. Li, and H. Zhu, "Recent advances in wearable tactile sensors: Materials, sensing mechanisms, and device performance," *Mater. Sci. Eng. R Reports*, vol. 115, pp. 1–37, 2017.

[119] C. G. Núñez, A. Vilouras, W. T. Navaraj, F. Liu, and R. Dahiya, "ZnO Nanowires-Based Flexible UV Photodetector System for Wearable Dosimetry," *IEEE Sens. J.*, vol. 18, no. 19, pp. 7881–7888, 2018, doi: 10.1109/JSEN.2018.2853762.

[120] S. Gupta, H. Heidari, A. Vilouras, L. Lorenzelli, and R. Dahiya, "Device Modelling for Bendable Piezoelectric FET-Based Touch Sensing System," *IEEE Trans. Circuits Syst. I Regul. Pap.*, vol. 63, no. 12, pp. 2200–2208, 2016, doi: 10.1109/TCSI.2016.2615108.

[121] A. Vilouras, H. Heidari, S. Gupta, and R. Dahiya, "Modeling of CMOS Devices and Circuits on Flexible Ultrathin Chips," *IEEE Trans. Electron Devices*, vol. 64, no. 5, pp. 2038–2046, 2017, doi: 10.1109/TED.2017.2668899.

[122] A. Vilouras, A. Christou, L. Manjakkal, and R. Dahiya, "Ultrathin Ion-Sensitive Field-Effect Transistor Chips with Bending-Induced Performance

Enhancement," *ACS Appl. Electron. Mater.*, vol. 2, no. 8, pp. 2601–2610, Aug. 2020, doi: 10.1021/acsaelm.0c00489.

[123] H.-J. Freund and G. Pacchioni, "Oxide ultra-thin films on metals: new materials for the design of supported metal catalysts," *Chem. Soc. Rev.*, vol. 37, no. 10, pp. 2224–2242, 2008.

[124] P. Zhao, N. Deng, X. Li, C. Ren, and Z. Wang, "Development of highly-sensitive and ultra-thin silicon stress sensor chips for wearable biomedical applications," *Sensors Actuators A Phys.*, vol. 216, pp. 158–166, 2014.

[125] P. Escobedo, M. Bhattacharjee, F. Nikbakhtnasrabadi, and R. Dahiya, "Smart Bandage With Wireless Strain and Temperature Sensors and Batteryless NFC Tag," *IEEE Internet Things J.*, vol. 8, no. 6, pp. 5093–5100, 2021, doi: 10.1109/JIOT.2020.3048282.

[126] X. Wang, L. Dong, H. Zhang, R. Yu, C. Pan, and Z. L. Wang, "Recent Progress in Electronic Skin," *Adv. Sci.*, vol. 2, no. 10, p. 1500169, Oct. 2015, doi: https://doi.org/10.1002/advs.201500169.

[127] Y. Liu, R. Bao, J. Tao, J. Li, M. Dong, and C. Pan, "Recent progress in tactile sensors and their applications in intelligent systems," *Sci. Bull.*, vol. 65, no. 1, pp. 70–88, 2020.

[128] C. G. Núñez, W. T. Navaraj, E. O. Polat, and R. Dahiya, "Energy-Autonomous, Flexible, and Transparent Tactile Skin," *Adv. Funct. Mater.*, vol. 27, no. 18, p. 1606287, May 2017, doi: https://doi.org/10.1002/adfm.201606287.

[129] M. Soni and R. Dahiya, "Soft eSkin: distributed touch sensing with harmonized energy and computing," *Philos. Trans. R. Soc. A Math. Phys. Eng. Sci.*, vol. 378, no. 2164, p. 20190156, Feb. 2020, doi: 10.1098/rsta.2019.0156.

[130] M. Zhu, M. Lou, J. Yu, Z. Li, and B. Ding, "Energy autonomous hybrid electronic skin with multi-modal sensing capabilities," *Nano Energy*, vol. 78, p. 105208, 2020.

[131] K. Dong *et al.*, "A stretchable yarn embedded triboelectric nanogenerator as electronic skin for biomechanical energy harvesting and multifunctional pressure sensing," *Adv. Mater.*, vol. 30, no. 43, p. 1804944, 2018.

[132] S. Park *et al.*, "Stretchable energy-harvesting tactile electronic skin capable of differentiating multiple mechanical stimuli modes," *Adv. Mater.*, vol. 26, no. 43, pp. 7324–7332, 2014.

[133] M. J. Allen, V. C. Tung, and R. B. Kaner, "Honeycomb Carbon: A Review of Graphene," *Chem. Rev.*, vol. 110, no. 1, pp. 132–145, Jan. 2010, doi: 10.1021/cr900070d.

[134] H. Park, S. Chang, X. Zhou, J. Kong, T. Palacios, and S. Gradečak, "Flexible Graphene Electrode-Based Organic Photovoltaics with Record-High Efficiency," *Nano Lett.*, vol. 14, no. 9, pp. 5148–5154, Sep. 2014, doi: 10.1021/nl501981f.

[135] Y. Shi, K. K. Kim, A. Reina, M. Hofmann, L.-J. Li, and J. Kong, "Work Function Engineering of Graphene Electrode via Chemical Doping," *ACS Nano*, vol. 4, no. 5, pp. 2689–2694, May 2010, doi: 10.1021/nn1005478.

[136] N. Kurra, Q. Jiang, P. Nayak, and H. N. Alshareef, "Laser-derived graphene: A three-dimensional printed graphene electrode and its emerging applications," *Nano Today*, vol. 24, pp. 81–102, 2019, doi: https://doi.org/10.1016/j.nantod.2018.12.003.

[137] X. Huang, Z. Zeng, Z. Fan, J. Liu, and H. Zhang, "Graphene-Based Electrodes," *Adv. Mater.*, vol. 24, no. 45, pp. 5979–6004, Nov. 2012, doi: https://doi.org/10.1002/adma.201201587.

[138] G. Jo, M. Choe, S. Lee, W. Park, Y. H. Kahng, and T. Lee, "The application of graphene as electrodes in electrical and optical devices," *Nanotechnology*, vol. 23, no. 11, p. 112001, 2012, doi: 10.1088/0957-4484/23/11/112001.

[139] C.-L. Choong *et al.*, "Highly Stretchable Resistive Pressure Sensors Using a Conductive Elastomeric Composite on a Micropyramid Array," *Adv. Mater.*, vol. 26, no. 21, pp. 3451–3458, Jun. 2014, doi:

https://doi.org/10.1002/adma.201305182.

[140] J. Ouyang, "'Secondary doping' methods to significantly enhance the conductivity of PEDOT: PSS for its application as transparent electrode of optoelectronic devices," *Displays*, vol. 34, no. 5, pp. 423–436, 2013.

[141] Y. Wen and J. Xu, "Scientific Importance of Water-Processable PEDOT–PSS and Preparation, Challenge and New Application in Sensors of Its Film Electrode: A Review," *J. Polym. Sci. Part A Polym. Chem.*, vol. 55, no. 7, pp. 1121–1150, Apr. 2017, doi: https://doi.org/10.1002/pola.28482.

[142] D. Alemu, H.-Y. Wei, K.-C. Ho, and C.-W. Chu, "Highly conductive PEDOT: PSS electrode by simple film treatment with methanol for ITO-free polymer solar cells," *Energy Environ. Sci.*, vol. 5, no. 11, pp. 9662–9671, 2012.

[143] B. W. An, S. Heo, S. Ji, F. Bien, and J.-U. Park, "Transparent and flexible fingerprint sensor array with multiplexed detection of tactile pressure and skin temperature," *Nat. Commun.*, vol. 9, no. 1, pp. 1–10, 2018.

[144] X.-Z. Jiang, Y.-J. Sun, Z. Fan, and T.-Y. Zhang, "Integrated Flexible, Waterproof, Transparent, and Self-Powered Tactile Sensing Panel," *ACS Nano*, vol. 10, no. 8, pp. 7696–7704, Aug. 2016, doi: 10.1021/acsnano.6b03042.

[145] B. Zhang *et al.*, "Dual functional transparent film for proximity and pressure sensing," *Nano Res.*, vol. 7, no. 10, pp. 1488–1496, 2014.

[146] E. Cagatay, P. Köhler, P. Lugli, and A. Abdellah, "Flexible capacitive tactile sensors based on carbon nanotube thin films," *IEEE Sens. J.*, vol. 15, no. 6, pp. 3225–3233, 2015.

[147] C. W. Park *et al.*, "Fabrication of well-controlled wavy metal interconnect structures on stress-free elastomeric substrates," *Microelectron. Eng.*, vol. 113, pp. 55–60, 2014.

[148] S. Béfahy, S. Yunus, V. Burguet, J.-S. Heine, M. Troosters, and P. Bertrand, "Stretchable gold tracks on flat polydimethylsiloxane (PDMS) rubber substrate," *J. Adhes.*, vol. 84, no. 3, pp. 231–239, 2008.

[149] T. Yamada *et al.*, "A stretchable carbon nanotube strain sensor for human-motion detection," *Nat. Nanotechnol.*, vol. 6, no. 5, pp. 296–301, 2011.

[150] A. M. K. Esawi, K. Morsi, A. Sayed, M. Taher, and S. Lanka, "Effect of carbon nanotube (CNT) content on the mechanical properties of CNT-reinforced aluminium composites," *Compos. Sci. Technol.*, vol. 70, no. 16, pp. 2237–2241, 2010.

[151] X.-M. Liu *et al.*, "Carbon nanotube (CNT)-based composites as electrode material for rechargeable Li-ion batteries: a review," *Compos. Sci. Technol.*, vol. 72, no. 2, pp. 121–144, 2012.

[152] M. Sianipar, S. H. Kim, F. Iskandar, and I. G. Wenten, "Functionalized carbon nanotube (CNT) membrane: progress and challenges," *RSC Adv.*, vol. 7, no. 81, pp. 51175–51198, 2017.

[153] V. D. Punetha *et al.*, "Functionalization of carbon nanomaterials for advanced polymer nanocomposites: A comparison study between CNT and graphene," *Prog. Polym. Sci.*, vol. 67, pp. 1–47, 2017.

[154] Y. Song *et al.*, "Highly Compressible Integrated Supercapacitor–Piezoresistance-Sensor System with CNT–PDMS Sponge for Health Monitoring," *Small*, vol. 13, no. 39, p. 1702091, Oct. 2017, doi: https://doi.org/10.1002/smll.201702091.

[155] M. Law, J. Goldberger, and P. Yang, "Semiconductor nanowires and nanotubes," *Annu. Rev. Mater. Res.*, vol. 34, pp. 83–122, 2004.

[156] N. Wang, Y. Cai, and R. Q. Zhang, "Growth of nanowires," *Mater. Sci. Eng. R Reports*, vol. 60, no. 1–6, pp. 1–51, 2008.

[157] C. M. Lieber and Z. L. Wang, "Functional nanowires," *MRS Bull.*, vol. 32, no. 2, pp. 99–108, 2007.

[158] E. Barrigón, M. Heurlin, Z. Bi, B. Monemar, and L. Samuelson, "Synthesis and applications of III–V nanowires," *Chem. Rev.*, vol. 119, no. 15, pp. 9170–9220, 2019.

[159] S. Gong *et al.*, "A wearable and highly sensitive pressure sensor with

ultrathin gold nanowires," *Nat. Commun.*, vol. 5, no. 1, pp. 1–8, 2014.

[160] T. Someya, T. Sekitani, S. Iba, Y. Kato, H. Kawaguchi, and T. Sakurai, "A large-area, flexible pressure sensor matrix with organic field-effect transistors for artificial skin applications," *Proc. Natl. Acad. Sci.*, vol. 101, no. 27, pp. 9966–9970, 2004.

[161] V. Maheshwari and R. F. Saraf, "High-resolution thin-film device to sense texture by touch," *Science (80-.).*, vol. 312, no. 5779, pp. 1501–1504, 2006.

[162] T. Someya *et al.*, "Conformable, flexible, large-area networks of pressure and thermal sensors with organic transistor active matrixes," *Proc. Natl. Acad. Sci.*, vol. 102, no. 35, pp. 12321–12325, 2005.

[163] S. El-Molla *et al.*, "Integration of a thin film PDMS-based capacitive sensor for tactile sensing in an electronic skin," *J. Sensors*, vol. 2016, 2016.

[164] X. Riedl, C. Bolzmacher, R. Wagner, K. Bauer, and N. Schwesinger, "A novel PDMS based capacitive pressure sensor," in *SENSORS, 2010 IEEE*, 2010, pp. 2255–2258.

[165] K. F. Lei, K.-F. Lee, and M.-Y. Lee, "A flexible PDMS capacitive tactile sensor with adjustable measurement range for plantar pressure measurement," *Microsyst. Technol.*, vol. 20, no. 7, pp. 1351–1358, 2014.

[166] K. F. Lei, K.-F. Lee, and M.-Y. Lee, "Development of a flexible PDMS capacitive pressure sensor for plantar pressure measurement," *Microelectron. Eng.*, vol. 99, pp. 1–5, 2012.

[167] Y. Joo *et al.*, "Silver nanowire-embedded PDMS with a multiscale structure for a highly sensitive and robust flexible pressure sensor," *Nanoscale*, vol. 7, no. 14, pp. 6208–6215, 2015.

[168] D. Kwon *et al.*, "Highly sensitive, flexible, and wearable pressure sensor based on a giant piezocapacitive effect of three-dimensional microporous elastomeric dielectric layer," *ACS Appl. Mater. Interfaces*, vol. 8, no. 26, pp. 16922–16931, 2016.

[169] P. Roberts, D. D. Damian, W. Shan, T. Lu, and C. Majidi, "Soft-matter

capacitive sensor for measuring shear and pressure deformation," in *2013 IEEE International Conference on Robotics and Automation*, 2013, pp. 3529–3534, doi: 10.1109/ICRA.2013.6631071.

[170] X. Guo, Y. Huang, X. Cai, C. Liu, and P. Liu, "Capacitive wearable tactile sensor based on smart textile substrate with carbon black /silicone rubber composite dielectric," *Meas. Sci. Technol.*, vol. 27, no. 4, p. 45105, 2016, doi: 10.1088/0957-0233/27/4/045105.

[171] Y. Cha, J. Seo, J.-S. Kim, and J.-M. Park, "Human–computer interface glove using flexible piezoelectric sensors," *Smart Mater. Struct.*, vol. 26, no. 5, p. 57002, 2017.

[172] A. V Shirinov and W. K. Schomburg, "Pressure sensor from a PVDF film," *Sensors Actuators A Phys.*, vol. 142, no. 1, pp. 48–55, 2008.

[173] Y. R. Wang, J. M. Zheng, G. Y. Ren, P. H. Zhang, and C. Xu, "A flexible piezoelectric force sensor based on PVDF fabrics," *Smart Mater. Struct.*, vol. 20, no. 4, p. 45009, 2011.

[174] S. Choi and Z. Jiang, "A novel wearable sensor device with conductive fabric and PVDF film for monitoring cardiorespiratory signals," *Sensors Actuators A Phys.*, vol. 128, no. 2, pp. 317–326, 2006.

[175] Y. Xin *et al.*, "The use of polyvinylidene fluoride (PVDF) films as sensors for vibration measurement: A brief review," *Ferroelectrics*, vol. 502, no. 1, pp. 28–42, 2016.

[176] I. Lee and H. J. Sung, "Development of an array of pressure sensors with PVDF film," *Exp. Fluids*, vol. 26, no. 1, pp. 27–35, 1999.

[177] Y. Tanaka, D. P. Nguyen, T. Fukuda, and A. Sano, "Wearable skin vibration sensor using a PVDF film," in *2015 IEEE World Haptics Conference (WHC)*, 2015, pp. 146–151.

[178] G. Kang and Y. Cao, "Application and modification of poly (vinylidene fluoride)(PVDF) membranes–a review," *J. Memb. Sci.*, vol. 463, pp. 145–165, 2014.

[179] Y. Wan, Y. Wang, and C. F. Guo, “Recent progresses on flexible tactile sensors,” *Mater. Today Phys.*, vol. 1, pp. 61–73, 2017, doi: https://doi.org/10.1016/j.mtphys.2017.06.002.

[180] X. Wang, Y. Gu, Z. Xiong, Z. Cui, and T. Zhang, “Silk-Molded Flexible, Ultrasensitive, and Highly Stable Electronic Skin for Monitoring Human Physiological Signals,” *Adv. Mater.*, vol. 26, no. 9, pp. 1336–1342, Mar. 2014, doi: https://doi.org/10.1002/adma.201304248.

[181] L. Pan *et al.*, “An ultra-sensitive resistive pressure sensor based on hollow-sphere microstructure induced elasticity in conducting polymer film,” *Nat. Commun.*, vol. 5, no. 1, p. 3002, 2014, doi: 10.1038/ncomms4002.

[182] H.-B. Yao *et al.*, “A Flexible and Highly Pressure-Sensitive Graphene–Polyurethane Sponge Based on Fractured Microstructure Design,” *Adv. Mater.*, vol. 25, no. 46, pp. 6692–6698, Dec. 2013, doi: https://doi.org/10.1002/adma.201303041.

[183] J. Park *et al.*, “Tactile-Direction-Sensitive and Stretchable Electronic Skins Based on Human-Skin-Inspired Interlocked Microstructures,” *ACS Nano*, vol. 8, no. 12, pp. 12020–12029, Dec. 2014, doi: 10.1021/nn505953t.

[184] Q. Tan *et al.*, “A High Temperature Capacitive Pressure Sensor Based on Alumina Ceramic for in Situ Measurement at 600 °C,” *Sensors* , vol. 14, no. 2. 2014, doi: 10.3390/s140202417.

[185] S. C. B. Mannsfeld *et al.*, “Highly sensitive flexible pressure sensors with microstructured rubber dielectric layers,” *Nat. Mater.*, vol. 9, no. 10, pp. 859–864, 2010, doi: 10.1038/nmat2834.

[186] J.-Y. Sun, C. Keplinger, G. M. Whitesides, and Z. Suo, “Ionic skin,” *Adv. Mater.*, vol. 26, no. 45, pp. 7608–7614, Dec. 2014, doi: https://doi.org/10.1002/adma.201403441.

[187] L. Viry *et al.*, “Flexible Three-Axial Force Sensor for Soft and Highly Sensitive Artificial Touch,” *Adv. Mater.*, vol. 26, no. 17, pp. 2659–2664, May 2014, doi: https://doi.org/10.1002/adma.201305064.

[188] L. Persano *et al.*, “High performance piezoelectric devices based on aligned arrays of nanofibers of poly(vinylidenefluoride-co-trifluoroethylene),” *Nat. Commun.*, vol. 4, no. 1, p. 1633, 2013, doi: 10.1038/ncomms2639.

[189] W. Wenzhuo, W. Xiaonan, and W. Z. Lin, “Taxel-Addressable Matrix of Vertical-Nanowire Piezotronic Transistors for Active and Adaptive Tactile Imaging,” *Science (80-.).*, vol. 340, no. 6135, pp. 952–957, May 2013, doi: 10.1126/science.1234855.

[190] G. Buchberger, R. Schwödiauer, and S. Bauer, “Flexible large area ferroelectret sensors for location sensitive touchpads,” *Appl. Phys. Lett.*, vol. 92, no. 12, p. 123511, Mar. 2008, doi: 10.1063/1.2903711.

[191] X. Wang, Z. Xu, S. Tang, and R. A. Cheke, “Cumulative effects of incorrect use of pesticides can lead to catastrophic outbreaks of pests,” *Chaos, Solitons & Fractals*, vol. 100, pp. 7–19, 2017, doi: https://doi.org/10.1016/j.chaos.2017.04.030.

[192] Z. L. Wang, “Triboelectric Nanogenerators as New Energy Technology for Self-Powered Systems and as Active Mechanical and Chemical Sensors,” *ACS Nano*, vol. 7, no. 11, pp. 9533–9557, Nov. 2013, doi: 10.1021/nn404614z.

[193] M. Intelligence, “3D PRINTING MARKET - GROWTH, TRENDS, COVID-19 IMPACT, AND FORECASTS (2021 - 2026),” 2021. https://www.mordorintelligence.com/industry-reports/3d-printing-market (accessed Dec. 20, 2021).

[194] A. Haleem and M. Javaid, “Additive manufacturing applications in industry 4.0: a review,” *J. Ind. Integr. Manag.*, vol. 4, no. 04, p. 1930001, 2019.

[195] M. Javaid and A. Haleem, “Additive manufacturing applications in orthopaedics: a review,” *J. Clin. Orthop. trauma*, vol. 9, no. 3, pp. 202–206, 2018.

[196] M. Javaid and A. Haleem, “Additive manufacturing applications in medical cases: A literature based review,” *Alexandria J. Med.*, vol. 54, no. 4, pp. 411–422, 2018.

[197] A. Haleem, M. Javaid, and A. Saxena, “Additive manufacturing applications in cardiology: A review,” *Egypt. Hear. J.*, vol. 70, no. 4, pp. 433–441, 2018.

[198] A. Camposeo, L. Persano, M. Farsari, and D. Pisignano, “Additive manufacturing: applications and directions in photonics and optoelectronics,” *Adv. Opt. Mater.*, vol. 7, no. 1, p. 1800419, 2019.

[199] N. Guo and M. C. Leu, “Additive manufacturing: technology, applications and research needs,” *Front. Mech. Eng.*, vol. 8, no. 3, pp. 215–243, 2013.

[200] M. Javaid and A. Haleem, “Using additive manufacturing applications for design and development of food and agricultural equipments,” *Int. J. Mater. Prod. Technol.*, vol. 58, no. 2–3, pp. 225–238, 2019.

[201] T. J. Horn and O. L. A. Harrysson, “Overview of current additive manufacturing technologies and selected applications,” *Sci. Prog.*, vol. 95, no. 3, pp. 255–282, 2012.

[202] T. D. Ngo, A. Kashani, G. Imbalzano, K. T. Q. Nguyen, and D. Hui, “Additive manufacturing (3D printing): A review of materials, methods, applications and challenges,” *Compos. Part B Eng.*, vol. 143, pp. 172–196, 2018.

[203] H. Bikas, P. Stavropoulos, and G. Chryssolouris, “Additive manufacturing methods and modelling approaches: a critical review,” *Int. J. Adv. Manuf. Technol.*, vol. 83, no. 1–4, pp. 389–405, 2016.

[204] T. Yao, Z. Deng, K. Zhang, and S. Li, “A method to predict the ultimate tensile strength of 3D printing polylactic acid (PLA) materials with different printing orientations,” *Compos. Part B Eng.*, vol. 163, pp. 393–402, 2019.

[205] B. Ripley *et al.*, “3D printing from MRI data: harnessing strengths and minimizing weaknesses,” *J. Magn. Reson. Imaging*, vol. 45, no. 3, pp. 635–645, 2017.

[206] D. Mitsouras and P. C. Liacouras, “3D printing technologies,” in *3D printing in medicine*, Springer, 2017, pp. 5–22.

[207] J. A. Lewis, “Direct Ink Writing of 3D Functional Materials,” *Adv. Funct. Mater.*, vol. 16, no. 17, pp. 2193–2204, Nov. 2006, doi:

https://doi.org/10.1002/adfm.200600434.

[208] F. Zhao, D. Li, and Z. Jin, “Preliminary Investigation of Poly-Ether-Ether-Ketone Based on Fused Deposition Modeling for Medical Applications,” *Materials* , vol. 11, no. 2. 2018, doi: 10.3390/ma11020288.

[209] M. Saari, B. Xia, B. Cox, P. S. Krueger, A. L. Cohen, and E. Richer, “Fabrication and Analysis of a Composite 3D Printed Capacitive Force Sensor,” *3D Print. Addit. Manuf.*, vol. 3, no. 3, pp. 136–141, Sep. 2016, doi: 10.1089/3dp.2016.0021.

[210] S.-Y. Wu, C. Yang, W. Hsu, and L. Lin, “3D-printed microelectronics for integrated circuitry and passive wireless sensors,” *Microsystems Nanoeng.*, vol. 1, no. 1, p. 15013, 2015, doi: 10.1038/micronano.2015.13.

[211] R. Amin *et al.*, “3D-printed microfluidic devices,” *Biofabrication*, vol. 8, no. 2, p. 22001, 2016, doi: 10.1088/1758-5090/8/2/022001.

[212] X. Tian, J. Jin, S. Yuan, C. K. Chua, S. B. Tor, and K. Zhou, “Emerging 3D-Printed Electrochemical Energy Storage Devices: A Critical Review,” *Adv. Energy Mater.*, vol. 7, no. 17, p. 1700127, Sep. 2017, doi: https://doi.org/10.1002/aenm.201700127.

[213] J. Lee, H.-C. Kim, J.-W. Choi, and I. H. Lee, “A review on 3D printed smart devices for 4D printing,” *Int. J. Precis. Eng. Manuf. Technol.*, vol. 4, no. 3, pp. 373–383, 2017, doi: 10.1007/s40684-017-0042-x.

[214] S. Zhang, Y. Liu, J. Hao, G. G. Wallace, S. Beirne, and J. Chen, “3D-Printed Wearable Electrochemical Energy Devices,” *Adv. Funct. Mater.*, vol. n/a, no. n/a, p. 2103092, Jul. 2021, doi: https://doi.org/10.1002/adfm.202103092.

[215] J. Fan, C. Montemagno, and M. Gupta, “3D printed high transconductance organic electrochemical transistors on flexible substrates,” *Org. Electron.*, vol. 73, pp. 122–129, 2019, doi: https://doi.org/10.1016/j.orgel.2019.06.012.

[216] J. Kwon, Y. Takeda, R. Shiwaku, S. Tokito, K. Cho, and S. Jung, “Three-

dimensional monolithic integration in flexible printed organic transistors," *Nat. Commun.*, vol. 10, no. 1, p. 54, 2019, doi: 10.1038/s41467-018-07904-5.

[217] H. Nassar and R. Dahiya, "Fused Deposition Modeling-Based 3D-Printed Electrical Interconnects and Circuits," *Adv. Intell. Syst.*, vol. 3, no. 12, p. 2100102, Dec. 2021, doi: https://doi.org/10.1002/aisy.202100102.

[218] S. J. Leigh, R. J. Bradley, C. P. Purssell, D. R. Billson, and D. A. Hutchins, "A simple, low-cost conductive composite material for 3D printing of electronic sensors," *PLoS One*, vol. 7, no. 11, p. e49365, 2012.

[219] H. Ota *et al.*, "Application of 3D Printing for Smart Objects with Embedded Electronic Sensors and Systems," *Adv. Mater. Technol.*, vol. 1, no. 1, p. 1600013, Apr. 2016, doi: https://doi.org/10.1002/admt.201600013.

[220] C. Liu *et al.*, "3D Printing Technologies for Flexible Tactile Sensors toward Wearable Electronics and Electronic Skin," *Polymers* , vol. 10, no. 6. 2018, doi: 10.3390/polym10060629.

[221] E. Macdonald *et al.*, "3D Printing for the Rapid Prototyping of Structural Electronics," *IEEE Access*, vol. 2, pp. 234–242, 2014, doi: 10.1109/ACCESS.2014.2311810.

[222] M. Areir, Y. Xu, D. Harrison, and J. Fyson, "3D printing of highly flexible supercapacitor designed for wearable energy storage," *Mater. Sci. Eng. B*, vol. 226, pp. 29–38, 2017, doi: https://doi.org/10.1016/j.mseb.2017.09.004.

[223] J. T. Muth *et al.*, "Embedded 3D Printing of Strain Sensors within Highly Stretchable Elastomers," *Adv. Mater.*, vol. 26, no. 36, pp. 6307–6312, Sep. 2014, doi: https://doi.org/10.1002/adma.201400334.

[224] A. D. Valentine *et al.*, "Hybrid 3D Printing of Soft Electronics," *Adv. Mater.*, vol. 29, no. 40, p. 1703817, Oct. 2017, doi: https://doi.org/10.1002/adma.201703817.

[225] K. Sun, T.-S. Wei, B. Y. Ahn, J. Y. Seo, S. J. Dillon, and J. A. Lewis, "3D

Printing of Interdigitated Li-Ion Microbattery Architectures," *Adv. Mater.*, vol. 25, no. 33, pp. 4539–4543, Sep. 2013, doi: https://doi.org/10.1002/adma.201301036.

[226] A. J. Blake *et al.*, "3D Printable Ceramic–Polymer Electrolytes for Flexible High-Performance Li-Ion Batteries with Enhanced Thermal Stability," *Adv. Energy Mater.*, vol. 7, no. 14, p. 1602920, Jul. 2017, doi: https://doi.org/10.1002/aenm.201602920.

[227] E. R. Cholleti, "A Review on 3D printing of piezoelectric materials," *IOP Conf. Ser. Mater. Sci. Eng.*, vol. 455, p. 12046, 2018, doi: 10.1088/1757-899x/455/1/012046.

[228] J. Zhao *et al.*, "3D Printing Fiber Electrodes for an All-Fiber Integrated Electronic Device via Hybridization of an Asymmetric Supercapacitor and a Temperature Sensor," *Adv. Sci.*, vol. 5, no. 11, p. 1801114, Nov. 2018, doi: https://doi.org/10.1002/advs.201801114.

[229] M. Sajid, J. Z. Gul, S. W. Kim, H. B. Kim, K. H. Na, and K. H. Choi, "Development of 3D-Printed Embedded Temperature Sensor for Both Terrestrial and Aquatic Environmental Monitoring Robots," *3D Print. Addit. Manuf.*, vol. 5, no. 2, pp. 160–169, Jun. 2018, doi: 10.1089/3dp.2017.0092.

[230] S. Liu and L. Li, "Ultrastretchable and Self-Healing Double-Network Hydrogel for 3D Printing and Strain Sensor," *ACS Appl. Mater. Interfaces*, vol. 9, no. 31, pp. 26429–26437, Aug. 2017, doi: 10.1021/acsami.7b07445.

[231] T. Le *et al.*, "A novel strain sensor based on 3D printing technology and 3D antenna design," in *2015 IEEE 65th Electronic Components and Technology Conference (ECTC)*, 2015, pp. 981–986, doi: 10.1109/ECTC.2015.7159714.

[232] H. Kim, F. Torres, D. Villagran, C. Stewart, Y. Lin, and T.-L. B. Tseng, "3D Printing of BaTiO3/PVDF Composites with Electric In Situ Poling for Pressure Sensor Applications," *Macromol. Mater. Eng.*, vol. 302, no. 11, p. 1700229, Nov. 2017, doi: https://doi.org/10.1002/mame.201700229.

[233] M. Palmieri, J. Slavič, and F. Cianetti, "Single-process 3D-printed structures with vibration durability self-awareness," *Addit. Manuf.*, vol. 47, p. 102303,

2021, doi: https://doi.org/10.1016/j.addma.2021.102303.

[234] J. Qu, Q. Wu, T. Clancy, and X. Liu, “Design and calibration of 3D-printed micro force sensors,” in *2016 International Conference on Manipulation, Automation and Robotics at Small Scales (MARSS)*, 2016, pp. 1–4, doi: 10.1109/MARSS.2016.7561748.

[235] M. A. Skylar-Scott, J. Mueller, C. W. Visser, and J. A. Lewis, “Voxelated soft matter via multimaterial multinozzle 3D printing,” *Nature*, vol. 575, no. 7782, pp. 330–335, 2019, doi: 10.1038/s41586-019-1736-8.

[236] R. L. Truby *et al.*, “Soft Somatosensitive Actuators via Embedded 3D Printing,” *Adv. Mater.*, vol. 30, no. 15, p. 1706383, Apr. 2018, doi: https://doi.org/10.1002/adma.201706383.

[237] S.-Z. Guo, K. Qiu, F. Meng, S. H. Park, and M. C. McAlpine, “3D Printed Stretchable Tactile Sensors,” *Adv. Mater.*, vol. 29, no. 27, p. 1701218, Jul. 2017, doi: https://doi.org/10.1002/adma.201701218.

[238] M. Schouten, R. Sanders, and G. Krijnen, “3D printed flexible capacitive force sensor with a simple micro-controller based readout,” in *2017 IEEE SENSORS*, 2017, pp. 1–3, doi: 10.1109/ICSENS.2017.8233949.

[239] Y. Gao *et al.*, “3D-Printed Coaxial Fibers for Integrated Wearable Sensor Skin,” *Adv. Mater. Technol.*, vol. 4, no. 10, p. 1900504, Oct. 2019, doi: https://doi.org/10.1002/admt.201900504.

[240] A. Frutiger *et al.*, “Capacitive Soft Strain Sensors via Multicore–Shell Fiber Printing,” *Adv. Mater.*, vol. 27, no. 15, pp. 2440–2446, Apr. 2015, doi: https://doi.org/10.1002/adma.201500072.

[241] X.-Y. Yin, Y. Zhang, X. Cai, Q. Guo, J. Yang, and Z. L. Wang, “3D printing of ionic conductors for high-sensitivity wearable sensors,” *Mater. Horizons*, vol. 6, no. 4, pp. 767–780, 2019.

[242] J. F. Christ, N. Aliheidari, P. Pötschke, and A. Ameli, “Bidirectional and Stretchable Piezoresistive Sensors Enabled by Multimaterial 3D Printing of Carbon Nanotube/Thermoplastic Polyurethane Nanocomposites,” *Polymers*

, vol. 11, no. 1. 2019, doi: 10.3390/polym11010011.

[243] E. R. Cholleti, J. Stringer, M. Assadian, V. Battmann, C. Bowen, and K. Aw, “Highly Stretchable Capacitive Sensor with Printed Carbon Black Electrodes on Barium Titanate Elastomer Composite,” *Sensors* , vol. 19, no. 1. 2019, doi: 10.3390/s19010042.

[244] Z. Lei, Q. Wang, and P. Wu, “A multifunctional skin-like sensor based on a 3D printed thermo-responsive hydrogel,” *Mater. Horizons*, vol. 4, no. 4, pp. 694–700, 2017.

[245] Z. Pei, Q. Zhang, K. Yang, Z. Yuan, W. Zhang, and S. Sang, “A Fully 3D-Printed Wearable Piezoresistive Strain and Tactile Sensing Array for Robot Hand,” *Adv. Mater. Technol.*, vol. 6, no. 7, p. 2100038, Jul. 2021, doi: https://doi.org/10.1002/admt.202100038.

[246] L. Somappa *et al.*, “A 3D Printed Robotic Finger with Embedded Tactile Pressure and Strain Sensor,” in *2020 IEEE International Conference on Flexible and Printable Sensors and Systems (FLEPS)*, 2020, pp. 1–4, doi: 10.1109/FLEPS49123.2020.9239490.

[247] Z. Wang, X. Guan, H. Huang, H. Wang, W. Lin, and Z. Peng, “Full 3D Printing of Stretchable Piezoresistive Sensor with Hierarchical Porosity and Multimodulus Architecture,” *Adv. Funct. Mater.*, vol. 29, no. 11, p. 1807569, Mar. 2019, doi: https://doi.org/10.1002/adfm.201807569.

[248] R. Dahiya, “E-skin: from humanoids to humans [point of view],” *Proc. IEEE*, vol. 107, no. 2, pp. 247–252, 2019.

[249] D. Rus and M. T. Tolley, “Design, fabrication and control of soft robots,” *Nature*, vol. 521, no. 7553, pp. 467–475, 2015.

[250] M. A. McEvoy and N. Correll, “Materials that couple sensing, actuation, computation, and communication,” *Science (80-.).*, vol. 347, no. 6228, 2015.

[251] N. Yogeswaran *et al.*, “Piezoelectric graphene field effect transistor pressure sensors for tactile sensing,” *Appl. Phys. Lett.*, vol. 113, no. 1, p.

14102, 2018.

[252] N. Yogeswaran *et al.*, “New materials and advances in making electronic skin for interactive robots,” *Adv. Robot.*, vol. 29, no. 21, pp. 1359–1373, 2015.

[253] M. Ntagios, H. Nassar, A. Pullanchiyodan, W. T. Navaraj, and R. Dahiya, “Robotic Hands with Intrinsic Tactile Sensing via 3D Printed Soft Pressure Sensors,” *Adv. Intell. Syst.*, vol. 2, no. 6, p. 1900080, Jun. 2020, doi: https://doi.org/10.1002/aisy.201900080.

[254] M. Ntagios, W. T. Navaraj, and R. Dahiya, “3D Printed Phalanx Packaged with Embedded Pressure Sensor,” in *2018 IEEE SENSORS*, 2018, pp. 1–4, doi: 10.1109/ICSENS.2018.8589720.

[255] M. Pawlaczyk, M. Lelonkiewicz, and M. Wieczorowski, “Age-dependent biomechanical properties of the skin,” *Adv. Dermatology Allergol. Dermatologii i Alergol.*, vol. 30, no. 5, p. 302, 2013.

[256] M. Ntagios, P. Escobedo, and R. Dahiya, “3D Printed Robotic Hand with Embedded Touch Sensors,” in *2020 IEEE International Conference on Flexible and Printable Sensors and Systems (FLEPS)*, 2020, pp. 1–4, doi: 10.1109/FLEPS49123.2020.9239587.

[257] M. Ntagios and R. Dahiya, “3D Printed Soft and Flexible Insole with Intrinsic Pressure Sensing Capability,” *IEEE Sens. J.*, p. 1, 2022, doi: 10.1109/JSEN.2022.3179233.

[258] O. Ozioko, P. Karipoth, P. Escobedo, M. Ntagios, A. Pullanchiyodan, and R. Dahiya, “SensAct: The Soft and Squishy Tactile Sensor with Integrated Flexible Actuator,” *Adv. Intell. Syst.*, vol. 3, no. 3, p. 1900145, Mar. 2021, doi: https://doi.org/10.1002/aisy.201900145.

[259] M. Ntagios, P. Escobedo, and R. Dahiya, “3D printed packaging of photovoltaic cells for energy autonomous embedded sensors,” in *2020 IEEE SENSORS*, 2020, pp. 1–4, doi: 10.1109/SENSORS47125.2020.9278635.

[260] D. P. J. Cotton, I. M. Graz, and S. P. Lacour, “A Multifunctional Capacitive

Sensor for Stretchable Electronic Skins," *IEEE Sens. J.*, vol. 9, no. 12, pp. 2008–2009, 2009, doi: 10.1109/JSEN.2009.2030709.

[261] S. W. Park, P. S. Das, and J. Y. Park, "Development of wearable and flexible insole type capacitive pressure sensor for continuous gait signal analysis," *Org. Electron.*, vol. 53, pp. 213–220, 2018, doi: https://doi.org/10.1016/j.orgel.2017.11.033.

[262] S.-J. Woo, J.-H. Kong, D.-G. Kim, and J.-M. Kim, "A thin all-elastomeric capacitive pressure sensor array based on micro-contact printed elastic conductors," *J. Mater. Chem. C*, vol. 2, no. 22, pp. 4415–4422, 2014.

[263] M. Ying *et al.*, "Silicon nanomembranes for fingertip electronics," *Nanotechnology*, vol. 23, no. 34, p. 344004, 2012, doi: 10.1088/0957-4484/23/34/344004.

[264] Q. Zhang, Y. L. Wang, Y. Xia, X. Wu, T. V. Kirk, and X. D. Chen, "A low-cost and highly integrated sensing insole for plantar pressure measurement," *Sens. Bio-Sensing Res.*, vol. 26, p. 100298, 2019, doi: https://doi.org/10.1016/j.sbsr.2019.100298.

[265] P. Escobedo, M. Ntagios, D. Shakthivel, W. T. Navaraj, and R. Dahiya, "Energy Generating Electronic Skin With Intrinsic Tactile Sensing Without Touch Sensors," *IEEE Trans. Robot.*, vol. 37, no. 2, pp. 683–690, 2021, doi: 10.1109/TRO.2020.3031264.